FDL-TDR-64-41
Part II

STAGNATION POINT HEAT TRANSFER IN HIGH ENTHALPY GAS FLOWS

Part II. Shock Layer Radiative Emission During Hypervelocity Re-entry

TECHNICAL DOCUMENTARY REPORT NO. FDL-TDR-64-41, Part II

Flight Dynamics Laboratory
Research and Technology Division
Air Force Systems Command
Wright-Patterson Air Force Base, Ohio

Project No. 1366, Task No. 136615

(Prepared under Contract No. AF 33(657)-10110
by The Ohio State University, Columbus, Ohio;
Robert M. Nerem, author)

FOREWORD

This report was prepared by The Ohio State University Research Foundation under USAF Contract No. AF33(657)-10110. The contract was initiated under Project No. 1366, "Aerodynamics and Flight Mechanics," Task No. 136615, "Mechanisms and Magnitudes of Aerodynamic Heating at Hypervelocities." The work was administered under the direction of the Flight Dynamics Laboratory, Research and Technology Division, Mr. L. E. Hooks, Project Engineer.

This report covers work conducted from February 1963 to February 1964.

The author wishes to acknowledge the assistance of Mr. L. E. Hooks in the programing of the results of this investigation for computer analysis. The author also wishes to acknowledge the encouragement and support of Dr. John D. Lee, Director, The Ohio State University Aerodynamic Laboratory, and the assistance of Mr. George H. Stickford of The Ohio State University Aerodynamic Laboratory in the development of the experimental techniques and in the performance of the present measurements.

ABSTRACT

Experimental measurements of stagnation point equilibrium radiative heat transfer have been performed using The Ohio State University arc driven shock tube facility and over the range of simulated flight velocities between 26,000 and 52,000 feet per second, and at altitudes from 100,000 to 170,000 feet. These measurements have been compared with existing theoretical estimates; and wide disagreement is shown to exist at high temperatures and low densities where the continuum emission due to the de-ionization of N^+ and O^+ dominates the shock layer radiation. Using an approximate approach, a revised estimate is presented for the radiative emission from high temperature equilibrium air. This revised estimate is then applied to the determination of stagnation point equilibrium radiative heat transfer during re-entry at super-orbital velocities. A correlation for the shock layer emission rate useful in engineering design calculations is presented.

PUBLICATION REVIEW

This report has been reviewed and is approved.

FOR THE DIRECTOR

Demetrius Zonars

DEMETRIUS ZONARS
Ass't for Experimental Simulation
Flight Mechanics Division
AF Flight Dynamics Laboratory

CONTENTS

TABLES

ILLUSTRATIONS

ILLUSTRATIONS (continued)

ILLUSTRATIONS (continued)

SYMBOLS

B_ν	Planck black body distribution, equation (5)
c	speed of light
d	shock tube diameter
E_t	total radiative energy emission per unit volume into 4π steradians
F	characterizes electronic transition probability
F_1	shock layer shape correction factor
F_2	thin film gage geometric view factor
F_{2_A}	view factor for point A on thin film gage
h	Planck's constant
I	gage current
I_ν	monochromatic intensity in specified direction
J	total radiance - energy emitted per unit volume per steradian
k	Boltzmann gas constant
L_e	effective radius for radiation, equation (16)
M	Mach number
M_s	incident shock Mach number
P	pressure
$\dot{q}_{rad}$	radiative heat transfer rate-energy flux per unit area per unit time
Q_ν	total monochromatic emission from an element of volume due to both spontaneous and induced effects
r	radial coordinate
R	radial distance; also resistance
R_N	nose radius of hemispherical body
T	temperature, or transmissivity

SYMBOLS (continued)

t	time
V	gas velocity
V_s	traveling normal shock velocity

Greek

αR_o	$= \frac{\Delta R}{\Delta T}$, temperature dependence of gage resistance
α_G	absorptivity of thin film gage
β_m	thermal property of gage backing material
ΔE	variation in voltage drop across gage
δ	shock detachment distance
ϵ'	emissivity per unit length
ϕ	angle in spherical coordinate system (see Figure 4)
γ	radio of specific heats
Γ	energy loss parameter
λ	wavelength of radiation
μ_ν	monochromatic radiation absorption coefficient
μ'_ν	monochromatic radiation absorption coefficient allowing for induced emission
ν	frequency of radiation
ω	solid angle
ρ	gas density
ρ_o	reference density at STP conditions; $\rho_o = 2.50 \times 10^{-3}$ Slugs/Ft^3
σ	Stefan-Boltzmann constant
θ	angle in spherical coordinate system (see Figure 4)

θ' angle between tangent plane to stagnation point of blunt body and tangent plane to some local point

Subscripts

1 initial shock tube driven conditions

2 conditions behind traveling normal shock; free-stream conditions present experiment

G gage property

∞ flight free-stream conditions

t stagnation point gas property

I. INTRODUCTION

In the design of a space vehicle for entry at hyper-velocities into the Earth's atmosphere, one of the most important considerations is the energy transfer to the vehicle which accompanies its deceleration in the atmosphere. This energy transfer, for re-entry vehicles traveling at velocities not in excess of the Earth's satellite orbital velocity, is almost completely due to the aerodynamic heating associated with the boundary layer viscous dissipation. Thus for the re-entry of inter-continental ballistic missiles, for the satellite re-entry of such systems as the Discoverer and Mercury space capsules, and for the glide re-entry of the Asset vehicle, a determination of re-entry heating can be carried out through an analysis of the vehicle boundary layer characteristics. This particular problem of predicting aerodynamic heating for re-entry vehicles has received extensive consideration in the literature, i.e., references 1-4, and a discussion of the presently available knowledge concerning the stagnation point of a blunt nosed re-entry vehicle may be found in reference 5.

On the other hand, for re-entry vehicles traveling at super-orbital velocities, sizeable energy transfer to the vehicle during re-entry may also occur as a result of thermal radiation emitted from the high temperature gas in the vehicle shock layer. Extensive investigations of this phenomenon have been carried out.[6-20] These have generally been limited to consideration of the stagnation region heating since the magnitude of the radiative heat transfer falls off rapidly away from the stagnation point.[16] The study of this shock layer emission has been divided into a consideration of the thermal radiation from (1) shock-heated gas in chemical non-equilibrium, and (2) gas that has relaxed to the thermodynamic equilibrium state after passage through the bow shock. These two sources of radiative heating are denoted as non-equilibrium radiation and equilibrium radiation respectively.

Figure 1 illustrates the non-equilibrium phenomena behind a normal shock wave traveling into undisturbed air. The temperature overshoot is a result of the finite time required to transfer energy into the vibrational mode of the molecules and for dissociation and ionization to occur. At the instant of shock compression, only the translational and rotational degrees of freedom are excited and the translational temperature immediately behind the shock may be predicted using the Rankine-Hugoniot relationships for $\gamma = 1.4$. Thus, for $M_\infty^2 \gg 1$,

$$\frac{T_M}{T_\infty} = 0.974\ (1 + 0.2M_\infty^2) \quad , \qquad (1)$$

Manuscript released March, 1964, for publication as an FDL Technical Documentary Report.

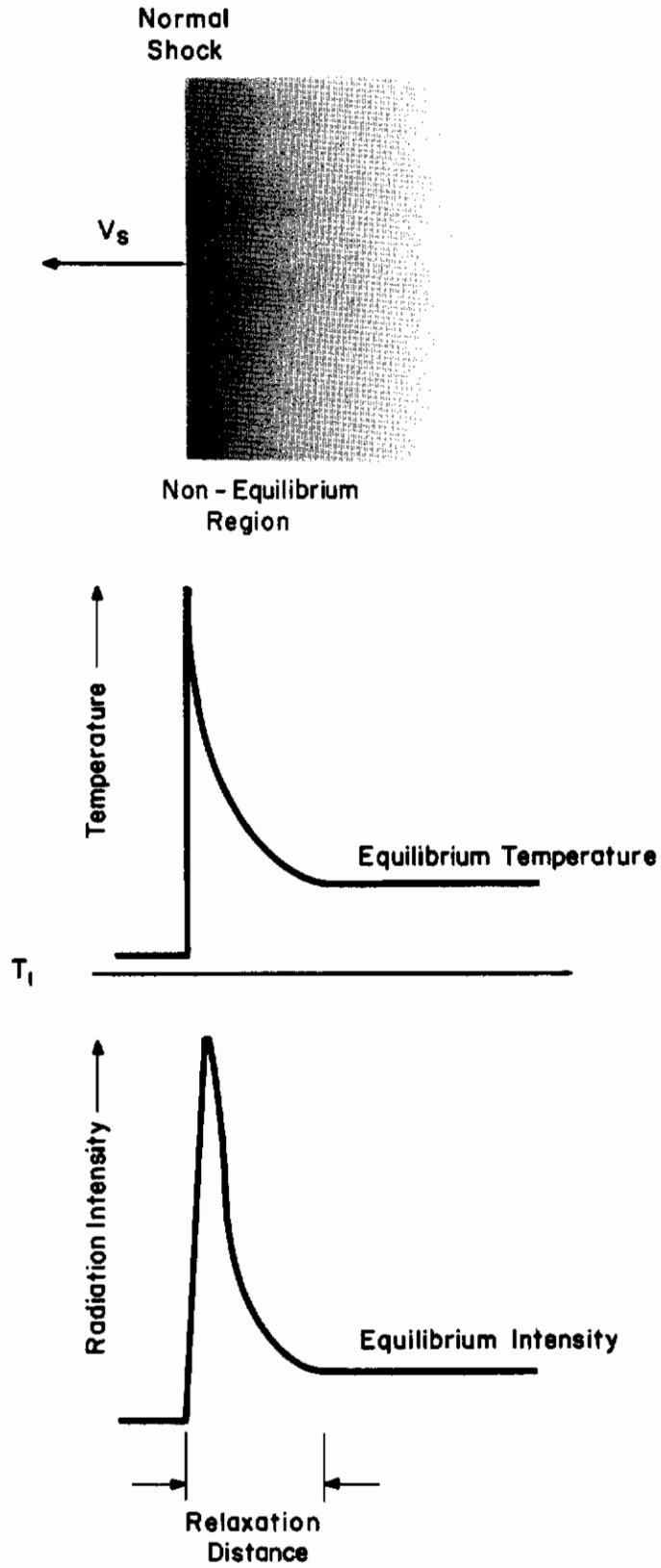

FIGURE 1. Illustration of Non-Equilibrium Phenomena Behind Normal Shock

where T_M is the maximum overshoot temperature. For shock velocities in the range of 30,000 - 50,000 feet per second, overshoot temperatures on the order of 50,000 to 100,000°K may ideally be attained. In the relaxation region following the shock, energy is transferred into the vibrational modes of the molecules, dissociation and ionization occurs, and finally chemical and thermodynamic equilibrium are attained. It should be noted that the various processes contributing to the attainment of the equilibrium state may be coupled together. The composition and thermodynamic properties corresponding to this equilibrium state can be determined through the application of the criteria for chemical equilibrium and the laws of conservation.[21-24]

In general, the radiative emission from high temperature air in thermodynamic equilibrium[6-9,11,19] has been considered to be dominated by the radiation of the molecular bands of nitrogen, oxygen, nitric oxide, and ionized molecular nitrogen; by the continuum radiation associated with the deionization of N^+ and O^+, and with the Bremsstrahlung emission of N and O; and by line radiative emission from nitrogen and oxygen atoms.[18] In addition, continuum radiation due to photoattachment to form the N^- ion has recently been identified as a possible source of a significant amount of radiative emission.[25] Figure 2 shows a comparison between the existing theoretical estimates for the radiative intensity of high temperature equilibrium air.[6-8,11,19] Indicated for each theory is the wavelength region considered. It can be seen there is wide disagreement between these various theories, and thus present estimates of radiative heating during re-entry are uncertain. This is particularly true at high temperatures where continuum radiation dominates.

The non-equilibrium radiation associated with the relaxation process behind the shock front is not nearly as well understood as the equilibrium radiation. There is also considerable uncertainty concerning the magnitude of its intensity. The biggest unknown is the excitation processes which lead to the population of upper electronic states and to dissociation and ionization within a few mean free paths of the shock front where the translational temperature may still be quite high. It is from such excited states of N_2, N_2^+, NO, and N that the non-equilibrium radiation originates. Without a proper understanding of excitation phenomena, it is impossible to predict theoretically the non-equilibrium radiative intensity; and the presently available knowledge of this phenomenon is based on the extensive experimental measurements carried out at the Avco-Everett Research Laboratory[10,14,18] and at the NASA Ames Research Center.[17]

As indicated earlier, the shock layer radiative emission makes an important contribution to the heat load associated with a super-orbital velocity re-entry vehicle. How important this contribution is can be seen in Fig. 3 where the relative contributions of the aerodynamic,[26] equilibrium radiative,[19] and non-equilibrium radiative[17] heating to the stagnation point heat transfer rate (assuming no coupling between these modes of energy transfer) are shown as a function of flight velocity for a vehicle at 200,000 feet in altitude and with a nose radius of 1 foot. It can be seen that as the flight velocity increases the radiative heating becomes increasingly important. Thus for planetary

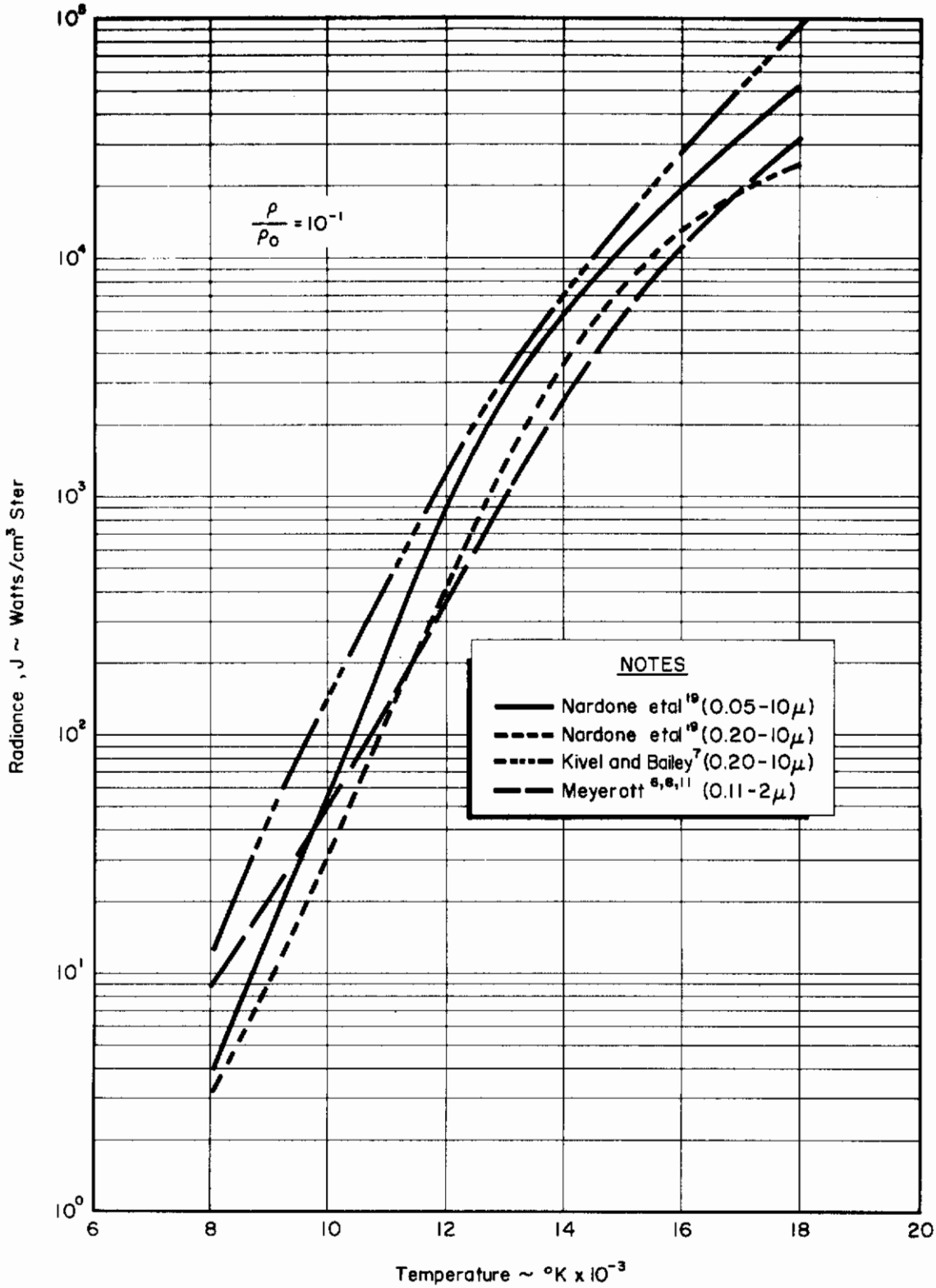

FIGURE 2. Comparison of Existing Theoretical Calculations of Radiance of High Temperature Air

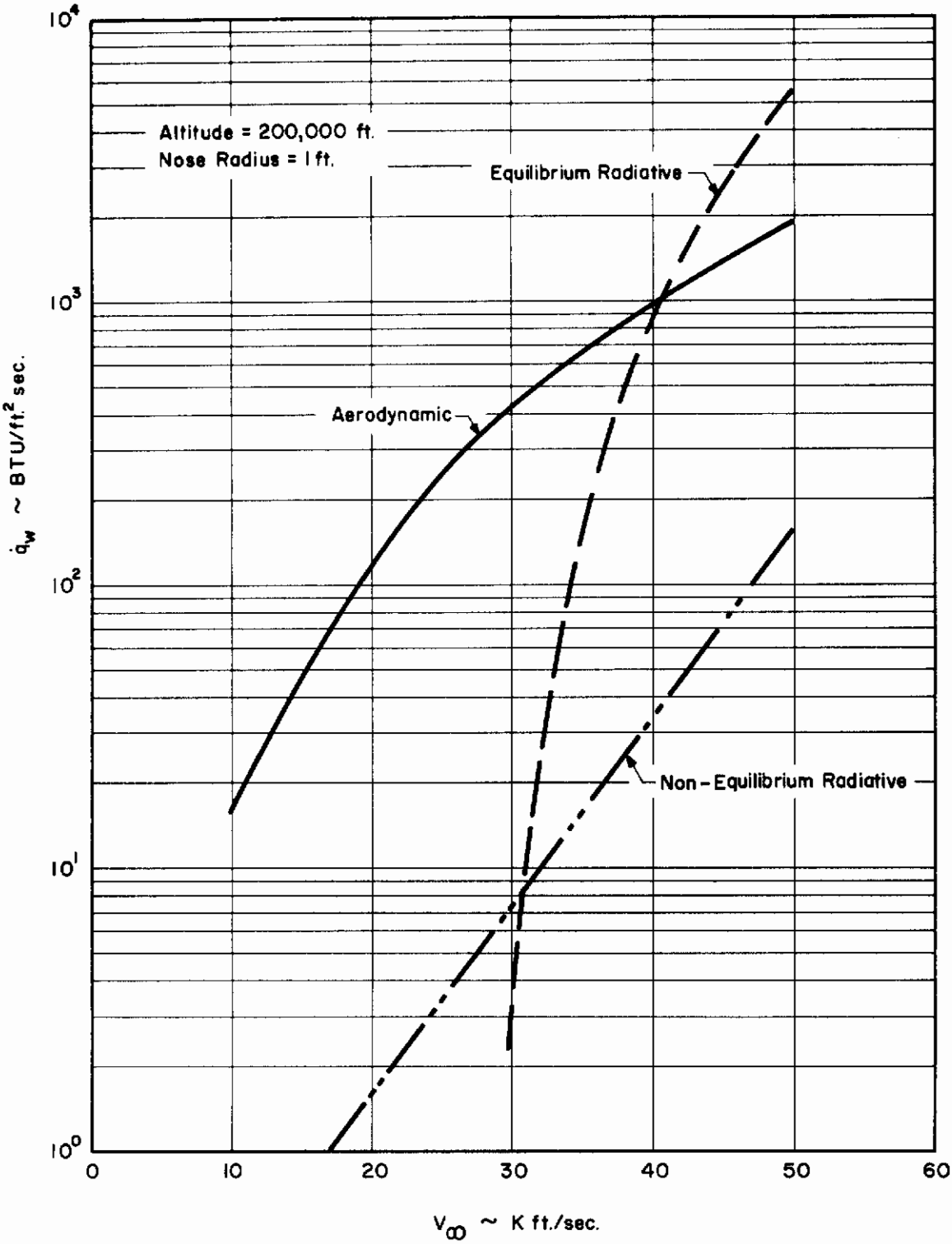

FIGURE 3. Comparison of Magnitude of Aerodynamic and Radiative Heating for a Re-entry Vehicle at 200,000 Feet

and solar probes re-entering the Earth's atmosphere at velocities ranging up to 75,000 feet per second, the radiative heating will actually dominate the re-entry heat load. Even for an initial re-entry velocity equal to the escape velocity from the Earth, the radiative heating makes an important, although not dominant, contribution.

The importance of shock layer radiative emission, with regard to the total heating to which a super-orbital velocity re-entry vehicle is exposed, is thus apparent. However, as previously indicated, there is considerable uncertainty as to its exact magnitude. For this reason, the present investigation of stagnation point radiative heating during hypervelocity re-entry was undertaken. Because of the importance of equilibrium radiation (as an example, see Fig. 3), the present study has been limited to an investigation of shock layer radiative emission from high temperature equilibrium air. The approach has been largely experimental, with measurements of the total stagnation point radiative heat flux in the wavelength region of 0.17 to 6.0 microns being performed over a range of simulated flight velocities from 26,000 to 52,000 feet per second at simulated altitudes from 100,000 to 170,000 feet. The facility used for these experimental measurements is The Ohio State University arc-driven shock tube facility[39-41] which is capable of generating hypervelocity flows with total enthalpies in excess of 60,000 BTU/lb_m. The measurements were carried out using a thin film radiative heat transfer gage developed as part of the investigation.

The purpose of this study has been to assess the accuracy of presently available theoretical estimates and, if necessary, to modify these analyses so as to provide more accurate information on radiative heating during re-entry for use in engineering design calculations. As will be seen in the discussion of results, existing theoretical estimates of shock layer radiation from high temperature equilibrium air are in wide disagreement with the data at extreme conditions where the de-ionization continuum radiation of N^+ and O^+ dominates the total emission rate. An improved estimate of this radiation is thus presented and applied to the determination of stagnation point radiative heat transfer during re-entry at super-orbital velocities.

II. THE STAGNATION POINT EQUILIBRIUM RADIATIVE HEAT TRANSFER PROBLEM

The problem to be considered in this investigation is the heat transfer rate at the stagnation point of a blunt body, re-entering the Earth's atmosphere at hypersonic velocities, due to the radiative emission from the equilibrium air in the shock layer. Before formulating the equation for the radiative heat flux at the stagnation point, the basic equation governing radiative transfer should be reviewed.[27,28] Consider a high temperature gas in thermodynamic equilibrium in which radiative emission and absorption occur, but in which there is no scattering or reflection of light. At any specified point in the gas having coordinates (x_1, x_2, x_3) and in a fixed direction $\vec{l}$, there exists a radiant flux with the monochromatic intensity in the direction of

propagation $\vec{l}$ being denoted as I_ν. The change in I_ν in the fixed direction $\vec{l}$ is due to both emission and absorption processes taking place in the gas. The emission from an element of gas consists of two parts[29,30]: (1) spontaneous emission, which is an isotropic radiation associated only with the quantum-mechanical properties of the gas and not depending on the collective action of the gas; (2) induced emission, which occurs as an effect associated with the absorption of radiant energy.

The total monochromatic emission from an element of volume in the fixed direction $\vec{l}$ due to both spontaneous and induced effects will be denoted here as Q_ν. The absorption in a gas is characterized by the monochromatic absorption coefficient per unit length, μ_ν; and the energy absorbed from a radiant flux in a fixed direction $\vec{l}$ having intensity I_ν is $\mu_\nu I_\nu$. Thus the equation for the transfer of radiation may be expressed in the form

$$\frac{dI_\nu}{dr} = Q_\nu - \mu_\nu I_\nu \quad , \tag{2}$$

where the derivative of I_ν is in the fixed direction $\vec{l}$.

For a gas in which there is an equilibrium distribution of energy, the two emission processes and the absorption process may be related to each other through the interrelation of their respective Einstein coefficients or transition probabilities. In this case the basic transfer equation becomes

$$\frac{dI_\nu}{dr} = \mu_\nu' (B_\nu - I_\nu) \quad , \tag{3}$$

where μ_ν' is the absorption coefficient allowing for induced radiation

$$\mu_\nu' = \mu_\nu \left[1 - e^{-h\nu/kT}\right] \quad , \tag{4}$$

and

$$B_\nu = \frac{2h\nu^3}{c^2} \exp\left[\left(\frac{h\nu}{kT}\right) - 1\right]^{-1} \tag{5}$$

is the Planck black body intensity distribution.

Integrating Eq. (3), where R is the length of gas in the direction $\vec{l}$ associated with a particular problem, results in [31]

$$I_\nu = c_1 e^{-\int_o^R \mu_\nu' dr} + e^{-\int_o^R \mu_\nu' dr} \int_o^R e^{\int_o^r \mu_\nu' dr} B_\nu \mu_\nu' dr \quad . \qquad (6)$$

If the length of gas in the direction $\vec{l}$ is zero, that is, R = o, then there can be no radiative flux in that direction due to the hot gas emission, and thus I_ν = o. Upon applying this boundary condition, Eq. (6) becomes

$$I_\nu = e^{-\int_o^R \mu_\nu' dr} \int_o^R e^{\int_o^r \mu_\nu' dr} B_\nu \mu_\nu' dr \quad . \qquad (7)$$

This equation specifies the monochromatic intensity of the radiation flux in a fixed direction $\vec{l}$ for a non-scattering medium.

The problem to be considered here is illustrated in Fig. 4. Consider a hemispherical blunt body with a detached shock wave in a hypersonic flow. The radiative heat flux to the stagnation point due to the shock layer emission may be expressed as

$$\dot{q}_{rad} = \int_o^\infty \int_{\omega=o}^{\omega=2\pi} I_\nu \cos\theta \, d\omega d\nu \quad , \qquad (8)$$

where the integration extends over all possible directions of incident radiation in a solid angle of 2π, and I_ν is as expressed in Eq. (7). The cos θ arises because incident radiation from a direction making an angle θ with the surface normal sees an element of area dA at the stagnation point as a projected area dA cos θ. In carrying out the integration of Eq. (8) with Eq. (7) inserted, R is the distance from the stagnation point to the shock wave measured in the direction as defined by the angle θ.

For the general case where the shock layer is non-uniform, the corrected absorption coefficient, μ_ν', is a function of position in the shock layer; and the integration of Eq. (8) can only be carried out with numerical techniques. However, if a simplified model is used to represent the stagnation point shock layer, an explicit relation may be determined for the stagnation point radiant heat flux. This model, illustrated in Fig. 5, assumes that the curved shock layer may be replaced by a semi-infinite slab of thickness equal to the stagnation point shock detachment distance, δ, and with constant properties equal to the equilibrium stagnation conditions. For this case, Eq. (7) reduces to

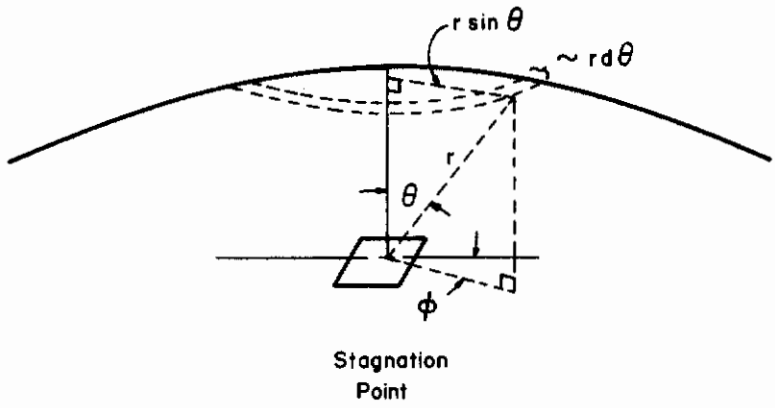

FIGURE 4. Schematic Diagram Defining Notation for Calculation of Stagnation Point Radiative Heat Transfer

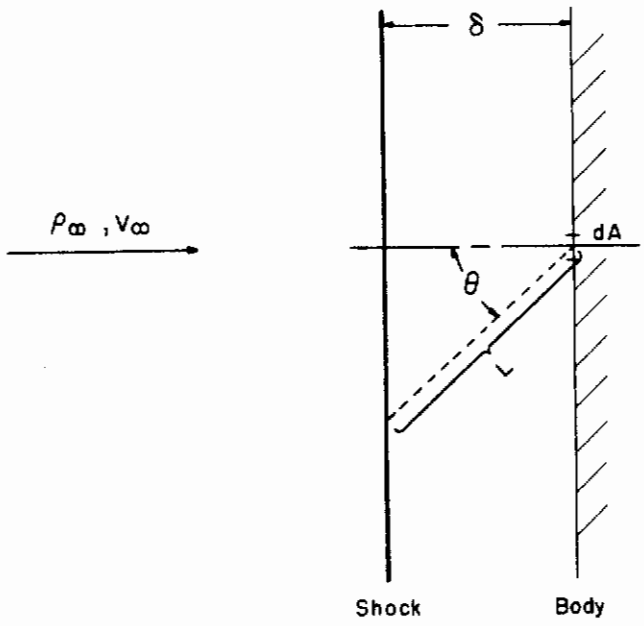

FIGURE 5. Approximate Model for Calculation of Stagnation Point Radiative Heating

the form

$$I_\nu = B_\nu \left(1 - e^{-\mu_\nu' R}\right) \quad . \qquad (9)$$

Furthermore, R may be expressed as $R = \delta/\cos\theta$ and thus the stagnation point equilibrium radiative flux becomes

$$\dot{q}_{rad} = \int_o^\infty d\nu \int_o^{2\pi} d\phi \int_o^{\pi/2} B_\nu \left(1 - e^{-\mu_\nu' \frac{\delta}{\cos\theta}}\right) \sin\theta \cos\theta \, d\theta \quad . \qquad (10)$$

For an opaque gas, that is, one where $\mu_\nu' \delta/\cos\theta \gg 1$,

$$\dot{q}_{rad} = \int_o^\infty d\nu \int_o^{2\pi} d\phi \int_o^{\pi/2} B_\nu \sin\theta \cos\theta \, d\theta = \sigma T^4 \quad , \qquad (11)$$

where σ is the Stefan-Boltzmann constant and T is the shock layer temperature. On the other hand, for an optically thin gas where $\mu_\nu \delta/\cos\theta \ll 1$,

$$e^{-\mu_\nu' \frac{\delta}{\cos\theta}} = 1 - \mu_\nu' \frac{\delta}{\cos\theta} + \cdots$$

and the stagnation point radiative flux becomes

$$\dot{q}_{rad} = \int_o^\infty d\nu \int_o^{2\pi} d\phi \int_o^{\pi/2} B_\nu \mu_\nu' \delta \sin\theta \, d\theta$$

$$= 2\pi \delta \int_o^\infty \mu_\nu' B_\nu d\nu = 2\pi \delta J \quad , \qquad (12)$$

where $J = \int_o^\infty \mu_\nu' B_\nu d\nu$ is the radiance of the high temperature equilibrium air and must be determined from a knowledge of the spectral characteristics of air. This will be discussed in Section III.

Exact calculations of the stagnation point radiative heat flux, which include effects of shock wave curvature and non-uniform shock layer properties, have indicated that the exact relation for an optically thin gas is of the form

$$\dot{q}_{rad} = 2\pi \delta F_1 J \qquad . \qquad (13)$$

F_1 is a correction factor which takes into account the above noted effects. Its value is on the order of 0.90, and is function of the shock layer properties and the shock detachment distance.[16-32]

With the use of Eq. (13) for an optically thin gas, the radiative heating due to shock layer thermal emission during re-entry may be evaluated. J is the radiance of high temperature air and, as noted previously, its determination will be discussed in the next section. The shock detachment distance, δ may be estimated with any one of several existing blunt body theoretical analyses or from experimental data.[33,34] For flight conditions in which the shock layer is neither optically thin nor opaque, Eq. (13) will overestimate the heat transfer and thus yield a conservative result which may be used in engineering design calculations. It should be noted that for non-optically thin shock layer conditions, the inviscid shock layer flow will not necessarily behave as an adiabatic process. Thus an exact analysis of re-entry heating in this case should include radiation effects in the governing energy equation. The shock layer in this case may be highly non-uniform and coupling between the convective and radiative transfer may occur. This will be discussed further in Section VIII.

It should also be noted that for the conditions of the present investigation, the shock layer is optically thin, and thus Eq. (13) is applicable. This will be discussed further in the next section.

III. THEORETICAL ESTIMATES OF THE RADIANCE OF HIGH TEMPERATURE AIR

There have been several calculations[6-8,19] of the radiance of high temperature air, J, where

$$J = \int_0^\infty \mu_\nu' B_\nu d\nu \qquad (14)$$

In any such calculation, the important gas characteristic to be evaluated is the spectral absorption coefficient allowing for induced emission, μ_ν'. This may be done by considering separately each specie which makes up the high temperature air at a particular condition, calculating its spectral absorption coefficient as a function of frequency or wavelength, and then summing up the individual specie contributions.

Those particle processes which generally have been considered to make important contributions to the radiative emission from high temperature air are as follows:

Ultraviolet-visible band spectra

The beta system of NO
The gamma system of NO
The Schumann-Runge system of O_2
The first positive system of N_2
The second positive system of N_2
The first negative system of N_2^+

Infrared band spectra

The vibration-rotation spectrum of NO

Free bound continua

The free bound continua of O
The de-ionization continuum of O^+
The de-ionization continuum of N^+

Free free continua

The free free continua of O, O^+, O^{++}
The free free continua of N, N^+, N^{++}

In addition, the atomic line radiation of N and O, and the emission accompanying the photo attachment of an electron to form N^- have recently been identified as possible contributors of a significant amount of radiative emission in high temperature air.[18,25] However, at the present there is still considerable uncertainty as to the magnitude of the radiation accompanying these processes, and none of the existing calculations of the radiance of high temperature air have included them.

CN is also a possible contributor to the emission from high temperature air due to the presence of CO_2 in the atmosphere. However, the calculations of Kivel and Bailey[7] for a realistic air atmosphere with approximately .03 per cent CO_2 indicate that the CN contribution is small.

Although no attempt will be made here to review the details of the methods used in the existing calculations of the radiance of high temperature air, a few general remarks are appropriate. Analytical expressions for the spectral absorption coefficient of an electronic band system have been developed under assumptions which result in a "smeared" structure and a continuous distribution of radiation within the wavelength limits of a particular band system. The important characteristic of a particular band system is the electronic transition probability which may be characterized by an electronic F-number. In Table 1 the F-numbers

used for the band systems previously indicated as being important are tabulated for the three existing calculations of radiative emission from high temperature air.[6-8,19] As can be seen, there is considerable disagreement in the F-number value used for some band systems in these three different calculations. The calculations of Nardone, Breene et al, are based on the most recent experimental F-number values. This calculation should be the most accurate for the temperature range in which electronic transitions in molecules dominate the radiative emission.

TABLE 1

COMPARISON OF F-NUMBERS FOR VARIOUS MOLECULAR BAND SYSTEMS

	F-number		
	Kivel and Bailey[7]	Meyerott[6,8,11]	Nardone et al[19]
NO Beta	.006	.008	.0015
NO Gamma	.001	.0025	.0024
N_2 First Positive	.025	.02	.0095
N_2 Second Positive	.09	.07	.04
N_2^+ First Negative	.18	.20	.04
O_2 Schumann-Runge	.028	.259	.163

The infrared radiation due to the vibration-rotation bands of NO may be approached in a similar manner as the radiation accompanying electronic transitions. This radiation is important only at temperatures on the order of 3000-4000°K and thus makes a negligible contribution in the temperature range of this present study.

The free bound continuum emission of oxygen, or nitrogen, may be described by the chemical equation

$$A + e \longrightarrow A^- + h\nu \quad ,$$

where $h\nu$ is the energy radiated and the symbol A denotes a neutral atom. Calculations of the intensity of this type of emission are based on the introduction

of an effective collision cross section for the photo attachment process. Branscomb et al[35] have made measurements of this cross section for oxygen, and these are generally used in radiance calculations. As indicated previously, no attempt has yet been made to include the nitrogen photo attachment emission in radiance calculations. However, Boldt[36] and Allen et al[25] have both detected enhanced continuum radiation at high temperatures and relatively high pressures which they explain as being due to the photo attachment of an electron to nitrogen.

Radiative emission associated with de-ionization phenomena, for example,

$$N^+ + e = N + h\nu \quad ,$$

has been estimated in all three existing calculations of the radiance of high temperature air for a hydrogen-like model. However, Biberman and Norman[37] have pointed out that the use of such a model will indeed give erroneous results and have suggested an improved technique for carrying out such calculations. Allen and Textoris[25] have carried out a limited number of calculations of the free free and free bound radiation of nitrogen at a wavelength of 5000 Å, using the method proposed by Biberman and Norman. These have been shown to be in reasonable agreement with spectroscopic shock tube measurements at low densities. Since the de-ionization continuum of N^+ is the dominant radiative emission at temperatures on the order of 16,000-18,000°K, it is obvious that it is important that more knowledge be gained concerning this radiation process. Present estimates must certainly be considered as highly approximate.

The total radiance of high temperaute air as calculated by Kivel and Bailey,[7] Meyerott,[6,8,11] and Nardone et al,[19] are shown in Figs. 6, 7, and 8. The emission of the N_2^+ first negative band system as predicted by Meyerott has been corrected through the use of an F-number of 0.04 by the present author, and the results in Fig. 7 include this correction. This value of 0.04 for the F-number is based on the experimental results of reference 38. The calculation of Kivel and Bailey was the earliest, and although based on the best information available at that time, appears to overestimate the radiative emission from high temperature air when compared with more recent calculations. The results of Meyerott[6,8,11] and Nardone et al[19] at high densities are in reasonable agreement, considering the present state of the knowledge. This can be seen from a comparison of the spectral distribution as predicted by these two different analyses for a particular condition, Fig. 9, and from a comparison of the total radiance as a function of temperature for $\rho/\rho_o = 10^{-1}$, Fig. 2. At low densities there is considerable disagreement. Because the calculations of Nardone et al are somewhat more detailed and inclusive than those of Meyerott, their calculations have been used as a basis for analyzing the results of the present experimental program. The calculations of Meyerott and his co-workers[6,8,11] must be considered as incomplete, since any radiation below 0.11 microns is omitted. On the other hand, the calculations of Nardone et al[19] predict extensive radiative emission at wavelengths between 0.05 and 0.15 microns, and at densities

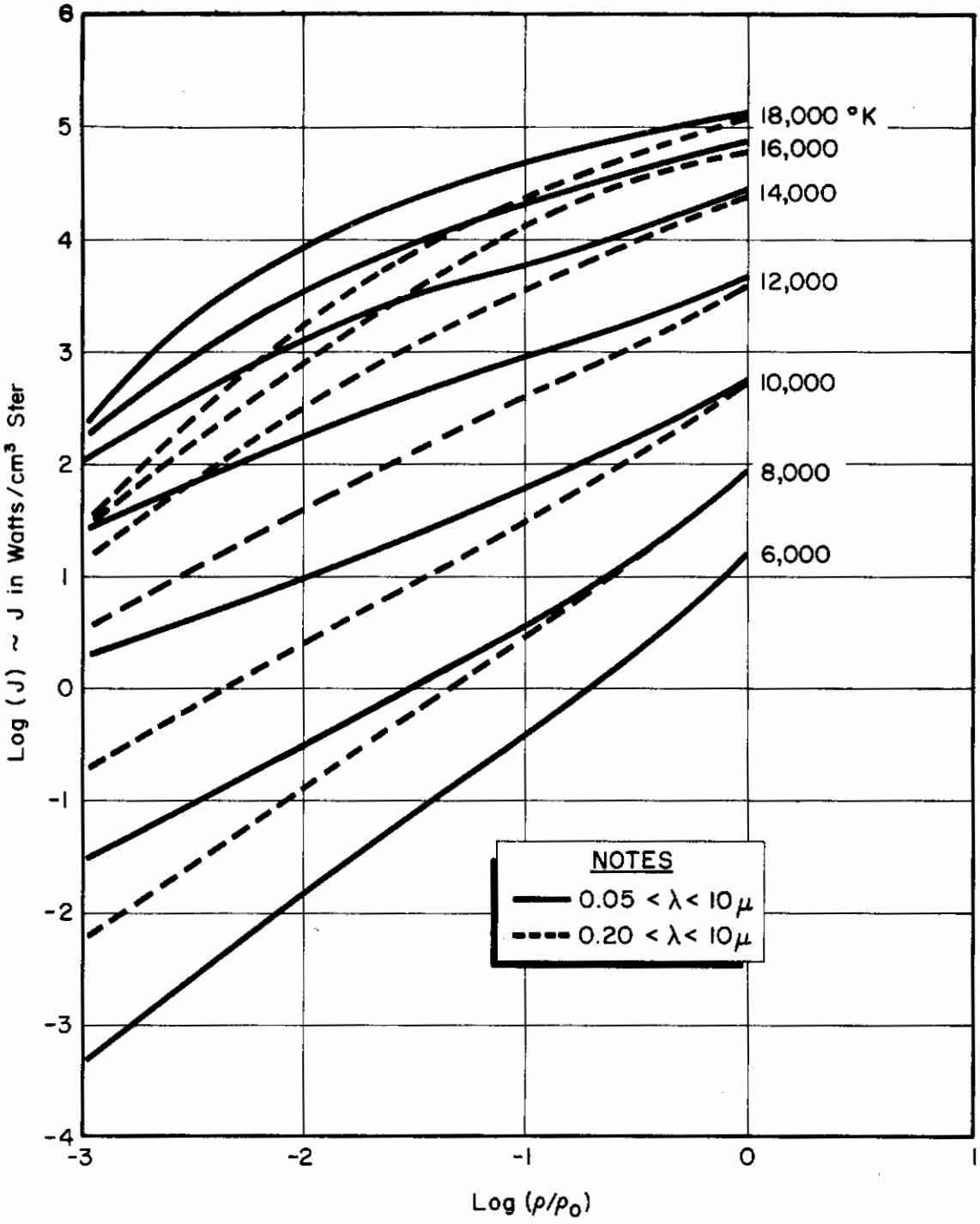

FIGURE 6. Radiance of High Temperature Air as Calculated by Nardone, Breene, Zeldin, and Riethof (Reference 19)

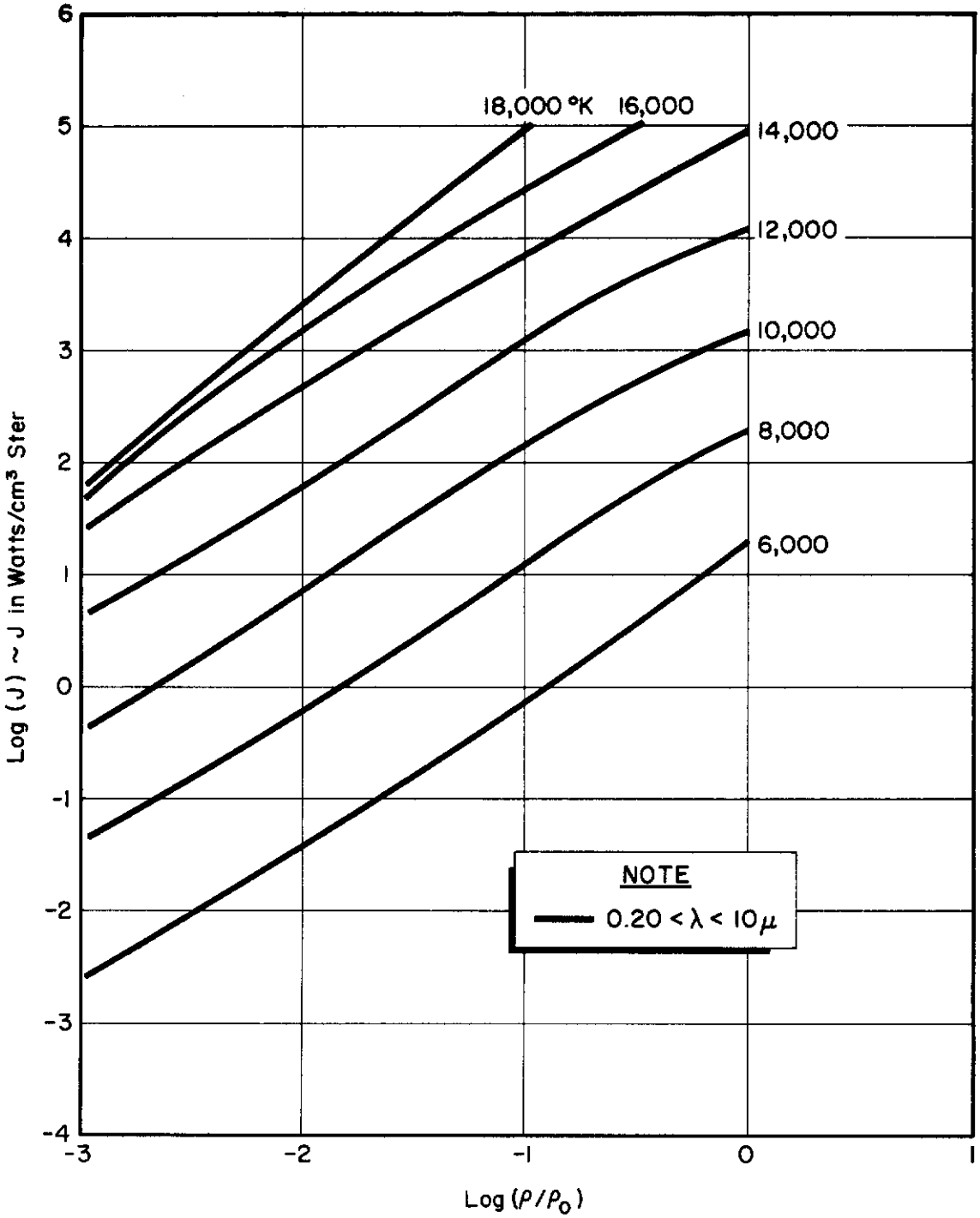

FIGURE 7. Radiance of High Temperature Air as Calculated by Kivel and Bailey (Reference 7)

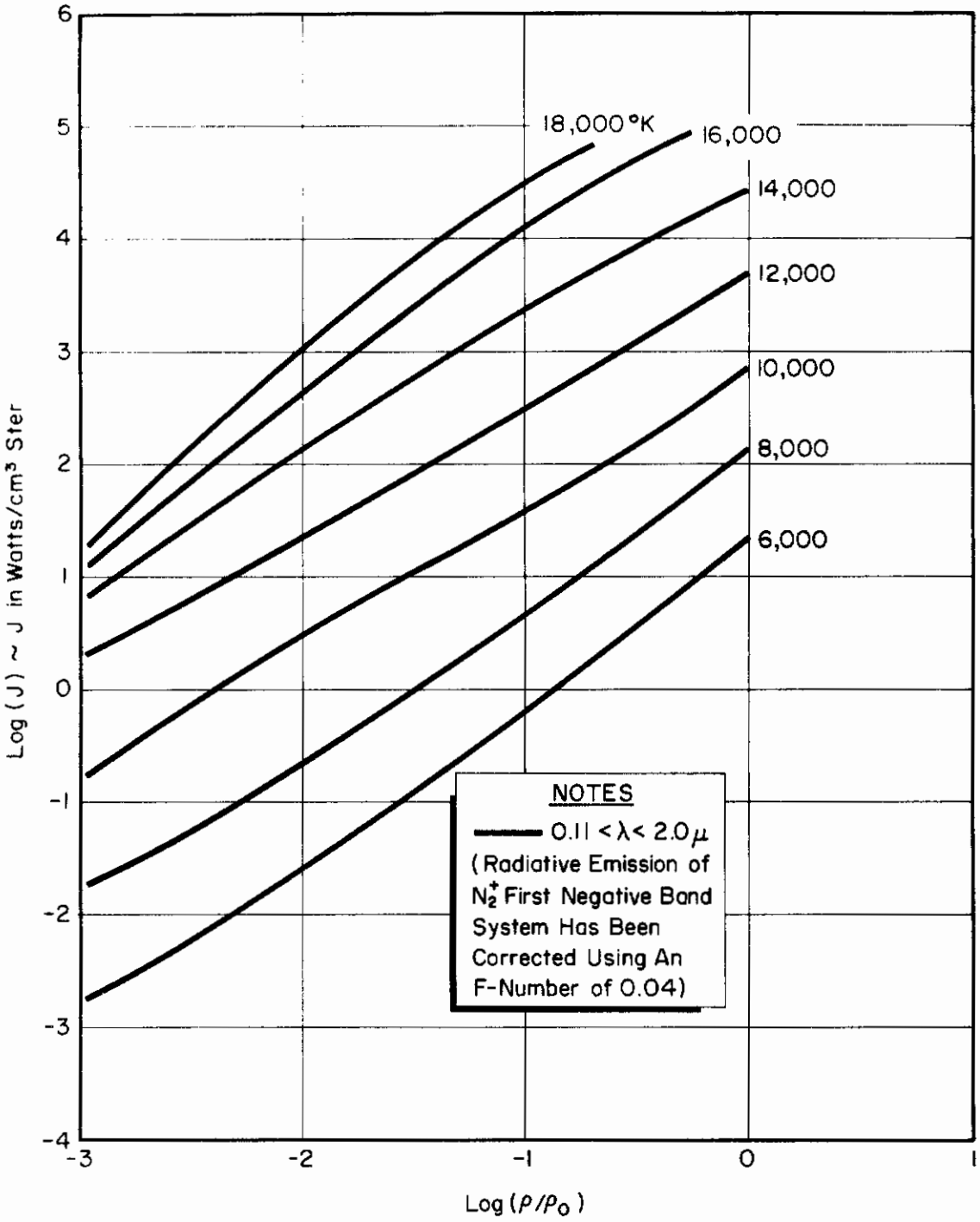

FIGURE 8. Radiance of High Temperature Air as Calculated by Meyerott and Coworkers (Reference 6, 8, 11)

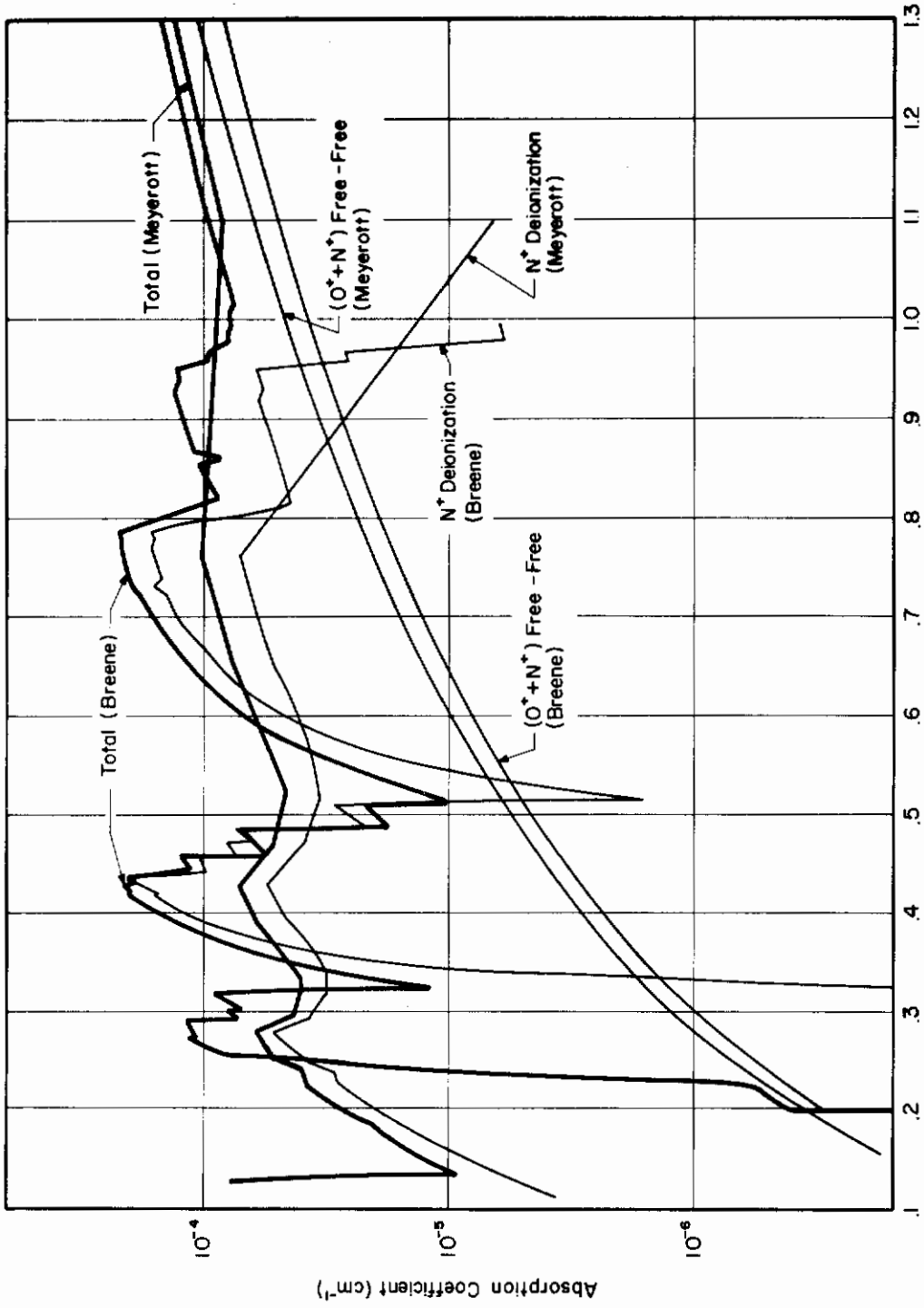

FIGURE 9. Comparison of Predictions: Spectral Absorption Coefficients of Equilibrium Air (Reference 19)

on the order of $\rho/\rho_o = 10^{-3} - 10^{-2}$. Figures 10, 11, and 12, taken from reference 19, show the relative contributions of the various species and processes to the total emission of high temperature air. The importance of the radiation due to N^+ and O^+ de-ionization in the wavelength region of 0.05 - 0.15 microns should be noted.

In Section II it was indicated that the shock layer for all conditions of the present experimental investtgation could be treated as being optically thin. For this to be true $\mu_\nu'\delta$ must be small compared to unity. That the shock layer is indeed optically thin can be shown if one considers the most extreme condition of the present investigation -- a stagnation temperature of 15,000°K and a density of $\rho/\rho_o = 10^{-1}$. From reference 6 it can be determined that μ_ν' is on the order of 10^{-2} to 10^{-1} cm^{-1}. Since δ is on the order of 10^{-1} cm., then $\mu_\nu'\delta$ is on the order of 10^{-3} to 10^{-2} and the shock layer is optically thin.

IV. THE APPLICATION OF AN ARC-DRIVEN SHOCK TUBE FACILITY TO THE STUDY OF RADIATIVE HEATING DURING RE-ENTRY

The present experimental investigation was preformed at The Ohio State University arc-driven shock tube facility.[39-41] This facility is capable of generating shock velocities in excess of 40,000 feet per second, with maximum equilibrium stagnation temperatures of more than 18,000°K being attained. Flight velocities of 60,000 feet per second and altitudes as high as 175,000 feet can be simulated.

A photograph of the shock tube and associated equipment is presented in Fig. 13. The driven tube is 4 inches in diameter (inside), about 28 feet in length, and fabricated from steel. The driver section is also 4 inches in diameter and contains a coaxial electrode assembly which is recessed in a T-arrangement. A condenser bank of 11,100 microfarads with a maximum voltage of 6000 volts (200,000 joules at full capacity) is connected in parallel through a coaxial collector ring to the electrode assembly. Triggering is accomplished through the use of an exploding wire mechanism.

With the exception of the energy addition process, the operation of an arc-driven shock tube resembles that of a conventional pressure-driven shock tube. Prior to firing, the gases in both the driver and driven chambers are at ambient room temperature. Helium is used as the driver gas while room air, which has been passed through a dry ice - acetone cold trap to remove the water vapor by condensation, is used as the test gas. After the establishment of the proper initial driver and driven tube conditions, energy stored in the capacitor bank is discharged into the driver chamber and the driver gas undergoes a constant-volume heat addition process. The diaphragm ruptures and a traveling normal shock wave is generated which propagates down the driven tube,

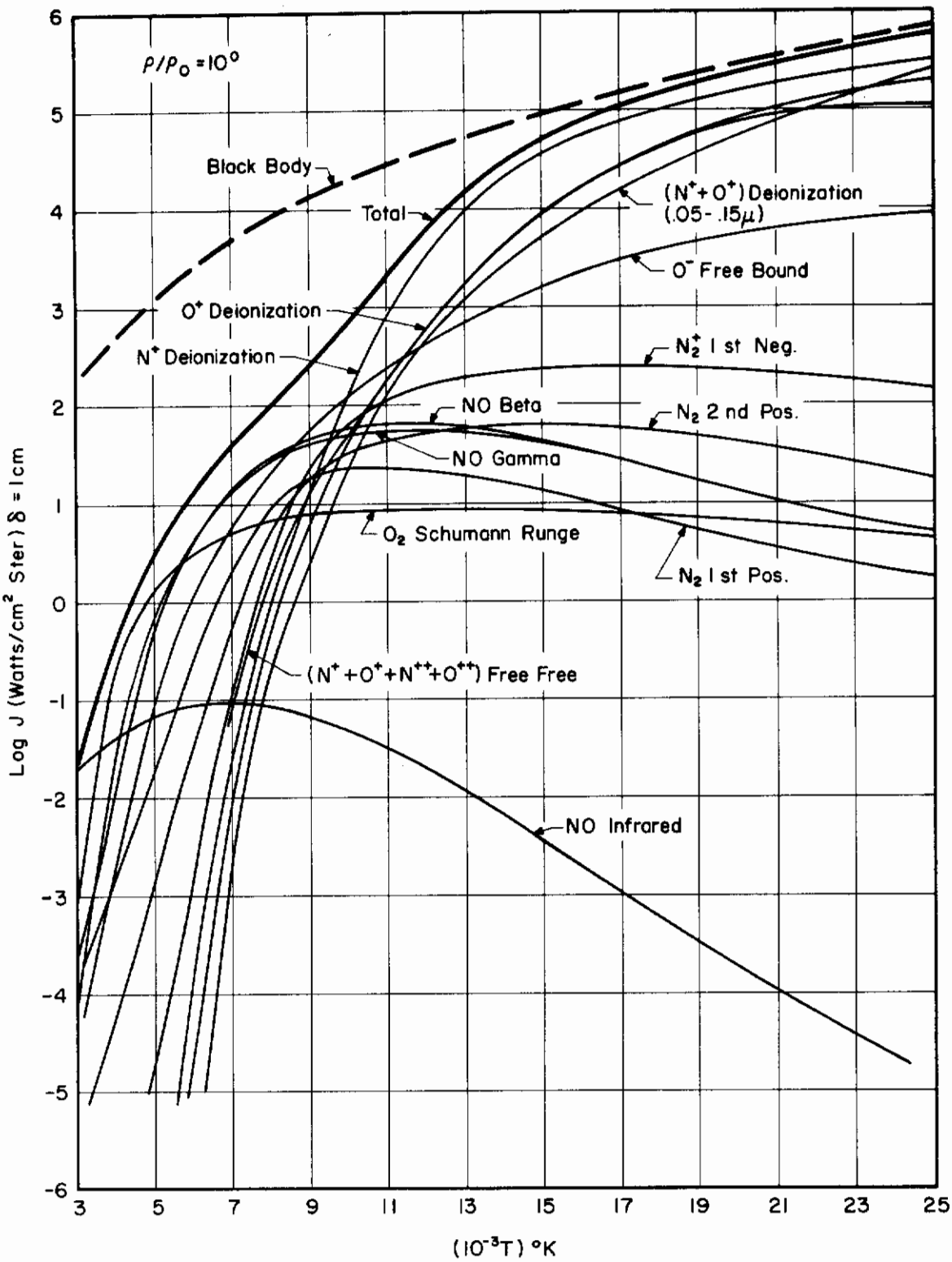

FIGURE 10. Radiance of Equilibrium Air Versus Temperature, $\rho/\rho_o = 10^o$ (Reference 19)

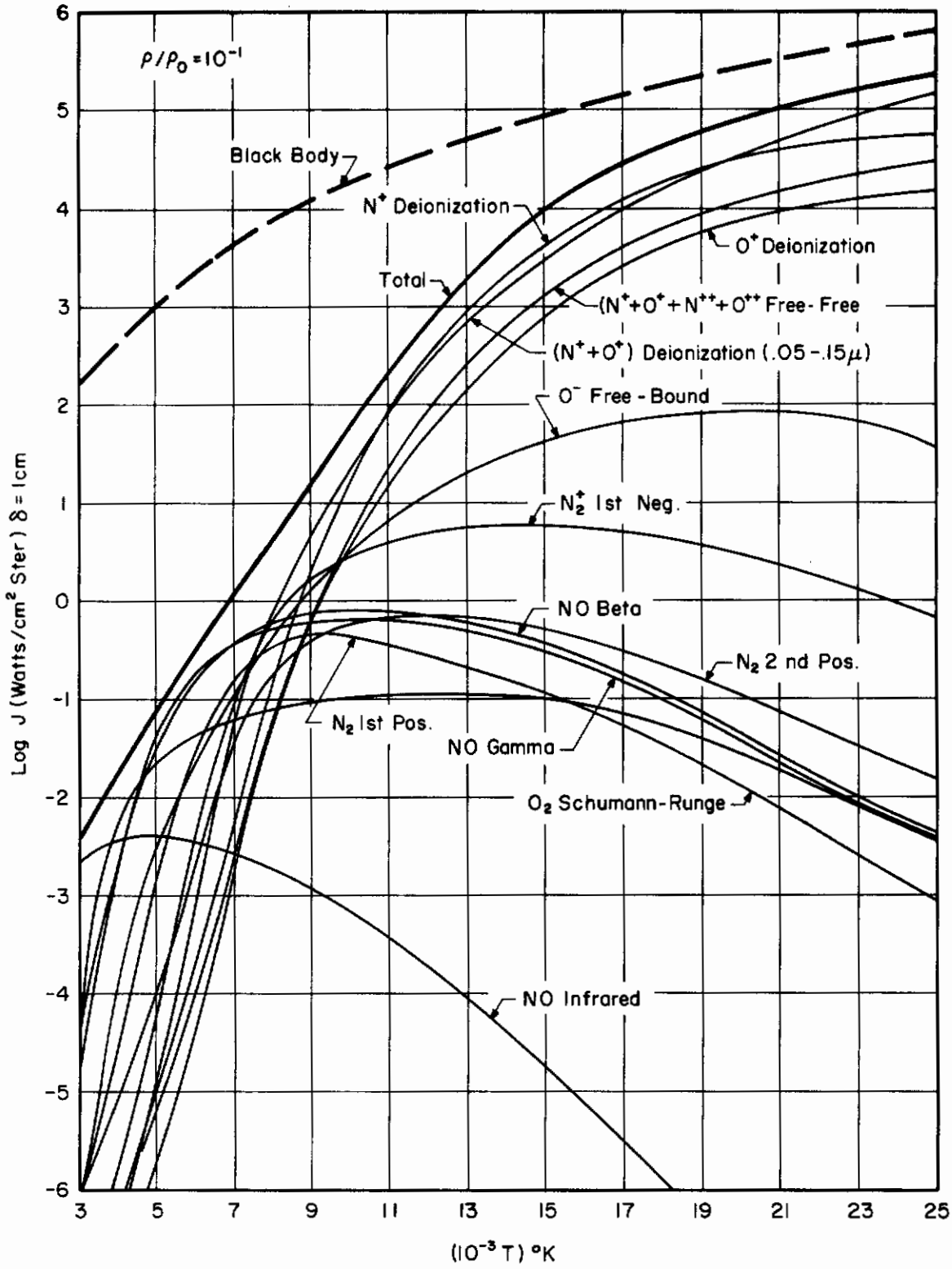

FIGURE 11. Radiance of Equilibrium Air Versus Temperature, $\rho/\rho_0 = 10^{-1}$ (Reference 19)

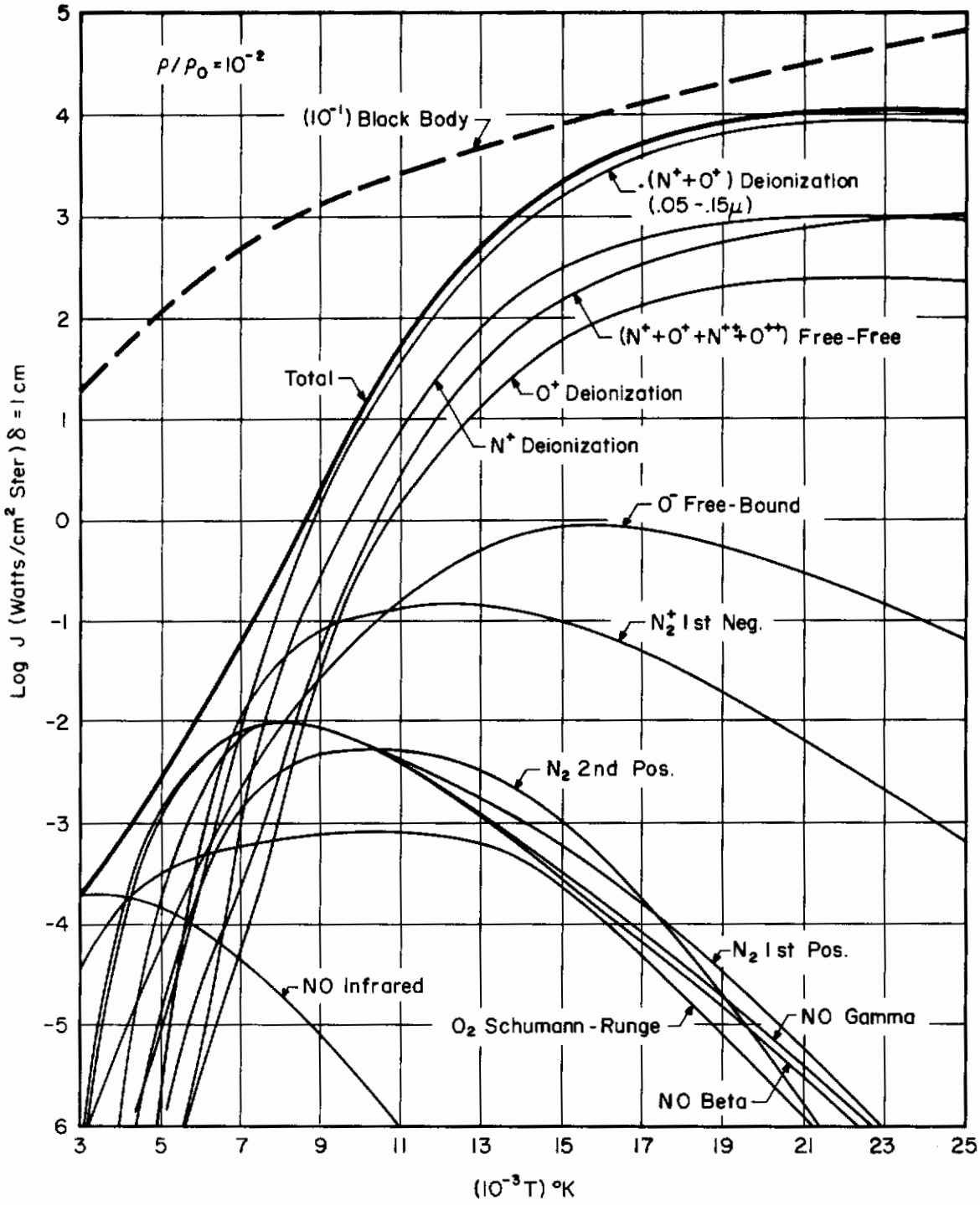

FIGURE 12. Radiance of Equilibrium Air Versus Temperature, $\rho/\rho_0 = 10^{-2}$ (Reference 19)

FIGURE 13. The Ohio State University Arc Driven Shock Tube Facility

heating and accelerating the driven tube gas as it goes. It is this shock heated and accelerated gas that serves as the test medium. A complete description of the facility and its operating characteristics is contained in references 39-41.

Measurements were performed using the shock generated flow and in the free-jet region formed where the driven tube terminates in a dump tank. Hemisphere-cylinder models, to be described in more detail in Section V, were mounted in this high enthalpy, supersonic flow as illustrated in Fig. 14, and stagnation point radiative heat transfer measurements were taken at pressures of 1.00, 0.200, and 0.060 mm Hg. The thermodynamic state of the high temperature air in the model stagnation region shock layer was determined from normal shock wave calculations for equilibrium air, as carried out by Ziemer[23] for shock tube conditions, together with measurements of the shock velocity and of the driven tube initial conditions. The shock velocity was determined using ionization probes, mounted 1 foot apart, to measure the time required for the shock wave to travel that distance. Although precursor ionization affects the performance of such probes, the use of proper probe voltages allows for accurate measurements. In this experimental program, the probe outputs were displayed on an oscilloscope. The shock velocity measurements are believed to have an accuracy of better than ± 2 per cent. The driven tube pressure was measured with a silicon fluid U-tube manometer board for pressures on the order of 1 mm Hg, and a CVC thermocouple gage for pressures of less than 500 microns. The thermocouple gage was frequently checked with a high vacuum McLeod gage as a standard. With the manometer board the accuracy of the pressure measurements is ± 2 per cent, while with the thermocouple gage the accuracy is ± 2 per cent at 60 microns and ± 5 per cent at 200 microns.

The re-entry flight conditions simulated were based on the establishment of the same stagnation region shock layer density and total enthalpy on the model as produced in flight. Since the stagnation point density and total enthalpy -- assuming the existence of chemical equilibrium in the shock layer -- depend on the shock velocity and initial driven tube conditions for a model mounted in a shock tube generated flow and on the flight velocity and atmospheric properties for a vehicle in free flight, then a particular shock tube run with known initial conditions and shock velocity may be likened to flight at a certain altitude and at a certain flight velocity. For hypervelocity shock tube flows, the flight velocity simulated, V_∞, may be related to the traveling shock velocity, V_s, through the relation

$$V_\infty = V_s\sqrt{2(1-\rho_1/\rho_2)} \quad ,$$

where ρ_2/ρ_1 is the density ratio across the traveling shock wave. The altitude simulated may be calculated using the results of Huber[24] for flight conditions and the shock tube calculations of Ziemer.[23] In the present investigation, the initial driver and driven tube conditions, together with the capacitor bank voltage, were set to deliver a pre-determined shock velocity such

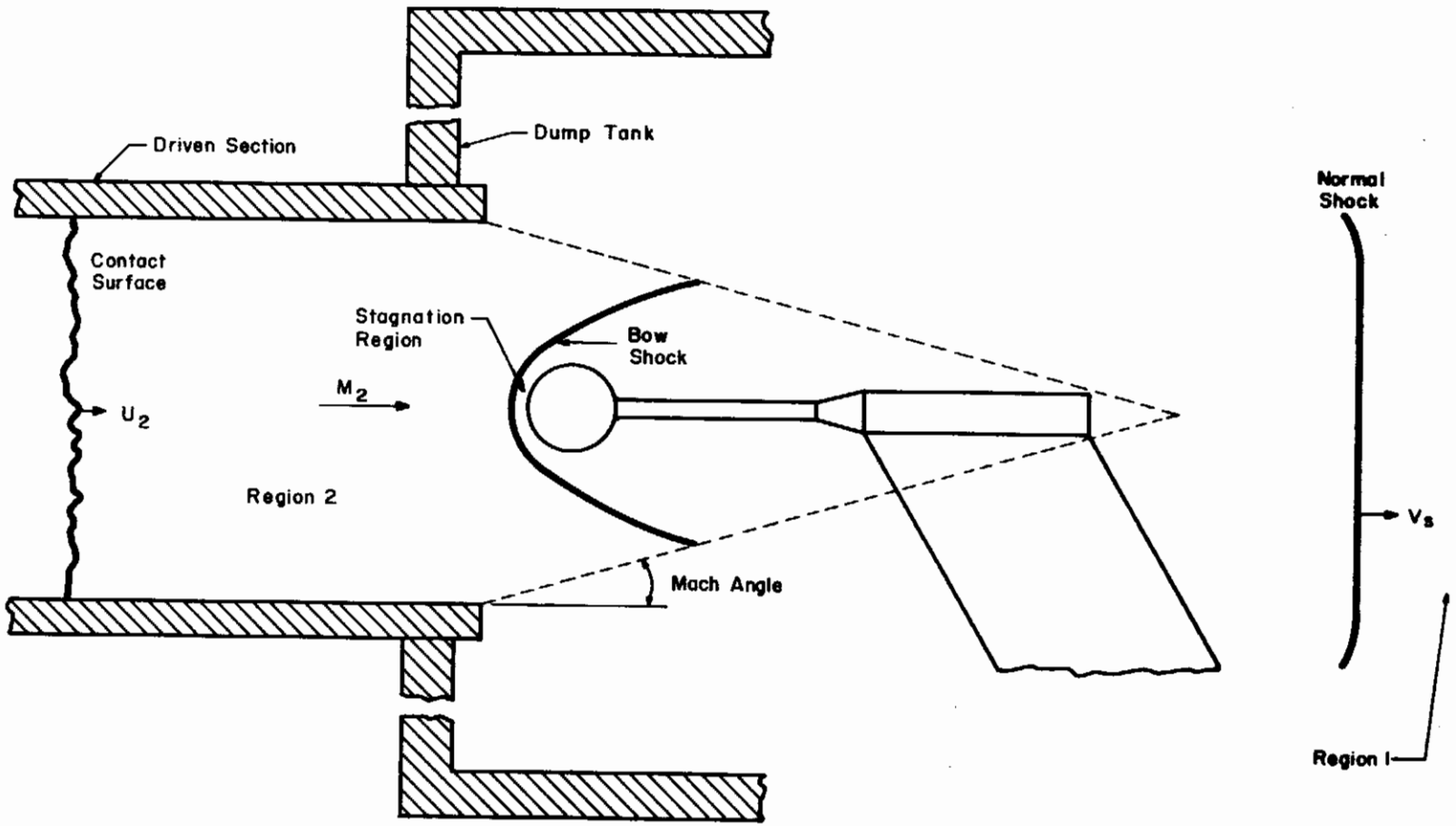

FIGURE 14. Test Region and Flow Pattern About Model

that a particular flight condition would be simulated. However, the actual flight condition simulated was based on the measured shock velocity using the above equation, and shock layer density calculations using the preset driven tube conditions and the measured shock velocity.

There are several aspects of shock tube testing that should be discussed. One of these is possible sources of contamination and their effect on the radiative emission from the high temperature air. Certainly the most common shock tube contaminant affecting the radiative intensity is CN. Although some CN is normally formed in shocked air because of the presence of traces of CO_2, excess CN can be formed because of contaminating carbon substances deposited on the tube walls which may be picked up in the shock tube wall boundary layer or may be present in the test gas due to outgassing from the wall. The presence of CN should increase the radiative intensity because of the strong band systems associated with it. This is in agreement with the results of James[42] who found that for CO_2-N_2 mixtures with less than 10 per cent CO_2, the radiative intensity increased with increasing CO_2 concentration.

In the present program, the operating procedure was to evacuate the driven tube to a pressure on the order of 5 microns or less, let in the test gas through a dry ice-acetone cold trap to remove the water vapor, and purge the tube through this same cold trap system at a pressure approximately equal to the initial pressure to be set for the subsequent test. The water vapor was removed because of its possible effect on electron density and thus on the continuum de-ionization and Bremsstrahlung radiation. Less than a minute before firing, the final driven tube conditions were established and the vacuum pump and intake valves were closed. Since the leak rate of the tube was approximately 3 microns per minute, any outgassing effects, which would show up as an effective leak rate, should be minimal.

Another source of contamination is metallic impurities in the driver gas which originate from the electrodes or from the diaphragm. This impurity emission could affect the present measurements; however, photomultiplier measurements of the time-history of radiative intensity behind the traveling normal shock indicate the driver gas to be relatively "clean" in terms of its emission rate. This is shown in Fig. 15.

Although the tube was cleaned after every test, undoubtedly some contaminants remained on the shock tube wall and were picked up in the boundary layer. Their presence should have been confined to the boundary layer, however, and thus it is felt that the test gas in the present program was a good representation of the media encountered by re-entry vehicles.

Another problem in shock tubes is ensuring sufficient test time with hypervelocity shock waves to allow the use of model-testing techniques. On passage of the traveling shock wave over a model mounted in a shock tube flow, such as illustrated in Fig. 14, a finite time on the order of 5 microseconds is required to establish a steady state flow field in the nose region of the model. Thus in order to have a minimum of 5 microseconds of steady state flow

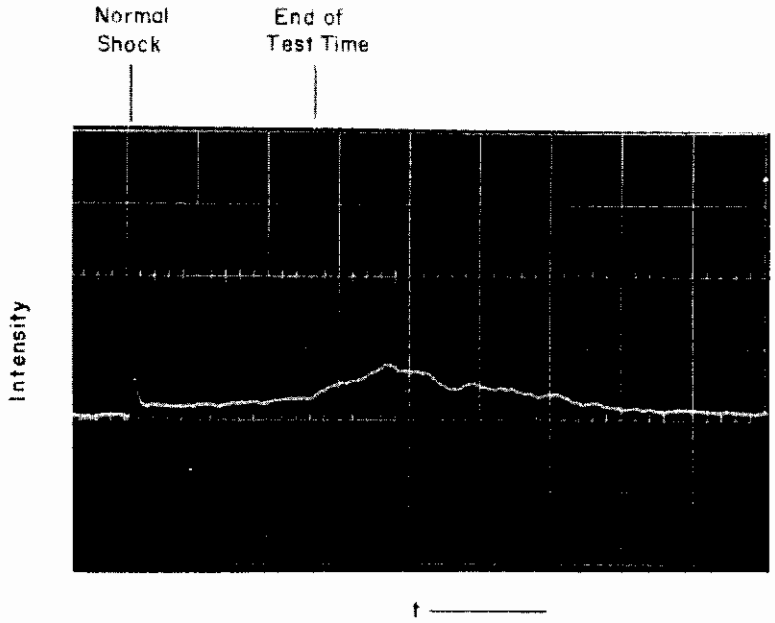

P_1 = 1.00 mm Hg V_S = 20.2 K ft/sec
Time Scale: 10 μ sec/cm

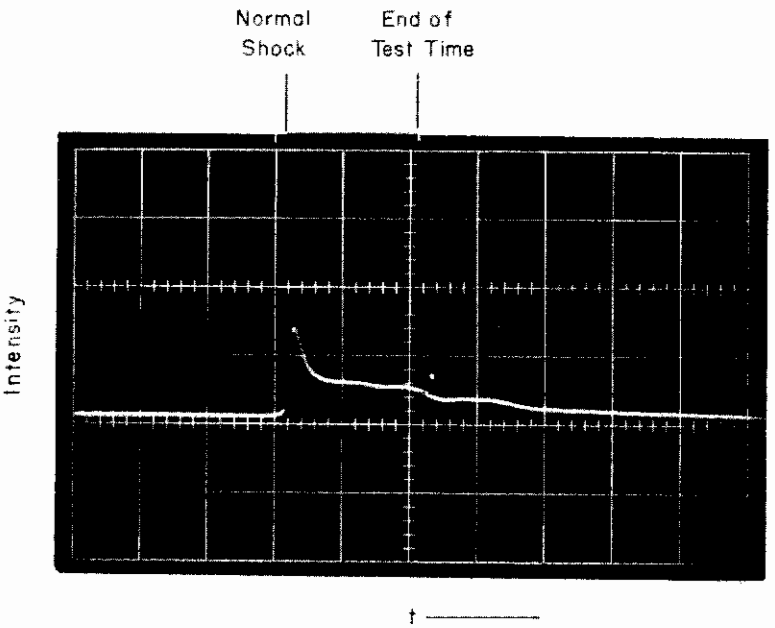

P_1 = 0.200 mm Hg V_S = 32.3 K ft/sec
Time Scale: 5 μ sec/cm

FIGURE 15. Typical Measurements of Time-History of Radiative Emission Behind Normal Shock

for testing, a total test time, as measured from passage of the incident shock, of 10 microseconds must be available. The test duration available in The Ohio State University facility has recently been the subject of an extensive investigation, in which optical, microwave, and radiation monitoring techniques were used to determine the uniformity of the flow. These results have previously been reported,[43] and, based on these results, a test time of at least 10 microseconds was expected at all test conditions. To ensure this, the time-history of the radiative intensity behind the traveling normal shock was monitored during all tests using a 1P22 photomultiplier looking across the flow through a collimated slit system. Typical traces which have obtained in this manner are shown in Fig. 15. These radiative intensity traces were used to separate out "good" shots, with sufficient test time and flow uniformity, from "bad" shots where the test conditions were not adequate. All of the data included here were thus taken with a minimum test time of 10 microseconds.

It should be noted that in monitoring the time-history of the radiative intensity, a measure of the flow uniformity was also obtained since the radiation of high temperature air is extremely sensitive to temperature changes.

In deriving the relation for the stagnation point equilibrium radiative heat transfer rate, Eq. (13), it was assumed that the shock layer was a uniform layer of constant thickness. In order to apply this equation to the conditions of the present measurements, it is necessary that the following be known: (1) the shock detachment distance, δ, for a shock tube generated flow; (2) the equilibrium properties of the shock layer; and (3) the extent of the non-equilibrium region behind the model bow shock and of the non-equilibrium radiative heating. Calculations of the equilibrium shock layer properties have already been discussed, and the determination of the shock detachment distance and possible non-equilibrium effects will now be considered.

Reference 44 contains the results of an extensive study of shock detachment distances and shock shapes on spherically blunted bodies in shock tube generated flows. The shock detachment distance for this case is shown to be a function of only the total enthalpy of the flow. The empirical curve correlating the data of reference 44, as presented in Fig. 16, has been used for the reduction of data contained herein and for theoretical calculations in support of the investigation.

A determination of the extent of non-equilibrium phenomena and the non-equilibrium radiative emission associated with the model bow shock is not so easily carried out. It is evident that such phenomena in this case will not be the same as in the free flight case. There the gas ahead of the shock is an undissociated, un-ionized gas possessing only translational and rotational energy; while in the shock tube case, the gas in front of the model bow shock will be vibrationally excited and highly dissociated for strong shock waves. Because of the weaker bow shock in the shock case, the maximum overshoot temperature will be much less in this case than in the free flight case. Figure 17 shows this in a comparison of the maximum overshoot temperature in these two cases for identical equilibrium conditions behind the shock. The free

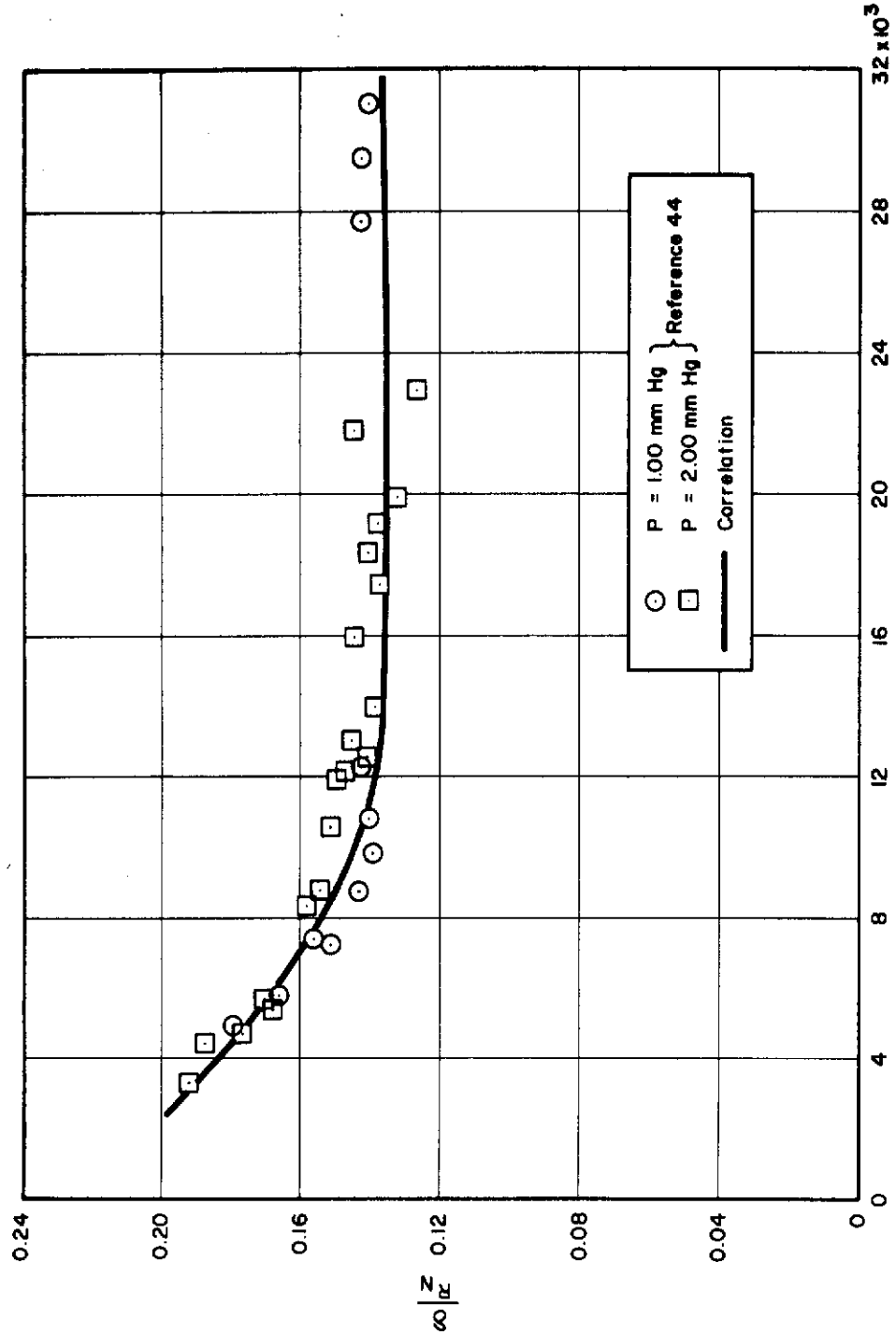

FIGURE 16. Shock Detachment Distance on Spherical Nosed Model in Shock Tube Generated Flow (Reference 44)

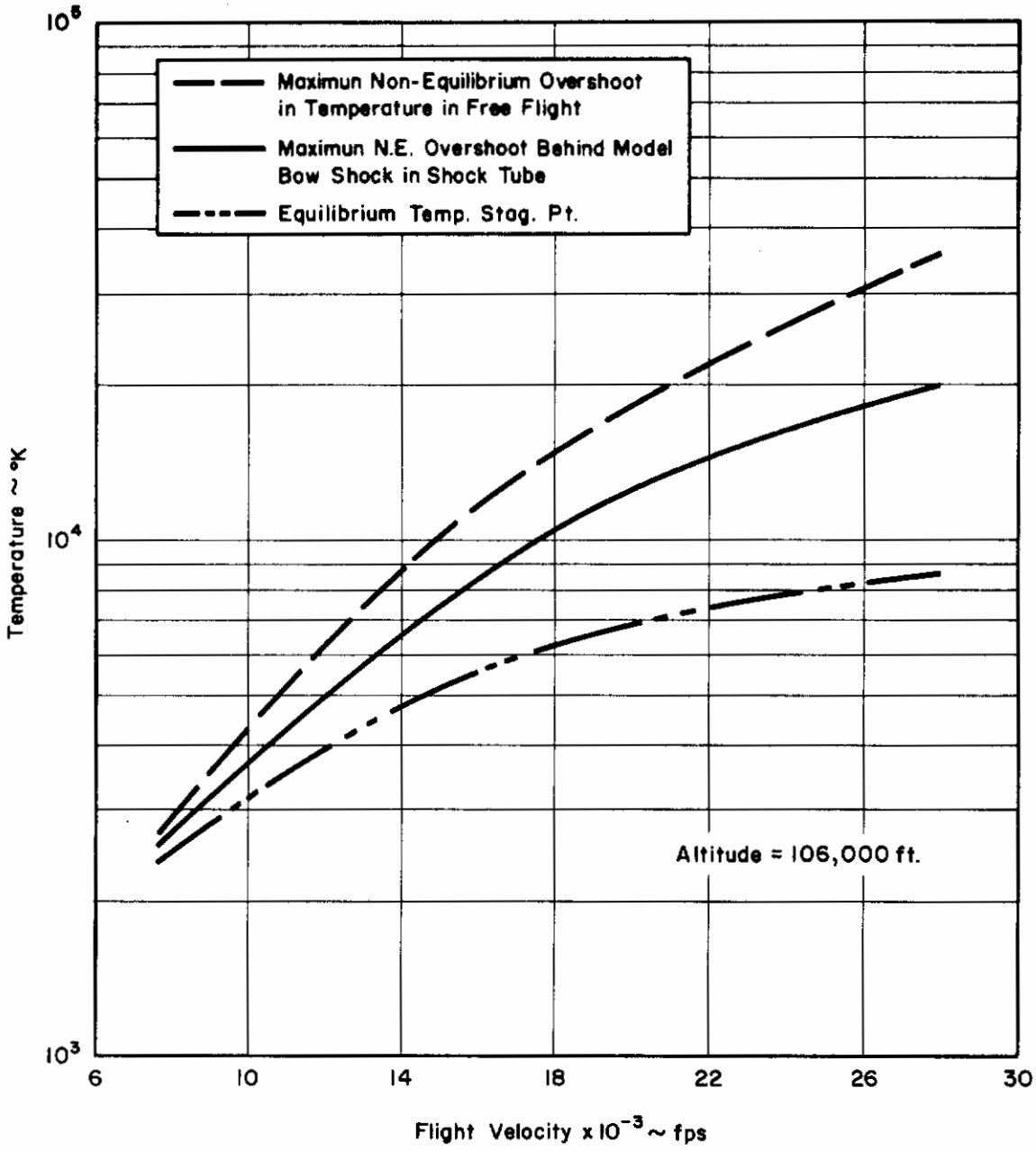

FIGURE 17. Non-Equilibrium Temperature Behind Normal Shock

flight temperature was obtained by using Eq. (1); the shock tube temperature was obtained assuming equilibrium conditions in front of the standing shock and a frozen composition and vibrational energy excitation on passage through the shock.

Figure 18 shows the relaxation distance behind a standing bow shock in a shock tube flow as calculated by Rose and Stankevics.[45] Also included in this figure is an estimate of a lower limit on the relaxation distance, which is based on initial results from a study of reflected shock phenomena. In this investigation, the models used had shock detachment distances on the order of 0.1 inch. For this shock detachment distance, and taking into account the exponential approach of the shocked gas to the equilibrium state, it can be seen from Fig. 18 that for an initial driven tube pressure of 1 mm Hg the shock layer should be in almost complete equilibrium; while at 0.200 mm Hg the shock layer will be in a near equilibrium state. At 0.060 mm Hg, the shock layer will be in a non-equilibrium state.

Based on the existing knowledge of non-equilibrium phenomena behind shock waves,[17,18] it would appear that any non-equilibrium effect should evidence itself as an increase in radiative heating due to the overshoot in radiative intensity (see Fig. 1). Because of the lower temperatures in the relaxation region for the shock tube case, as compared with the free flight case with the same equilibrium conditions, the importance of non-equilibrium radiative heating would be expected to be less for the conditions of this investigation than in the flight case being simulated.

It should be noted that the results of measurements currently being performed at Ohio State on non-equilibirum phenomena behind reflected shock waves in shock tube generated flows, indicate (1) that the integrated non-equilibrium intensity associated with a reflected shock wave is much less than that with the bow shock of a vehicle in free flight for the same equilibrium conditions behind the shock waves, and (2) that the relaxation rate behind a reflected shock may be slightly faster than that used by Rose and Stankevics[45] for their calculations shown in Fig. 18. Since the phenomenon associated with a reflected shock is quite similar to that for a standing bow shock in a shock tube flow, the above conclusion regarding the relative effect of non-equilibrium radiative heating, under the present conditions as compared to the free flight case, is borne out.

Non-equilibrium radiative heating becomes more important compared with equilibrium radiative heating as altitude is increased. Thus for the present measurements, non-equilibrium effects should be the most important at the lowest initial driven tube pressure -- in this case, 0.060 mm Hg. This corresponds to a simulated altitude of 170,000 feet. The flight velocities simulated at this condition range from 36,000 to 44,000 feet per second. For a vehicle in free flight, with the same nose radius as the present model used at this condition, the percentage of the total radiative emission arising due to the non-equilibrium overshoot is 50 per cent at a velocity of 36,000 feet per second and 6 per cent at a velocity of 44,000 feet per second. Since the

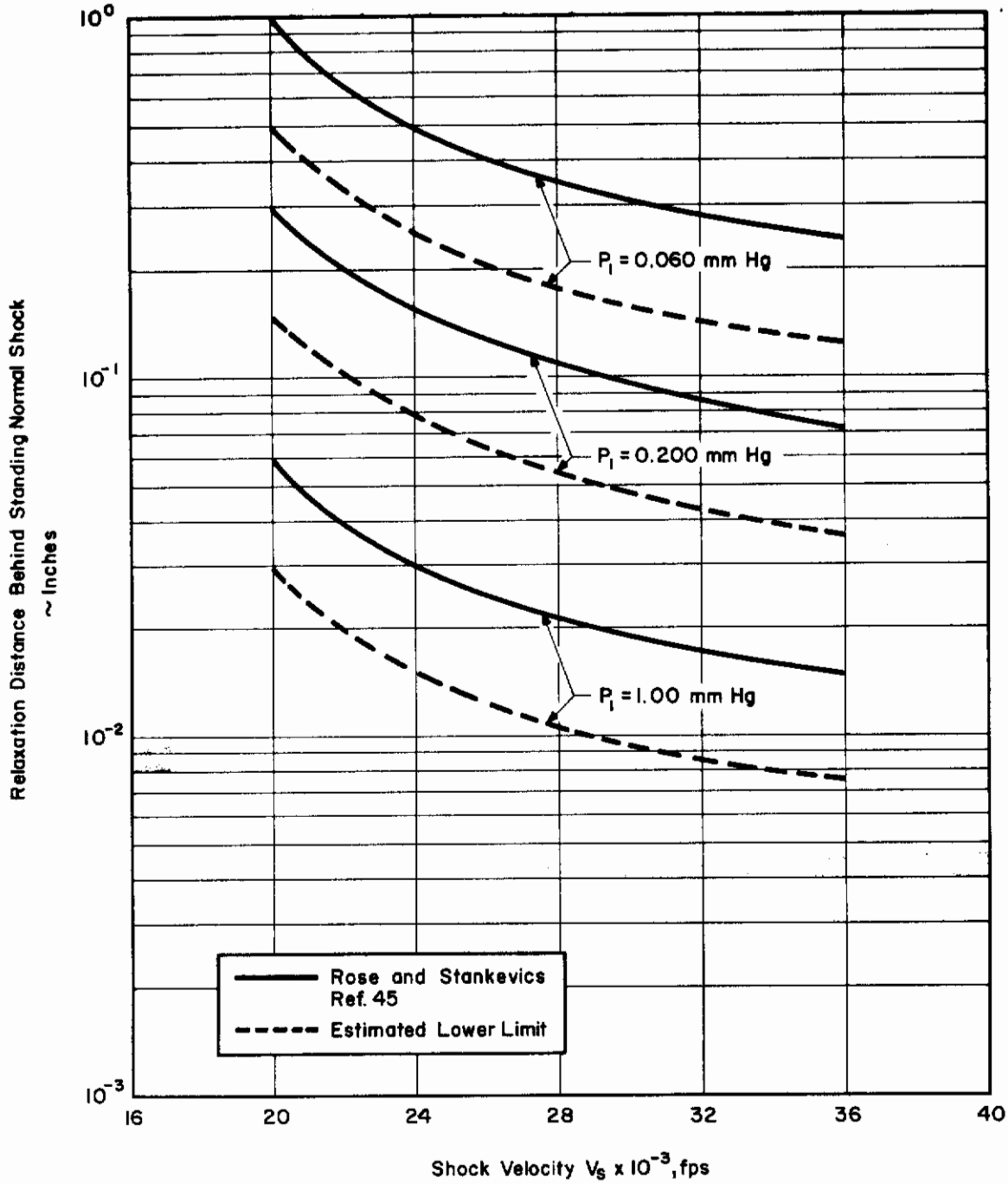

FIGURE 18. Relaxation Distance Behind Standing Normal Shock in Shock Tube Flow

non-equilibrium effect is considerably less in the present shock tube case as compared to the flight case, then any non-equilibrium effect has been neglected in the analysis of the data. However, it should be remembered that for the data taken at an initial driven tube pressure of 60 microns, the composition does not correspond completely with the equilibrium one, and that increased heating may be present.

One final consideration in the use of shock tube generated flows for measurements such as those performed here is the possible effect on the measured heat transfer rates of radiation from the high temperature air residing in front of the model bow shock layer. Calculations of the ratio of shock layer emitted radiation to this background radiation have been carried out as follows. The shock layer emitted radiation was calculated using the formula

$$\dot{q}_{\text{shock layer}} = \epsilon_t' \delta \sigma T_t^4 \quad , \qquad (15)$$

where ϵ_t' is the effective emissivity per unit length in the shock layer and δ is the shock detachment distance. The background radiation was expressed as[46]

$$\dot{q}_{\text{background}} = \epsilon_2' L_e \sigma T_2^4 \quad , \qquad (16)$$

where ϵ_2' is the effective emissivity per unit length of the normally shocked gas and L_e is the effective radius of the cylindrically shaped gas slug which emits the background radiation. For a circular cylinder of infinite height and diameter d, the effective radius is $L_e = 0.9d$, where d in this case is the shock tube diameter.

Results have been obtained for a tube diameter of 4 inches, a shock detachment distance of 0.1 inch, gas properties from reference 23, and emissivities from Kivel and Bailey.[7] For example, for a shock wave traveling at a Mach number of 24 into air at an initial driven tube pressure of 1 mm Hg, the following properties exist:

$T_2 = 7500^\circ K$	$T_t = 13100^\circ K$
$\rho_2/\rho_o = 2.1 \times 10^{-2}$	$\rho_t/\rho_o = 1.55 \times 10^{-1}$
$\epsilon_2' = 10^{-3.7}$ cm^{-1}	$\epsilon_t' = 10^{-0.9}$ cm^{-1}
$L_e = 9.15$ cm	$\delta = 0.254$ cm

For these conditions the ratio of shock layer radiation to background radiation is 163. Calculations for other shock tube conditions are presented in Table 2. It can be seen that for all these conditions the background radiation can be neglected.

TABLE 2

ESTIMATED EFFECTS OF BACKGROUND RADIATION

Shock detachment distance = 0.1 inch
Shock tube diameter = 4 inches

M_s	P_1 mm Hg	Shock layer radiation / background radiation
18	1	12.6
18	0.1	9.45
24	1	163
24	0.1	363
30	0.1	68.5

V. THE DEVELOPMENT OF A THIN FILM RADIATIVE HEAT TRANSFER GAGE

In order to measure experimentally the stagnation point radiative heat flux in a shock tube generated flow, standard thin film resistance thermometer heat transfer measurement techniques have been applied. These techniques have been chosen because their use in convective heating measurements in impulse devices, such as shock tubes, is well understood and quite extensively documented in the literature.[47,48]

A thin film gage, in essence, consists of a thin layer of metal (the sensing element) mounted on an insulator backing. The metal sensor acts as a resistive element in a dc-powered constant current circuit. When the sensing element is exposed to a heat flux, its resistance changes as its temperature increases. This changes the voltage drop across the element which can be measured. In this manner, a measurement of the surface temperature can be obtained; this can be related to the heat transfer rate when the insulator acts as a semi-infinite slab.

The performance of a thin film heat transfer gage may be analyzed as follows. Consider a semi-infinite slab of an insulating material on which is mounted a thin film of metal, illustrated in Fig. 19. Incident on the thin film surface is a transient heat flux, $\dot{q}(t)$ which is applied at time $t = 0$. When the thermal effects of the thin film can be ignored, and assuming the thermal properties in the insulating material are constant, the general solution relating the surface temperature and the applied heat flux is[47]

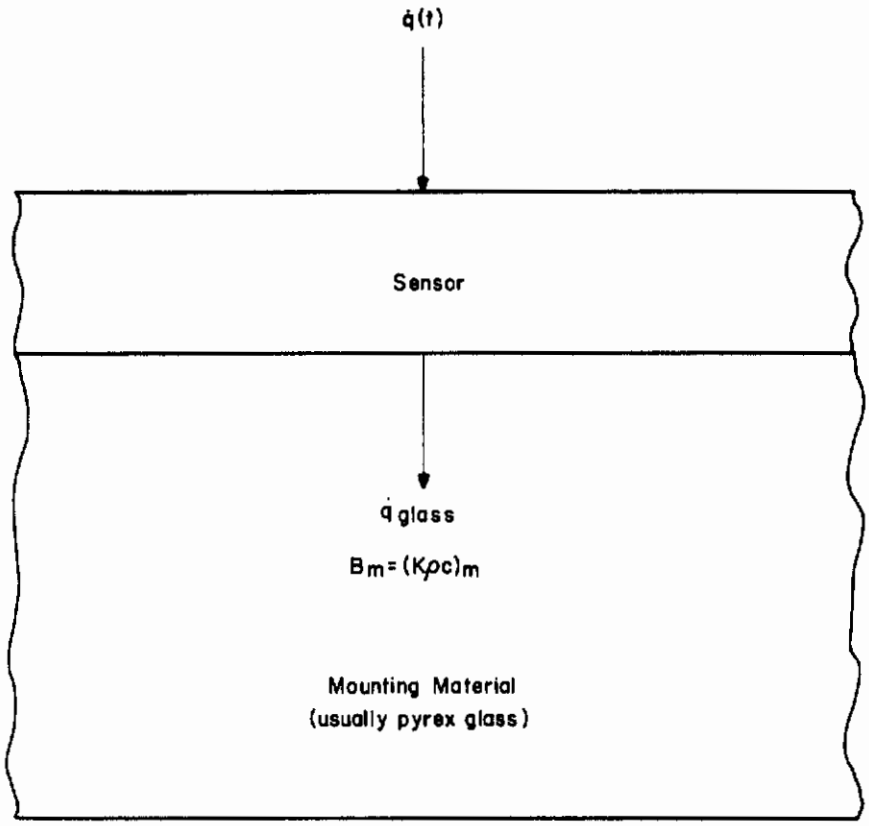

FIGURE 19. Model Used for Analysis of Thin Film Gage Performance

$$T(t) = \frac{1}{\sqrt{\pi\beta_m}} \int_0^t \frac{\dot{q}(\tau)}{\sqrt{t - \tau}} d\tau \qquad (17)$$

or

$$\dot{q}(t) = \sqrt{\frac{\beta_m}{\pi}} \frac{\partial}{\partial t} \left\{ \int_0^t \frac{T(\tau)}{\sqrt{t - \tau}} d\tau \right\} . \qquad (18)$$

Here β_m is a property of the insulating material and may be expressed as $\beta_m = (K\rho c)_m$ where K, ρ, and c are, respectively, the thermal conductivity, density, and heat capacity of the mounting material. T is the increment of temperature above the initial temperature at t = 0. If it is further specified that the applied heat flux is invariant with time, that is, a step-function heat pulse is applied, then from the above equations it can be shown that

$$\dot{q}(t) = \frac{1}{2}\sqrt{\pi\beta_m} \frac{T(t)}{\sqrt{t}} . \qquad (19)$$

Thus for the case of a constant heat flux, the heat transfer rate to a thin film gage may be readily calculated using Eq. (19) by determining the surface temperature time history through a measurement of the thin film resistance.

In applying this technique to the measurement of integrated radiative fluxes, it is desirable that the thin film sensing element have a relatively high absorptivity which is approximately independent of the wavelength of the incident radiation. Platinum, which is the material normally used in thin film resistance thermometer gages for convective heating measurements, has a high reflectivity which varies considerably over the wavelength region of interest ($0.2 < \lambda < 2.0$ microns). It was therefore desirable for the present investigation to consider other materials which might possibly be applicable.

Of the materials investigated, two were considered promising. Thin film radiative heat transfer gages have been constructed using both these materials. These two materials are Hanovia Luster Black No. 4771 and Hanovia Bright Gold EF No. 31-A. Both of these materials are manufactured by Hanovia Liquid Gold Division, Engelhard Industries, 1 West Central Avenue, East Newark, New Jersey, and obtained as liquid metal suspensions. They may be applied as thin films on glass or ceramics by brushing them on, followed by firing in a ventilated oven at a temperature of approximately 700°F for 5 minutes and at 1250°F for 15 minutes. At the lower temperature, the liquid solvent is evaporated; at the higher temperature the glass softens and the thin film bonds with the glass. Specific details regarding the application of these materials to glass surfaces

may be found in references 49 and 50. The spectral radiation characteristics of these two materials are shown in Figs. 20 and 21 in terms of the wavelength dependence of their transmissivity and reflectivity. It can be seen that the use of Bright Gold EF No. 31-A would allow measurement of only the radiation below a wavelength of 5500 Å, and that in this region below 5500 Å, approximately 75-80 per cent of the incident radiation would be absorbed. On the other hand, the use of Luster Black No. 4771 would allow the measurement of incident radiation over a much wider wavelength region. Below a wavelength of one micron, approximately 80-85 per cent of the incident radiation would be absorbed; however, in the infrared region above one micron a considerable portion of the incident radiation would be transmitted. Based on surface characteristics, the Luster Black appeared to be the superior material.

Because of development problems encountered initially with the Luster Black material, a few radiative measurements, which were carried out in the early stages of the present investigation, were obtained using a thin film gage with the Bright Gold EF No. 31-A as the sensing element. The Luster Black thin films were, for all practical purposes, non-conducting and thus could not be used as the resistive element of an electrical circuit. In order to circumvent this problem, a thin film radiative heat transfer gage has been built in which the thin film sensing element actually consists of two layers -- the top layer, which is exposed to the incident radiation, is Luster Black; the bottom layer is Hanovia Bright Platinum No. 05-X which is an electrically conducting material also obtained as a liquid metal suspension. This gage, illustrated in Fig. 22, is constructed by first brushing a thin film of Bright Platinum No. 05-X on a pyrex ball and firing the ball in an oven as previously described. A thin film of Luster Black No. 4771 is then brushed on and the gage is again fired in an oven. Finally electric leads are soldered on and the pyrex ball is mounted to the model with epoxy cement. Virtually all of the measurements taken as part of this program were obtained by using this double layer thin film gage. Because of the low transmissivity of the Bright Platinum No. 05-X, this double layer gage has a high absorptivity even in the infrared wavelength region.

It should be noted that the exact spectral characteristics of thin films depend on the thickness and uniformity of the film, and therefore will vary from gage to gage. However, such variations will have a small effect on the absorptivity of the gages used here. For example, since the reflectivity of the Luster Black double-layer gage is approximately 20 per cent and its transmissivity is negligible in the wavelength region of interest, then an obviously extreme deviation of 50 per cent in the reflectivity of the gage from that shown in Fig. 21 will result in a change in the absorptivity from 80 per cent to 70 per cent. This is only a 12 per cent change in the absorptivity. Investigators at the Cornell Aeronautical Laboratory, in measuring the spectral characteristics of thin films made from Hanovia liquid preparations, have noted deviations of up to 25 per cent between the measured values and those in reference 49.[51] Such a deviation for the gages used here would produce only a 6 per cent change in the absorptivity, thus small variations in gage properties have been neglected. It should further be noted that three different Luster

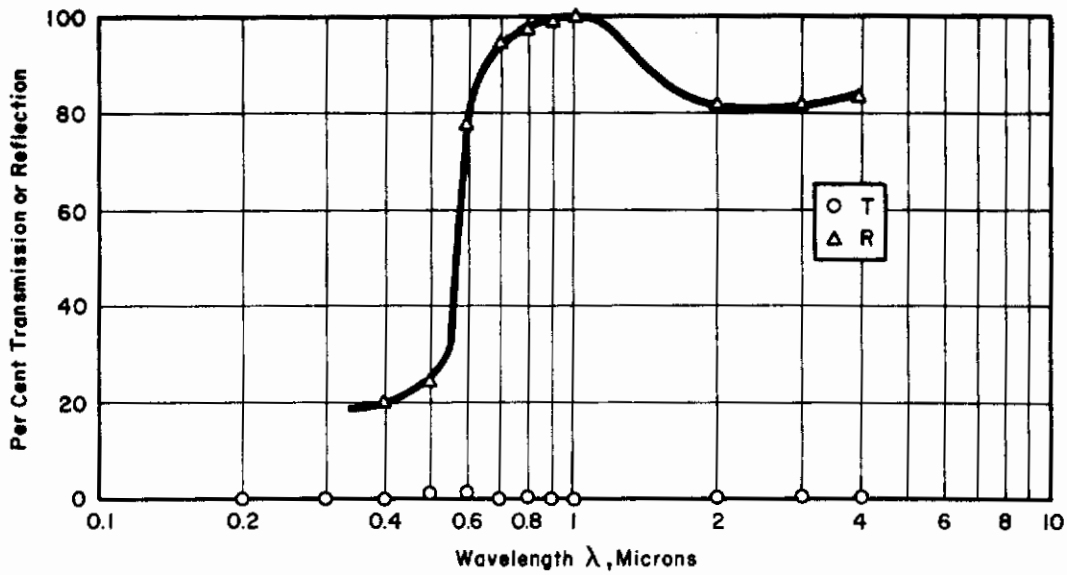

FIGURE 20. Transmission and Reflection Characteristics of Bright Gold EF No. 31-A (Reference 49)

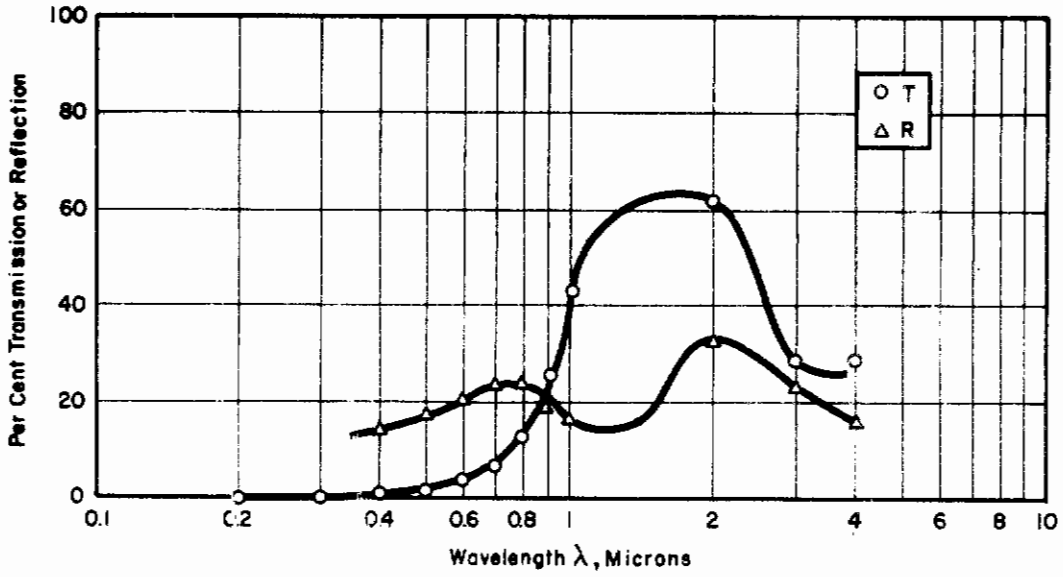

FIGURE 21. Transmission and Reflection Characteristics of Luster Black No. 4771 (Reference 49)

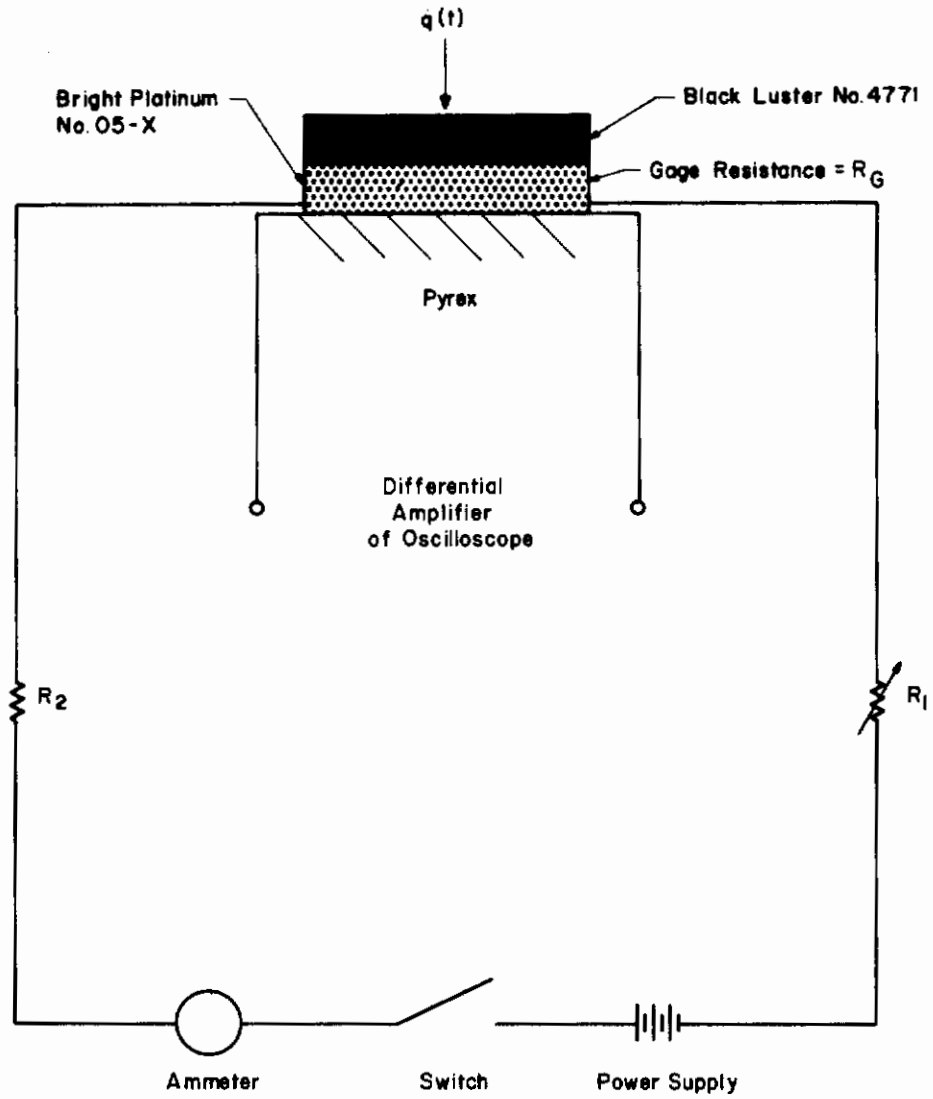

Power Supply	0-16 Volts
R_1	700 ohms
R_2	700 ohms
R_G	$\simeq$ 100 ohms
ΔR_G	< 10 ohms

FIGURE 22. Schematic of Thin Film Gage and Electrical Circuit

Black gages were used during the course of this investigation under all types of varying conditions, and any difference due to small variations in spectral characteristics alone are indiscernible compared with the normal data scatter.

In order to sense only radiative fluxes with this gage, it was necessary to shield the gage from convective heating inputs. Thus, hemisphere-cylinder models, such as shown in Figs. 23 and 24, were built for stagnation point radiative heat transfer measurements. Each of these models has a sapphire window, 0.25 inch in diameter and 0.020 inch thick, mounted at the stagnation point. The radiative heat transfer gage is mounted on a pyrex ball and positioned behind the sapphire window. The sides of the hole leading through the model to the gage is blackened with Luster Black. The electrical circuit (shown in Figure 22), of which this gage is a part, is designed to measure the time history of the voltage drop across the gage, ΔE. A similar circuit is discussed in more detail in reference 5. The heat transfer rate may be expressed in terms of ΔE and the time length of exposure to the heat flux, t, through the relation

$$\dot{q} = \frac{1}{2}\sqrt{\pi\beta_m}\,\frac{1}{\alpha I R_o}\,\frac{\Delta E}{\sqrt{t}} \quad , \qquad (20)$$

where $\alpha R_o = \Delta R/\Delta T$ is a property of the sensing element and assumed to be constant, and I is the gage current which is kept constant during each test. Equation (20) follows directly from Eq. (19).

For the measurements to be presented here, the value[52] of $\sqrt{\beta_m}$ was taken to be constant at 0.0743 $BTU/ft^2 sec^{1/2} {}^oF$. A correction for variable backing material thermal properties was applied using the results of reference 53. αR_o was determined from static calibrations of each gage in the laboratory. These calibrations were carried out in an oven using a thermocouple to measure the oven temperature and a Wheatstone bridge to measure the gage resistance. A typical calibration is shown in Fig. 25 where the different symbols correspond to different calibration suns.

These thin film radiative heat transfer gages were also checked dynamically through the use of a Xenon flash lamp to provide a pulse of radiation. These pulses, as determined with a 1P22 photomultiplier, had a rise time of 4 microseconds and the heat flux remained relatively constant for 20-25 microseconds. Thus the time scale for these test was on the order of that in the shock tube experiments. The purpose of these dynamic tests was to provide (1) a check on the linearity of the gage, (2) an indication of any possible effects due to a non-negligible thermal capacity of the thin sensing element, and (3) an overall check on the operational characteristics of the gage. Figure 26 shows a comparison of the variation in the Xenon flash lamp produced radiation pulse as measured with both a photomultiplier and the thin film radiative heat transfer gage; it can be seen that there is reasonable agreement. Figure 27 shows the variation of the heat transfer rate, as measured by the thin film gage,

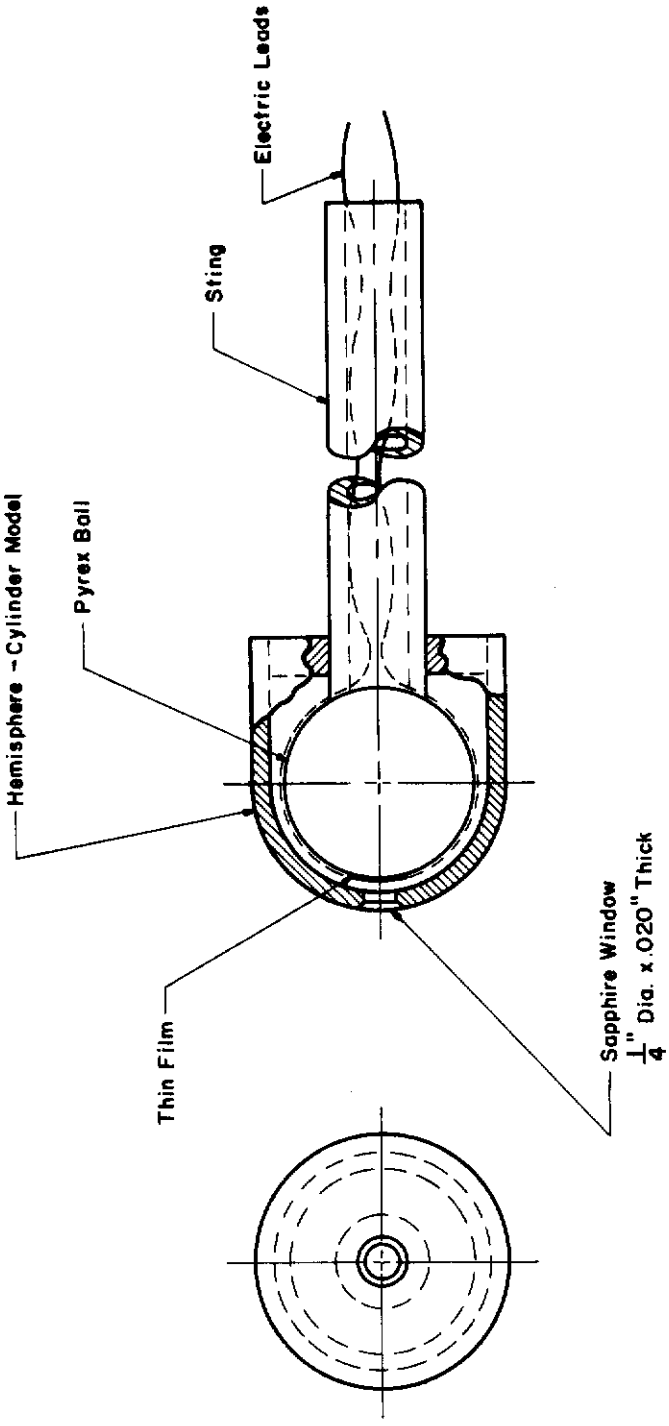

FIGURE 23. Diagram of Radiation Heat Transfer Models

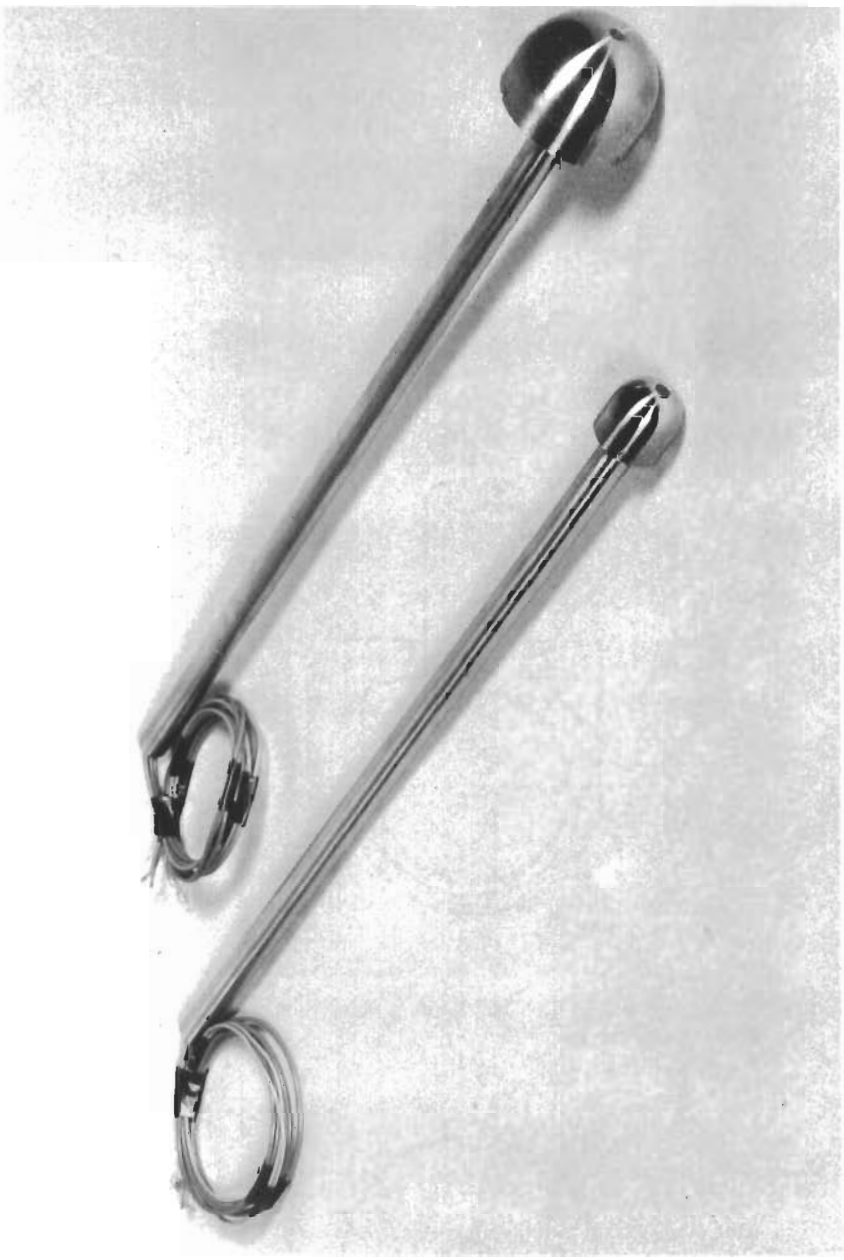

FIGURE 24. Radiation Heat Transfer Models

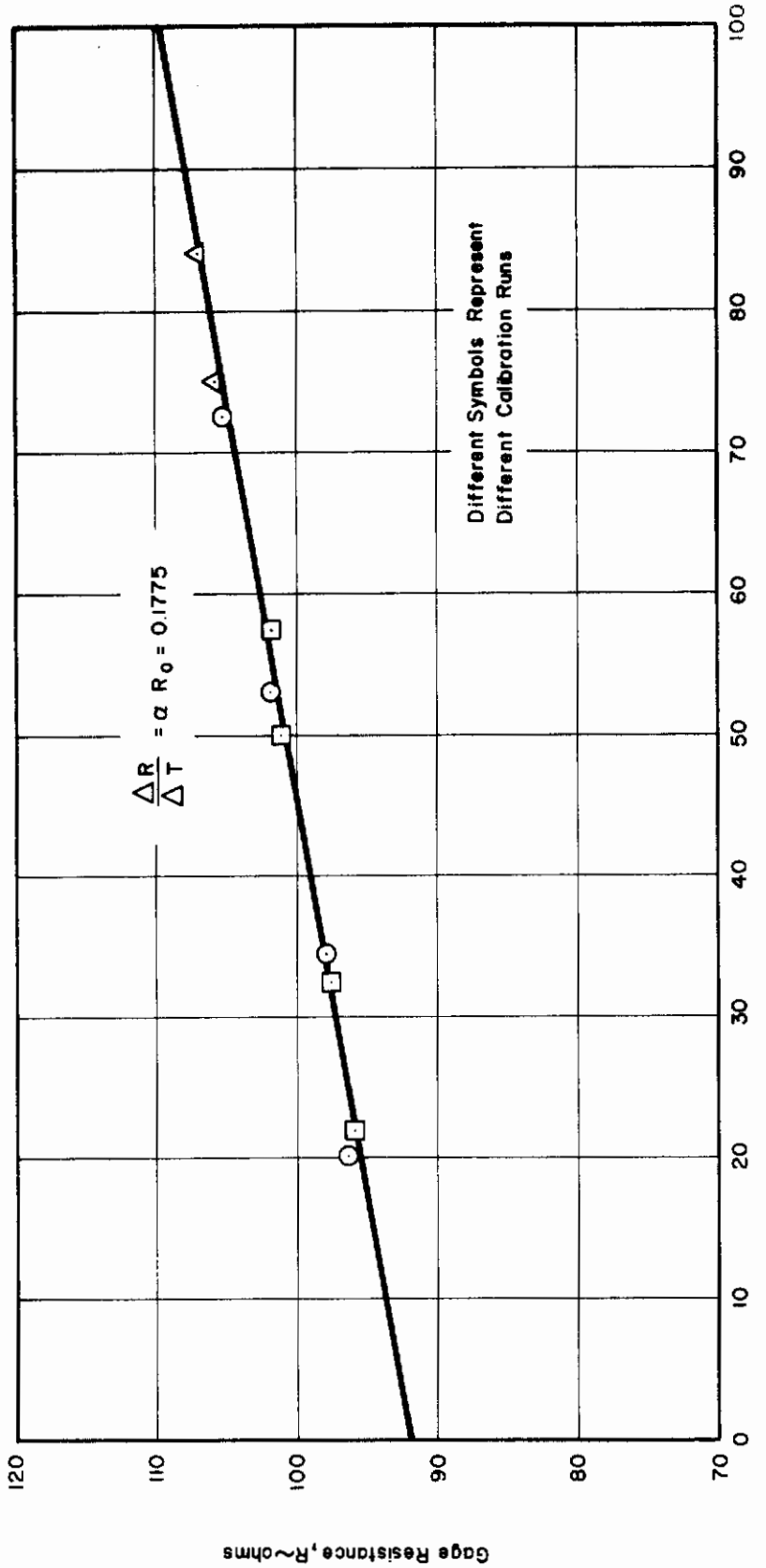

FIGURE 25. Typical Radiative Thin Film Gage Static Calibration

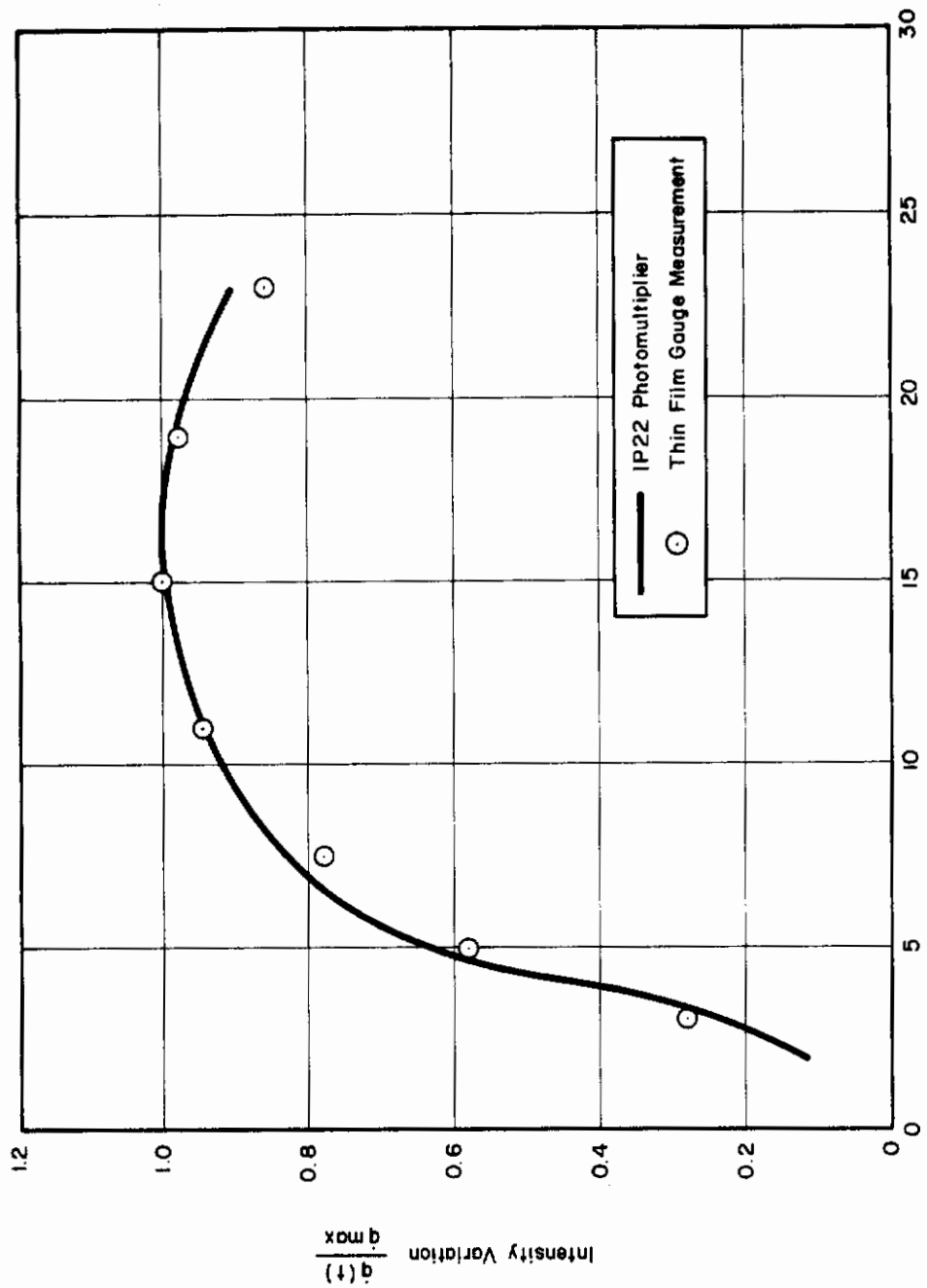

FIGURE 26. Dynamic Calibration of Thin Film Radiative Gage

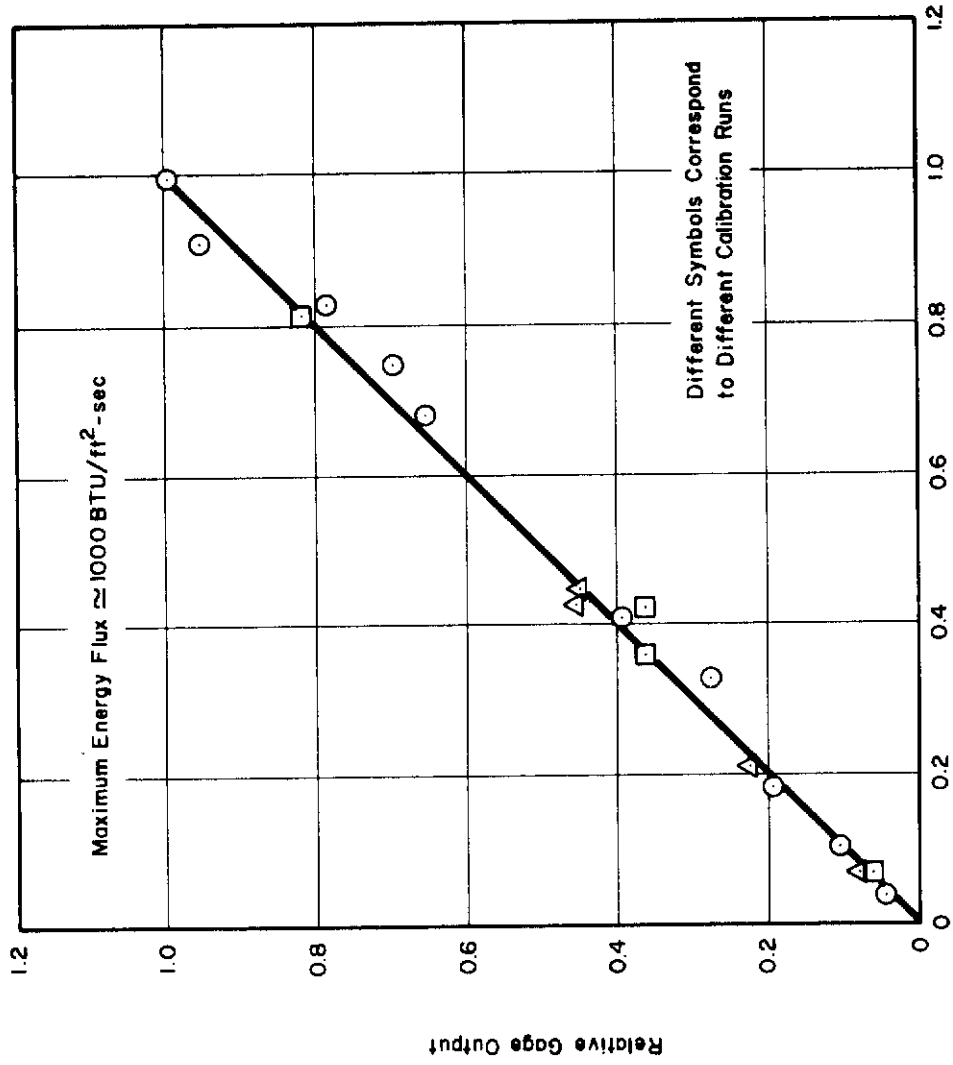

FIGURE 27. Thin Film Gage Output for Varying Energy Inputs

with varying energy inputs as determined with a photomultiplier. The maximum energy flux here was approximately 1000 BTU/ft^{2}sec, and as may be seen in Fig. 27, the response of the gage is linear.

It should be noted that in thin film resistance thermometer gages the sensing element must be thin in order to minimize any effects due to the thermal capacity. Such an effect becomes increasingly important as the heat flux exposure time, t, becomes shorter and manifests itself in an inability of the gage to follow a highly transient heat flux. For the thin film radiative heat transfer gage developed as part of this investigation it is felt that the results shown in Fig. 26 indicate clearly the ability of the gage to measure transient fluxes. Thus any effect due to the thermal capacity of the sensing element has been assumed to be negligible.

In analyzing data obtained using the hemisphere-cylinder model previously described, consideration must be given to the transmission characteristics of the sapphire window, the absorption characteristics of the surface of the thin film gage, and the geometrical view factor relating the stagnation point radiative heat transfer rate to the average heat transfer rate at the gage surface.

The transmission characteristics of sapphire are well-known and are shown in Fig. 28.[54-57] For the thickness windows used here, and in the wavelength region of interest, the spectral absorptivity[56] is less than 0.001 and absorption losses may be neglected. Thus the results shown in Fig. 28 are based on measurements of the refractive index. It can be seen from Fig. 28 that in the wavelength region of 0.25 to more than 2.0 microns the transmissivity is approximately constant at 84 per cent. The infrared cut-off occurs in the neighborhood of 6.0 microns, and the ultra-violet cut-off, as shown in Fig. 28, occurs at 1750 Å.

The surface characteristics of the thin film radiative heat transfer gage used here are shown in Figs. 20 and 21. For the Luster Black No. 4771 thin film gages, an absorptivity of 0.80 was used in the reduction of the data.

The view factor of the gage may be determined from straightforward geometrical considerations. This view factor takes into account the fact that the radiative heat transfer gage, which is located at the bottom of a cylindrical well, sees a lower heat transfer rate than the surface. In order to calculate this view factor, a flat surface with a cylindrical well and which is covered by a constant thickness layer of optically thin gas is used as a model. This model is illustrated in Fig. 29. The heat transfer rate to the top surface is given by Eq. (12). However, for a point A at the bottom of the well, the heat flux is

$$\dot{q}_{rad_{gage}} = \int_0^\infty d\nu \int_0^{2\pi} d\phi \int_0^{\theta_1} B_\nu \mu_\nu' \, \delta \sin\theta \, d\theta \quad , \qquad (21)$$

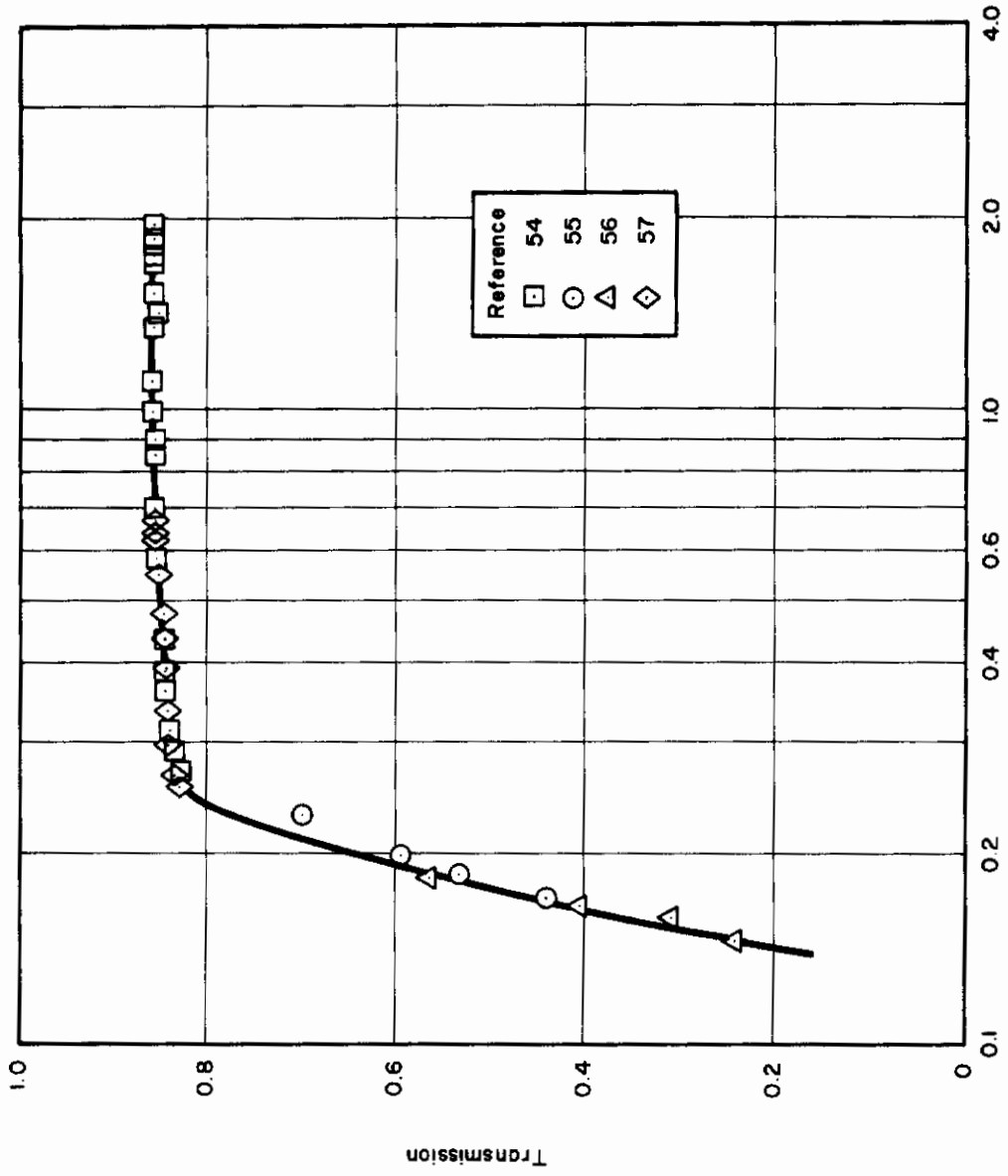

FIGURE 28. Transmission of Sapphire Windows with Negligible Absorption

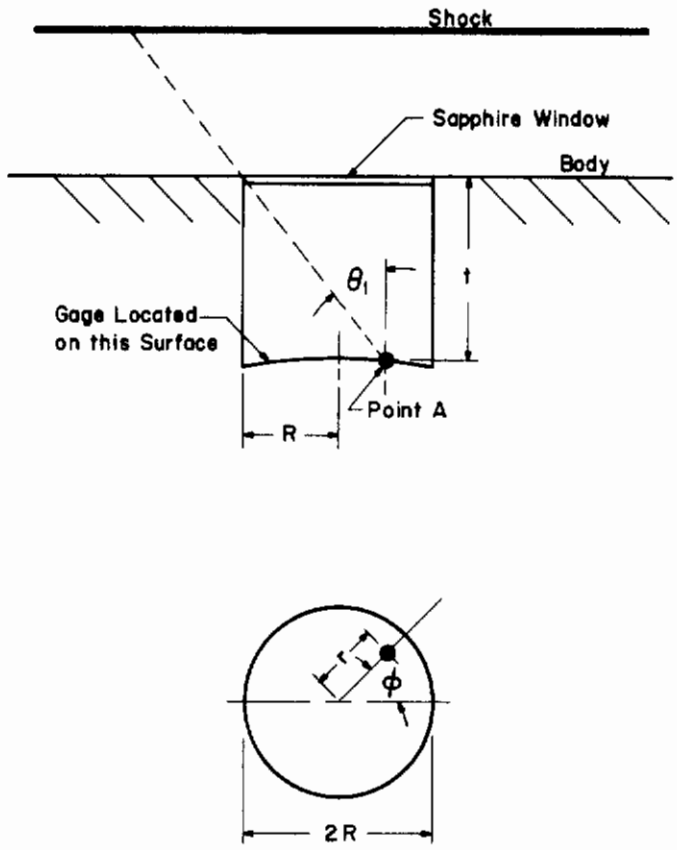

FIGURE 29. Model for Evaluation of View Factor

where θ_1 is a function of ϕ and depends on the dimensions of the cylindrical well. Note that reflections off the side of the hole are neglected since the side is coated with Luster Black and is highly absorbing. The geometrical view factor for point A, F_{2A}, thus can be expressed as

$$F_{2A} = \frac{\int_0^{2\pi} d\phi \int_0^{\theta_1} \sin\theta \, d\theta}{2\pi}$$

$$= \frac{1}{2\pi} \int_0^{2\pi} (1-\cos\theta_1) d\phi \quad . \qquad (22)$$

For a cylinder such as illustrated in Fig. 29, where t is the height from some point A to the top surface, R is the cylinder radius, and r is the radial distance from the center of the cylinder to point A, $\cos\theta_1$ can be expressed as

$$\cos\theta_1 = \frac{t}{\sqrt{2r^2\cos^2\phi + R^2 - r^2 + t^2 - 2r\cos\phi \left| \sqrt{r^2\cos^2\phi + R^2 - r^2} \right|}} \quad , \qquad (23)$$

and thus the local view factor may be expressed as

$$F_{2A} = 1 - \frac{1}{2\pi} \int_0^{2\pi} \frac{t/R}{\sqrt{\frac{2r^2}{R^2}\cos^2\phi + 1 - \frac{r^2}{R^2} + \frac{t^2}{R^2} - \frac{2r}{R}\cos\phi \left| \sqrt{\frac{r^2}{R^2} + 1 - \frac{r^2}{R^2} + \cos^2\phi} \right|}} d\phi \quad . \qquad (24)$$

This integration can be readily carried out using numerical or graphical techniques.

In analyzing the radiative heat transfer measurements, an average view factor for the entire gage, F_g, must be used. F_g can be expressed as

$$F_2 = \frac{1}{L} \int_0^L F_{2A}\, dx \qquad , \qquad (25)$$

where L is the length of the gage as measured over its surface and the integration is carried out over this length. Because the gage is extremely narrow, it has been treated here as having an infinitesimal width in deriving the expression for the view factor. The view factor, F_2, was evaluated separately for each model by numerical techniques. As an example of the value of this view factor, F_2, for the 1-inch nose radius model, the diameter of the hole is 0.225 inch, the distance from the outer surface of the window to the center of the gage is 0.050 inch, and F_2 is 0.56. If the view factor, the transmissivity of sapphire, and the absorptivity of the sensing element are known, the characteristics of the thin film radiative heat transfer gage are completely specified.

VI. STAGNATION POINT RADIATIVE HEAT TRANSFER MEASUREMENTS

Stagnation point radiative heat transfer measurements have been performed at three initial driven tube pressures of 1 mm, 200 microns, and 60 microns Hg, and over a range of shock velocities from 18,000 to 39,000 feet per second. Two hemisphere cylinder models, such as discussed in Section V, have been used; one had a nose radius of 0.5 inch and the other 1.0 inch. The simulated flight velocity range extends from 26,000 to 52,000 feet per second, and the simulated altitude range from 100,000 feet to 170,000 feet. Figure 30 shows the operating range of The Ohio State University facility and also the flight conditions simulated during this investigation for each of the two size models used. Figure 31 is a Schlieren photograph of one of the radiative heat transfer models during a test. The rapid decay in radiative intensity away from the stagnation point should be noted.

The measured heat transfer rates have been reduced into the form of the radiance as a function of shock tube conditions. The radiance may be expressed as

$$J = \frac{\dot{q}_{rad_{stag\ pt}}}{2\pi\delta F_1}$$

$$= \frac{\dot{q}_{rad_{gage}}}{2\pi\ \delta F_1 F_2(T)\alpha_G} \qquad , \qquad (26)$$

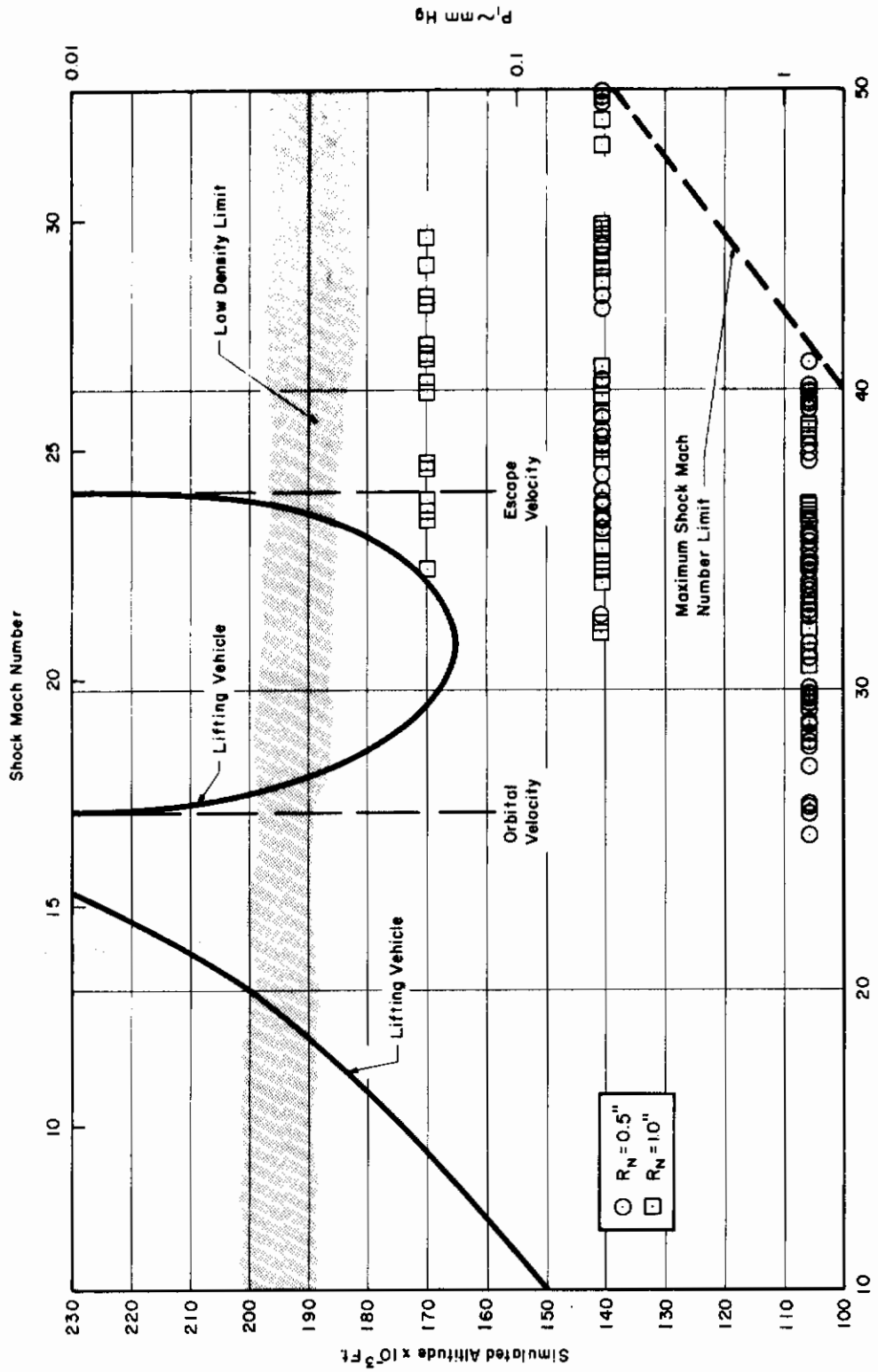

FIGURE 30. Operating Range for The Ohio State University Arc Driven Shock Tube Facility Including Free Flight Conditions Simulated During Present Investigations

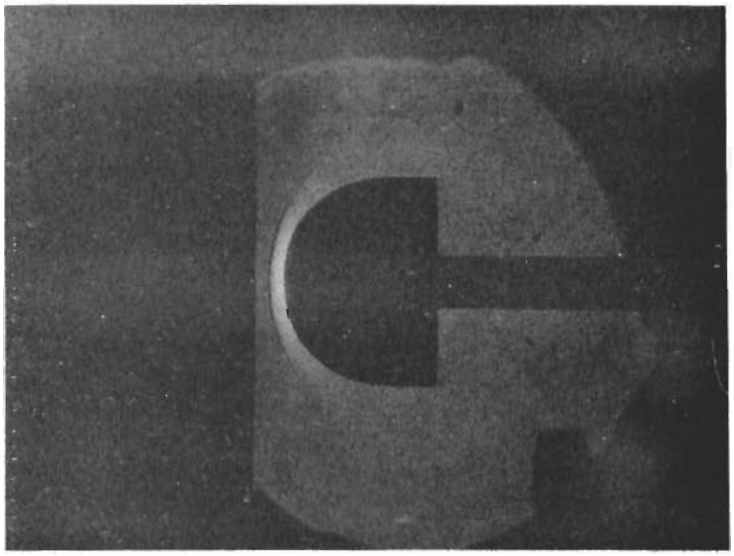

V_s = 29,500 fps
P_1 = 1mm Hg

FIGURE 31. Schlieren Photograph of Radiation Model During Test

where $\dot{q}_{rad_{gage}}$ is the heat transfer rate measured by the gage; $\dot{q}_{rad_{stag\ pt}}$ is the associated stagnation point heat transfer rate; F_1 is the correction factor, introduced in Section II to account for non-uniform shock layer properties; F_2 is the view factor; T is the average transmission coefficient over the wavelength region, 0.2 - 10μ, of the sapphire window, taken here to be 0.82; and α_G is the average absorptivity of the gage, which is taken to be 0.80. The gage heat transfer rate has been evaluated using Eq. (20) where a current of 10 ma was used in virtually all tests.

The experimental measurements of the radiance are presented in Figs. 32-34 in the form of the radiance of high temperature equilibrium air as a function of shock velocity. These data are also tabulated in Tables 3 and 4. Unless otherwise noted, the data were obtained by using the double layer Luster Black thin film gage. As can be seen, there is considerable scatter in the data. This scatter is a result of the extreme sensitivity of the radiative intensity to the shock velocity and initial pressure. An error of one per cent in the shock velocity measurement, together with a two per cent error in the pressure, will result in an error of the order of 15 per cent in the radiative intensity for the measured condition.

Typical gage outputs are shown in Fig. 35 for both the Bright Gold EF No. 31-A gage and the double layer Luster Black thin film gage. It should be noted that because of the finite time required to develop a steady state flow around a model, the heat transfer gage is not exposed to a constant heat flux starting with passage of the incident shock. It was found that Eq. (20) could still be used in data reduction if an effective starting time were chosen. Exact calculations using Eq. (18) have shown good agreement with this approximate technique. A typical data reduction is shown in Fig. 36.

It should be noted that the few data points obtained by using the Bright Gold EF No. 31-A gage were corrected so as to also represent measurements of the integrated intensity over a wavelength region of 0.17 to 6 microns. This was done by using the theoretical wavelength dependence of intensity as calculated by Meyerott,[6,8,11] together with the spectral transmissivity of the sapphire window (Fig. 28) and the spectral absorbtivity of the Bright Gold EF No. 31-A (Fig. 20). The ratio of the measured radiative intensity to the total radiative intensity in the wavelength region of approximately 0.17 to 6 microns is

$$\frac{\int \alpha_G(T)\ \mu'_\nu B_\nu d_\nu}{\int \mu'_\nu B_\nu d_\nu} ,$$

where the integration in both integrals is carried out over the wavelength region, $0.17 < \lambda < 6.0\mu$. T is the transmissivity of the sapphire window and

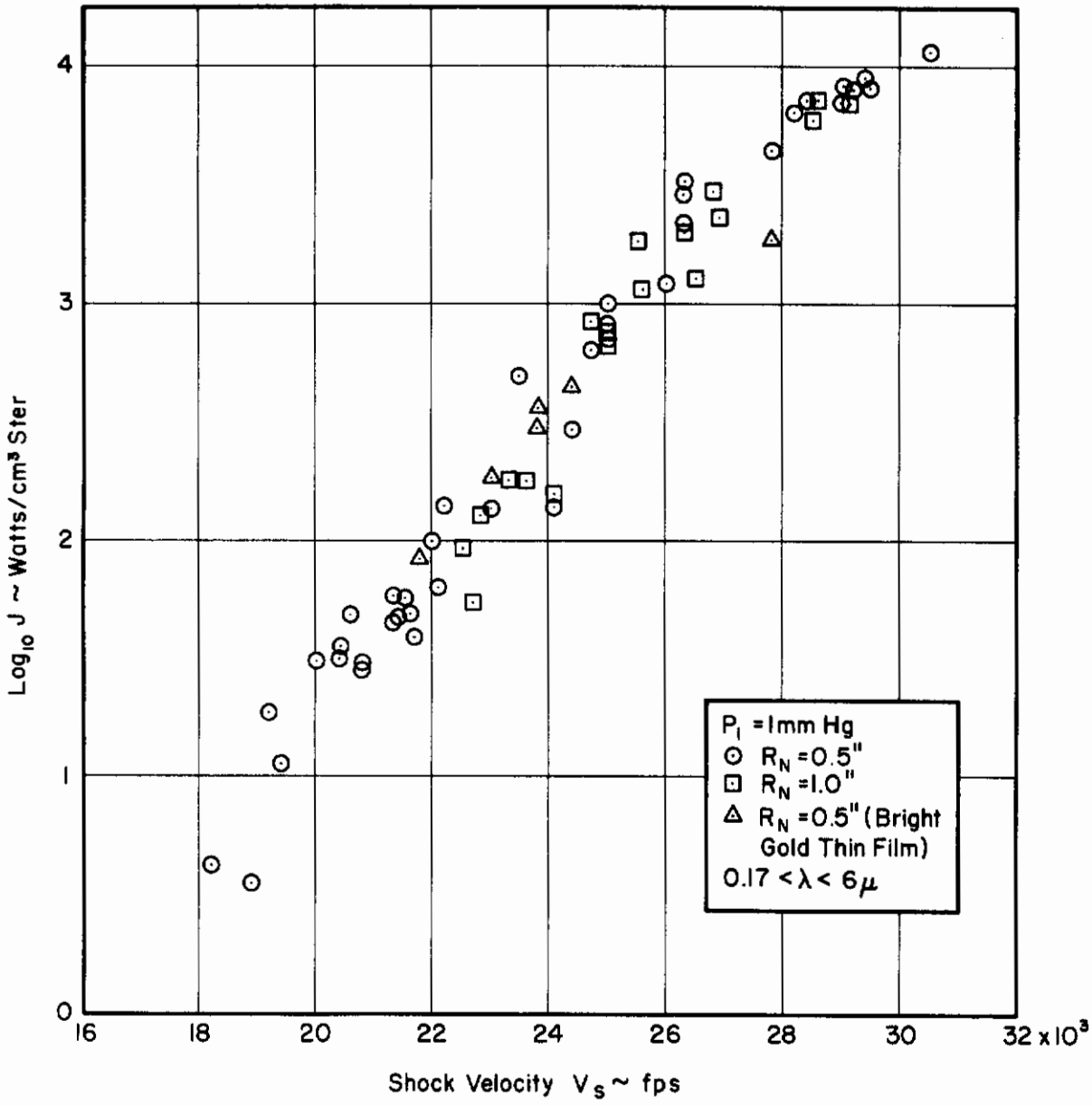

FIGURE 32. Experimental Stagnation Point Radiative Heat Transfer Data, P_1 = 1 mm Hg

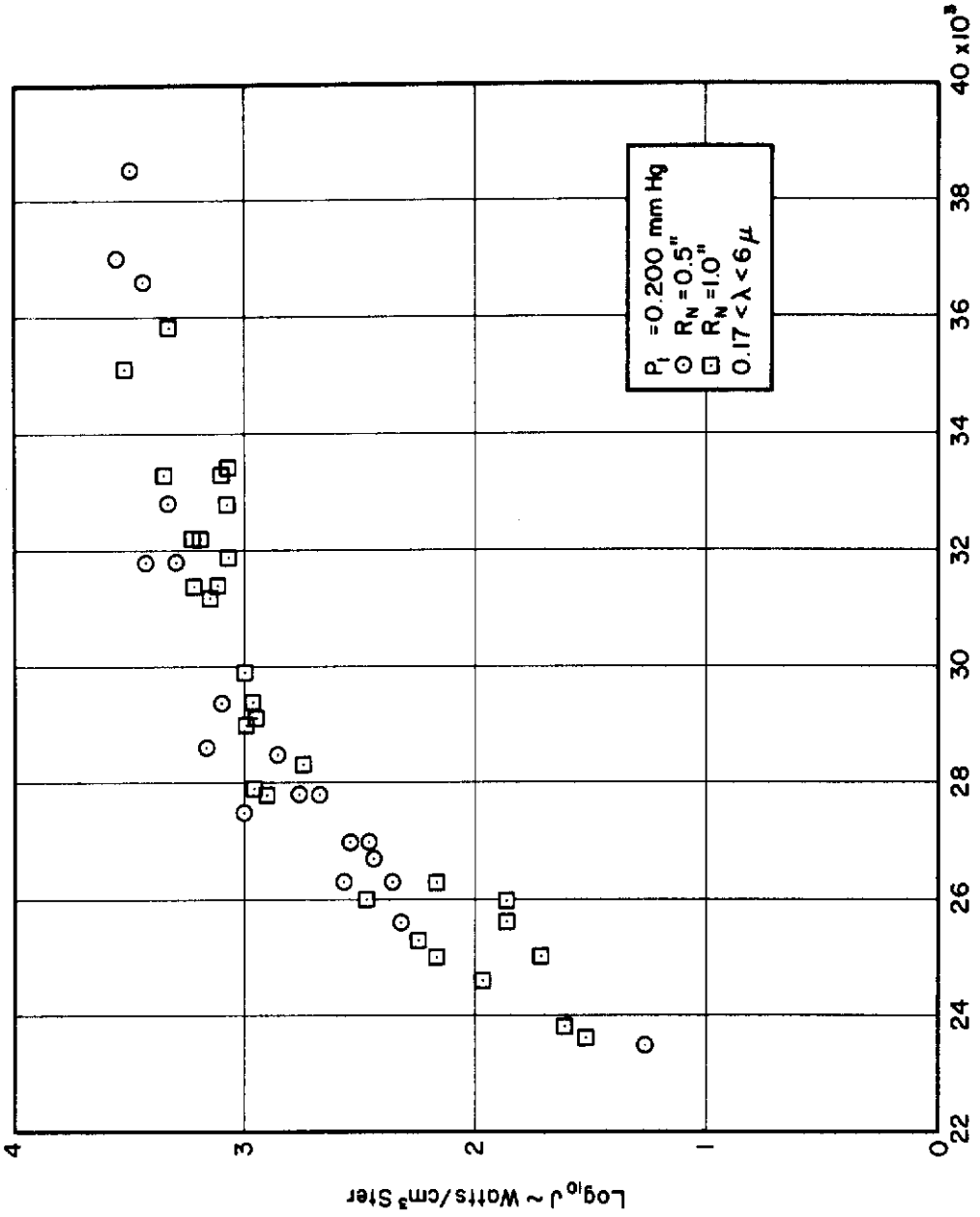

FIGURE 33. Experimental Stagnation Point Radiative Heat Transfer Data, P_1 = 0.20 mm Hg

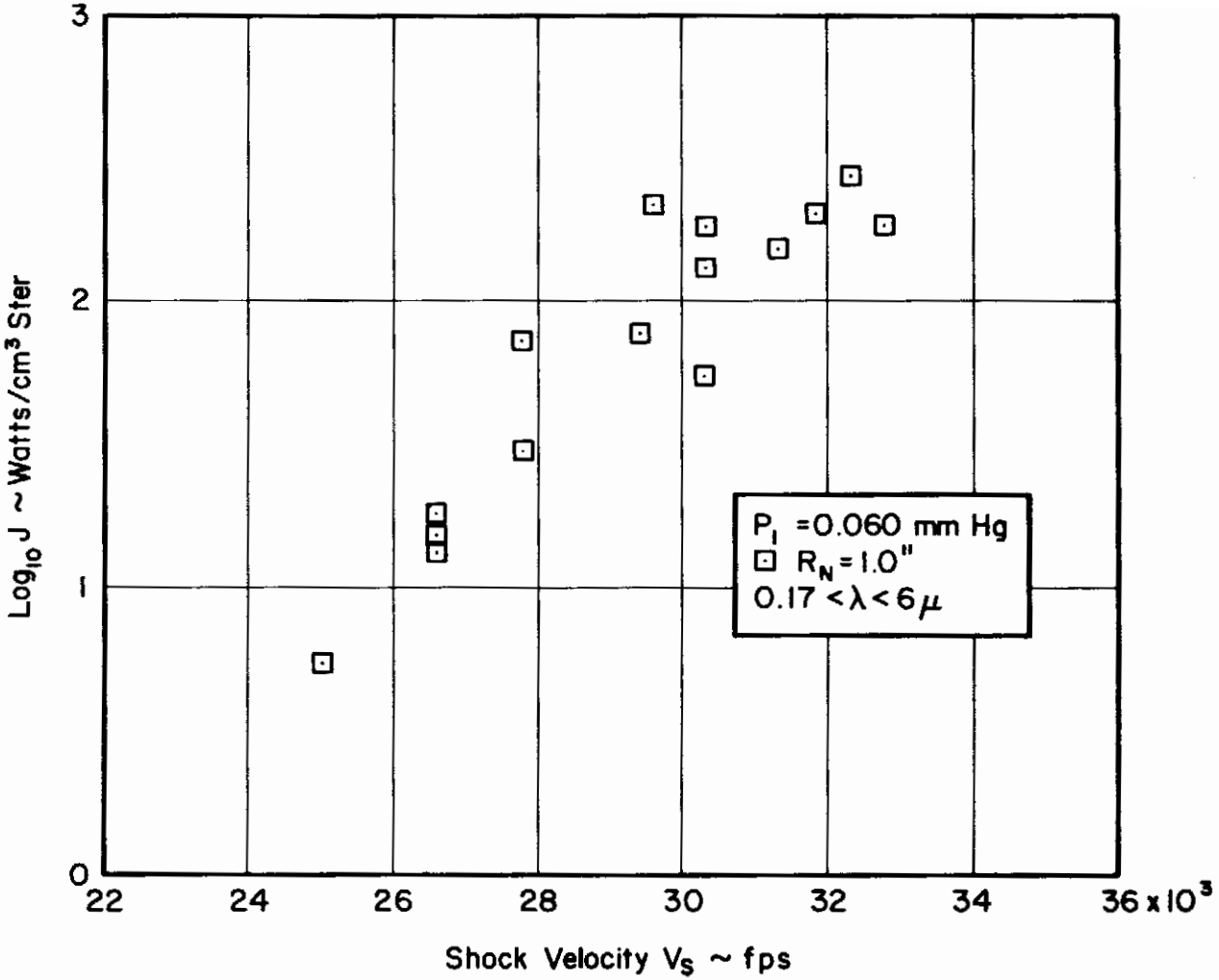

FIGURE 34. Experimental Stagnation Point Radiative Heat Transfer Data, P_1 = 0.06 mm Hg

TABLE 3

EXPERIMENTAL SHOCK TUBE DATA
ON RADIANCE OF HIGH TEMPERATURE AIR ($0.17 < \lambda < 6.0\mu$)

R_N = 0.5 inch

Run No.	P_1 mm Hg	V_s Kft/sec	$\dot{q}_{rad_{gage}}$ Watts/cm^2	$\dot{q}_{rad_{stag\ pt}}$ Watts/cm^2	J Watts/cm^3Ster	$Log_{10}J$
2707	1.00	18.2	1.35	4.29	4.40	0.644
2703	1.00	18.9	1.07	3.41	3.49	0.543
2722	1.00	19.2	5.76	18.3	18.8	1.27
2699	1.00	19.4	3.40	10.8	11.1	1.05
2719	1.00	20.0	9.17	29.1	29.8	1.48
2692	1.00	20.4	9.42	29.9	30.6	1.49
2721	1.00	20.4	11.0	34.9	35.8	1.55
2696	1.00	20.6	14.6	46.2	47.3	1.68
2694	1.00	20.8	9.07	28.8	29.5	1.47
2634	1.00	20.8	8.60	27.3	28.0	1.45
2628	1.00	21.3	17.6	56.0	57.4	1.76
2693	1.00	21.3	13.4	42.6	43.6	1.64
2631	1.00	21.4	14.3	45.3	46.4	1.67
2632	1.00	21.5	17.5	55.6	57.0	1.76
2633	1.00	21.6	14.5	46.0	47.1	1.68

TABLE 3 (Cont'd)

Run No.	P_1 mm Hg	V_s Kft/sec	$\dot{q}_{rad_{gage}}$ Watts/c_m^2	$\dot{q}_{rad_{stag\ pt}}$ Watts/c_m^2	J Watts/c_m^3Ster	$Log_{10}J$
2691	1.00	21.7	11.6	37.0	37.9	1.58
2700	1.00	22.0	30.0	95.2	97.6	1.99
2630	1.00	22.1	18.9	60.0	61.5	1.79
2771	1.00	22.2	42.8	136	139	2.14
2754	1.00	23.0	41.3	131	134	2.13
2704	1.00	23.5	151	478	490	2.69
2743	1.00	24.1	41.3	131	134	2.13
30.9	1.00	24.4	90.7	288	296	2.47
2755	1.00	24.7	200	634	650	2.81
2710	1.00	25.0	241	765	784	2.90
2748	1.00	25.0	298	947	970	2.99
2752	1.00	25.0	215	683	700	2.85
2715	1.00	26.0	365	1160	1190	3.08
2714	1.00	26.3	658	2090	2140	3.33
2719	1.00	26.3	857	2720	2790	3.45
2753	1.00	26.3	1010	3200	3280	3.51
2749	1.00	27.8	1340	4260	4360	3.64
3013	1.00	28.2	2000	6360	6520	3.81
3015	1.00	28.4	2220	7060	7230	3.86
2774	1.00	29.0	2120	6740	6910	3.84
2778	1.00	29.2	2410	7660	7850	3.90
3014	1.00	29.0	2570	8160	8360	3.92
3018	1.00	30.5	3870	12300	12600	4.10
3016	1.00	29.4	2800	8880	9100	3.96
3017	1.00	29.5	2510	7960	8160	3.91

TABLE 3 (Cont'd)

Run No.	P_1 mm Hg	V_s Kft/sec	$\dot{q}_{rad_{gage}}$ Watts/c_m^2	$\dot{q}_{rad_{stag_{pt}}}$ Watts/c_m^2	J Watts/c_m^3Ster	$Log_{10}J$
2387*	1.00	21.8	25.7	81.7	83.7	1.92
2390*	1.00	23.0	56.4	179	183	2.26
2391*	1.00	25.0	201	639	655	2.82
2409*	1.00	24.4	135	428	439	2.64
2411*	1.00	27.8	554	1760	1800	3.26
2412*	1.00	23.8	110	348	357	2.55
2414*	1.00	23.8	90.4	287	294	2.47
2995	0.200	23.5	5.67	18.0	18.5	1.27
3001	0.200	25.6	63.6	202	207	2.32
2997	0.200	26.3	68.4	217	222	2.35
3007	0.200	26.3	114	361	370	2.57
2999	0.200	26.7	83.2	264	270	2.43
2998	0.200	27.0	102	325	333	2.53
2994	0.200	27.0	85.0	270	277	2.45
3006	0.200	27.5	307	974	998	3.00
3003A	0.200	27.8	143	454	465	2.67
3004	0.200	27.8	174	551	565	2.76
3003B	0.200	28.5	211	671	688	2.84
3005	0.200	28.6	441	1400	1430	3.16
3006	0.200	29.4	365	1160	1190	3.08

*These data were obtained with a Bright Gold EF No. 31-A sensing element.

TABLE 3 (Cont'd)

Run No.	P_1 mm Hg	V_s Kft/sec	$\dot{q}_{rad_{gage}}$ Watts/c_m^2	$\dot{q}_{rad_{stag\_pt}}$ Watts/c_m^2	J Watts/c_m^3Ster	$Log_{10}J$
3008	0.200	31.8	576	1830	1880	3.28
3009	0.200	31.8	813	2580	2640	3.42
3010	0.200	32.8	633	2010	2060	3.32
3021	0.200	36.6	819	2600	2660	3.43
3022	0.200	38.5	784	2940	3010	3.48
3023	0.200	37.0	1060	3360	3440	3.54

TABLE 4

EXPERIMENTAL SHOCK TUBE DATA
ON RADIANCE OF HIGH TEMPERATURE AIR ($0.17 < \lambda < 6.0\mu$)

R_N = 1.0 inch

Run No.	P_1 mm Hg	V_s Kft/sec	$\dot{q}_{rad_{gage}}$ Watts/c_m^2	$\dot{q}_{rad_{stag_2pt}}$ Watts/c_m^2	J Watts/c_m^3Ster	$Log_{10}J$
2786	1.00	22.5	66.2	180	91.9	1.96
2785	1.00	22.7	38.3	104	53.0	1.73
2783	1.00	22.8	93.1	253	129	2.11
2927	1.00	23.3	128	349	178	2.25
2784	1.00	23.6	124	337	172	2.24
2782	1.00	24.1	109	296	151	2.18
2789	1.00	24.7	604	1640	836	2.92
2787	1.00	25.0	534	1450	741	2.87
2790	1.00	25.0	475	1290	660	2.82
2800	1.00	25.5	1320	3590	1830	3.26
2792	1.00	25.6	813	2210	1130	3.06
2797	1.00	26.3	1430	3880	1980	3.30
2791	1.00	26.5	894	2430	1240	3.10
2794	1.00	26.8	217	5900	3010	3.48
2796	1.00	26.9	166	4510	2300	3.36
2799	1.00	28.5	423	1150	5860	3.77
2798	1.00	28.6	522	1420	7240	3.86
2801	1.00	29.1	500	1360	6960	3.84
2932	0.200	23.6	24.0	65.1	33.2	1.52
2930	0.200	23.8	28.3	76.8	39.2	1.60

TABLE 4 (Cont'd)

Run No.	P_1 mm Hg	V_s Kft/sec	$\dot{q}_{rad_{gage}}$ Watts/c_m^2	$\dot{q}_{rad_{stag_2pt}}$ Watts/c_m^2	J Watts/c_m^3Ster	$Log_{10}J$
2956	0.200	24.6	65.5	178	90.6	1.96
2933	0.200	25.0	35.6	96.8	49.4	1.70
2934	0.200	25.0	104	282	144	2.16
2935	0.200	25.3	125	341	174	2.24
2931	0.200	25.6	52.2	142	72.4	1.86
2950	0.200	26.0	210	572	292	2.47
2959	0.200	26.0	52.2	142	72.4	1.86
2957	0.200	26.3	104	282	144	2.16
2973	0.200	27.8	567	1540	787	2.90
2949	0.200	27.9	633	1720	876	2.94
2958	0.200	28.3	383	1040	532	2.73
2972	0.200	29.0	677	1840	940	2.98
2965	0.200	29.1	607	1650	840	2.93
2970	0.200	29.4	633	1720	880	2.95
2948	0.200	29.9	684	1860	948	2.98
2947	0.200	31.2	986	2680	1370	3.14
2943	0.200	31.4	1170	3180	1620	3.21
2939	0.200	31.4	916	2490	1270	3.11
2951	0.200	31.9	821	2230	1140	3.06
2937	0.200	32.2	1070	2920	1490	3.18
2941	0.200	32.2	1130	3060	1560	3.20
2946	0.200	32.8	843	2290	1170	3.07
2938	0.200	33.3	1580	4290	2190	3.34
2940	0.200	33.3	887	2410	1230	3.09
2953	0.200	33.4	813	2210	1130	3.06

TABLE 4 (Cont'd)

Run No.	P_1 mm Hg	V_s Kft/sec	$q_{rad_{gage}}$ Watts/c_m^2	$q_{rad_{stag\ pt}}$ Watts/c_m^2	J Watts/c_m^3Ster	$Log_{10}J$	
2976	0.200	35.1	2330	6330	3230	3.51	
2975	0.200	35.8	1490	4040	2060	3.32	
2981	0.060	25.0	3.90	10.6	5.39	.731	(N)*
2983	0.060	26.6	13.1	35.7	18.2	1.26	(N)
2985	0.060	26.6	10.5	28.6	14.6	1.17	(N)
2988	0.060	26.6	9.38	25.5	13.0	1.12	(N)
2986	0.060	27.8	21.3	57.8	29.5	1.47	(N)
2991	0.060	27.8	51.9	141	71.7	1.86	(N)
2977	0.060	29.4	54.1	147	75.2	1.88	(N)
2989	0.060	29.6	154	419	214	2.33	(N)
2984	0.060	30.3	92.4	251	128	2.11	(N)
2987	0.060	30.3	131	355	181	2.26	(N)
2990	0.060	30.3	38.6	105	53.8	1.73	(N)
2978	0.060	31.3	108	294	150	2.18	(N)
2992	0.060	31.8	144	390	199	2.30	(N)
2979	0.060	32.2	132	359	183	2.26	(N)
2980	0.060	32.3	195	529	270	2.43	(N)

*The "N" indicates conditions at which effects due to chemical non-equilibrium in the shock layer may exist. See discussion in this section.

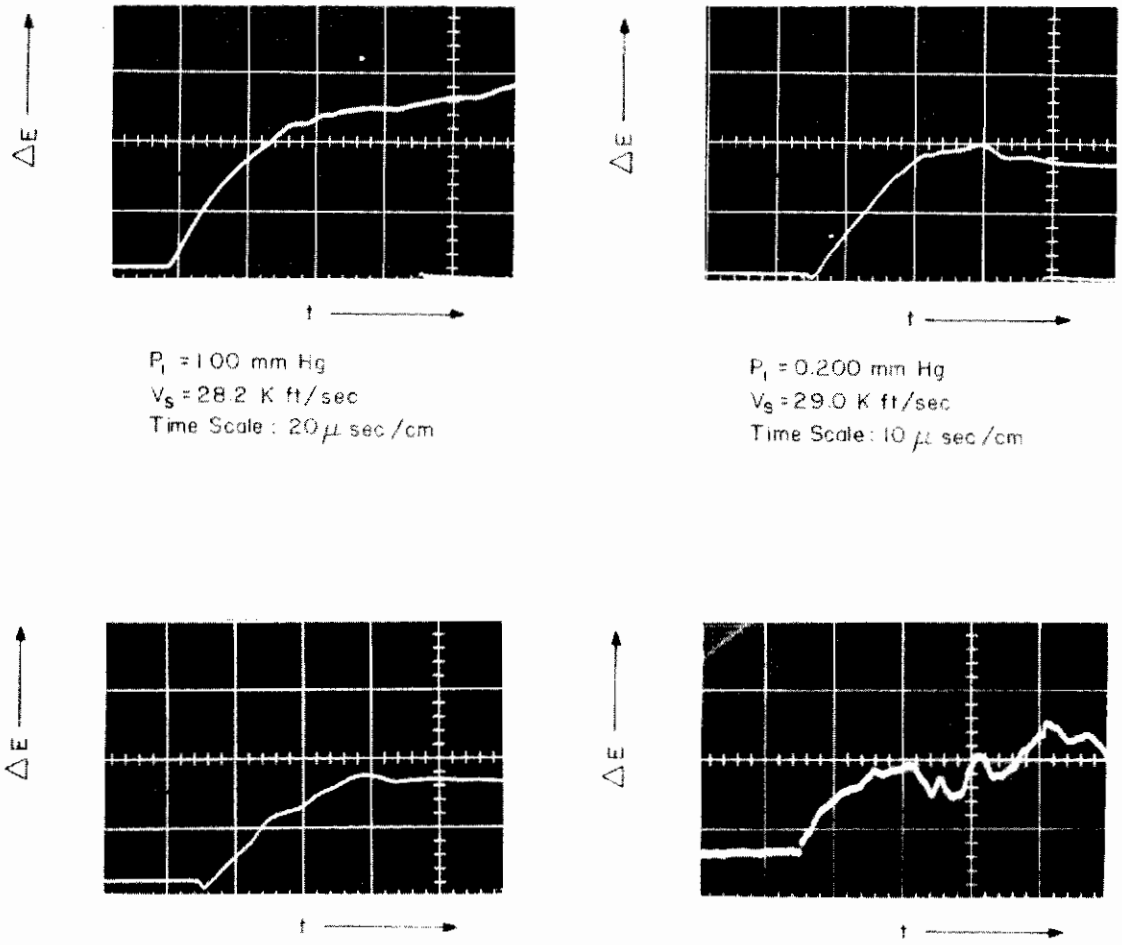

FIGURE 35. Typical Thin Film Radiative Gage Outputs

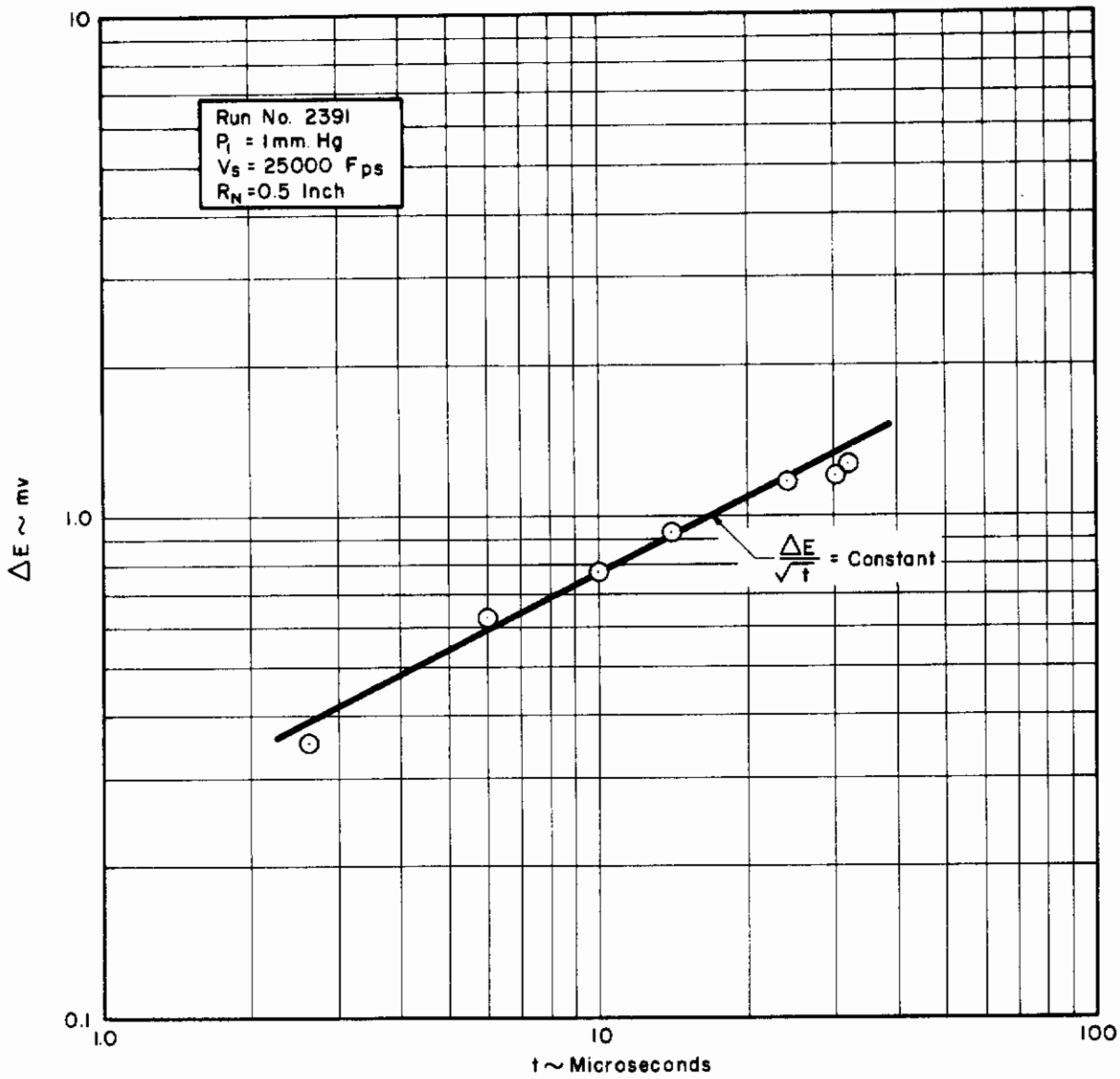

FIGURE 36. Typical Data Reduction

α_G is the absorptivity of the gage. Both are wavelength dependent. For a typical case, such as run no. 2411, the evaluation of this integral numerically gave a value of 0.565 for the ratio of measured intensity to actual total intensity in the indicated wavelength region. These corrected data points are seen to be in good agreement with the data obtained using the double layer Luster Black gage.

At two pressures, 1 mm Hg and 200 microns, data were obtained using both size models, and it can be seen from Figs. 32 and 33 that there is no discernible difference between the measured radiances of the two models. This indiscernible difference has been regarded as evidence of a negligible influence of non-equilibirum effects on the present measurements at these pressures. For the data taken at an initial driven tube pressure of 0.060 mm Hg, chemical non-equilibrium exists in the shock layer. These conditions are indicated by an "N" in Tables 3 and 4. This non-equilibrium effect is not believed to be important.

VII. ANALYSIS AND DISCUSSION OF RESULTS

In order to analyze the present experimental results, the data shown in Figs. 32-34 have been treated statistically. If it is assumed that the scatter in the data, corresponding to a particular shock velocity and initial driven tube pressure, is due to inherent random inaccuracies and not due to a consistent error in experimental technique, then the average of the experimental data points at that condition should be representative of the true value which would have been measured experimentally had there not been random inaccuracies. On this basis, the present data at each driven tube pressure have been grouped, such that all data points in a group have a velocity within a 1,000 feet per second range, and linearily averaged. For example, the measured intensities of all points at 1 mm Hg with shock velocities between 22,500 and 23,500 feet per second have been averaged. These average data points, as tabulated in Tables 5 and 6, have been considered in analyzing the results obtained here. In this manner the data scatter has been greatly reduced and a meaningful analysis of the data has been made possible. In this analysis, only the data obtained with the Luster Black sensing element gage have been considered. The Bright Gold data were too limited for a statistical analysis.

Using the average points, the experimental results obtained here at an initial driven tube pressure of 1 mm Hg are presented in Fig. 37 in the form of the radiance of high temperature air as a function of temperature. The shock layer density corresponding to this initial driven tube pressure is $\rho/\rho_o = 0.16$. Also shown in Fig. 37 are the results of the three existing calculations of the radiance of high temperature air.[6-8,11,19] It can be seen that the experimental results are in excellent agreement with the results of Nardone et al,[19] except at extremely high temperatures. The theoretical results of Meyerott and his co-workers[6,8,11] are seen to also be in reasonable agreement with this data. However, the theoretical calculations of Kivel and Bailey[7] are consistently high.

TABLE 5

AVERAGED SHOCK TUBE DATA
ON RADIANCE OF HIGH TEMPERATURE AIR ($0.17 < \lambda < 6.0\mu$)

R_N = 0.5 inch

P_1 mm Hg	V_s Kft/sec	V_∞ Kft/sec	ρ/ρ_o	T °K	J Watts / cm^3 Ster
1.00	19.2	26.2	0.16	8650	11.1
1.00	20.3	27.7	0.16	9100	32.0
1.00	20.7	28.3	0.16	9350	34.8
1.00	21.3	29.1	0.16	9700	49.1
1.00	21.6	29.5	0.16	9920	47.3
1.00	22.1	30.2	0.16	10200	99.1
1.00	24.0	32.8	0.16	11450	307
1.00	24.9	34.0	0.16	12200	775
1.00	26.2	35.8	0.16	13150	2350
1.00	28.1	38.4	0.16	14400	6040
1.00	29.1	39.8	0.16	15000	7690
1.00	29.8	40.7	0.16	15500	9950
0.200	26.1	35.8	0.032	12200	266
0.200	26.9	36.9	0.032	12850	294
0.200	27.7	38.0	0.032	13300	676
0.200	28.8	39.5	0.032	14000	1090
0.200	32.1	44.0	0.032	15500	2190
0.200	37.3	51.1	0.032	17600	3040

TABLE 6

AVERAGED SHOCK TUBE DATA
ON RADIANCE OF HIGH TEMPERATURE AIR ($0.17 < \lambda < 6.0\mu$)

R_N = 1.0 inch

P_1 mm Hg	V_s Kft/sec	V_∞ Kft/sec	ρ/ρ_o	T °K	J Watts/cm^3Ster	
1.00	22.7	31.2	0.16	10500	91.1	
1.00	23.7	32.5	0.16	11300	167	
1.00	24.9	34.2	0.16	12000	746	
1.00	25.8	35.4	0.16	12800	1650	
1.00	26.7	36.6	0.16	13500	2180	
1.00	28.7	39.4	0.16	14800	6680	
0.200	23.7	32.5	0.032	10375	36.2	
0.200	25.0	34.2	0.032	11475	114	
0.200	26.0	35.6	0.032	12150	145	
0.200	28.0	38.4	0.032	13450	749	
0.200	29.2	40.0	0.032	14150	886	
0.200	31.3	42.9	0.032	15150	1410	
0.200	32.1	44.0	0.032	15500	1400	
0.200	33.2	45.2	0.032	15900	1430	
0.200	35.4	48.5	0.032	16900	2640	
0.060	26.6	35.6	0.011	12000	15.2	(N)*
0.060	27.8	38.2	0.011	12700	50.5	(N)
0.060	29.5	40.5	0.011	13450	144	(N)
0.060	30.3	41.6	0.011	13850	121	(N)
0.060	31.5	43.3	0.011	14350	175	(N)
0.060	32.5	44.6	0.011	14700	227	(N)

*The "N" indicates conditions at which effects due to chemical non-equilibrium in the shock layer may possibly exist. See discussion in Section VI.

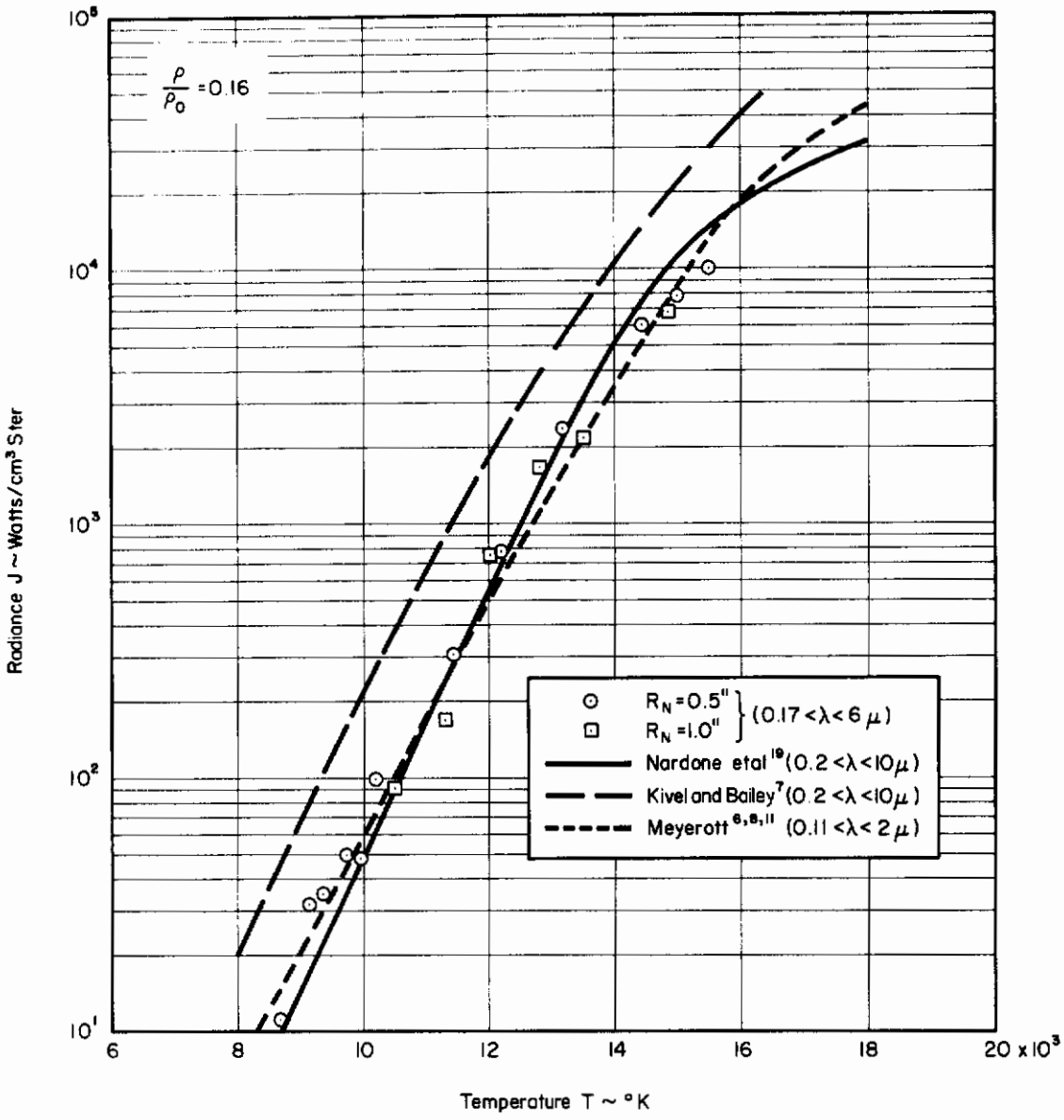

FIGURE 37. Comparison of Experimental Results and Theoretical Calculations on Radiance of High Temperature Air, P_1 = 1 mm Hg

At the lower pressures of 0.20 and 0.06 mm Hg, no one theoretical calculation was in agreement with the experimental results over the entire temperature range. However, a comparison of the results of Nardone et al[19] with the results of this investigation showed a consistent pattern in which the deviation between the theory and experiment increased with increasing temperature and decreasing density. It will be shown that this trend can be explained, based on recent developments reported in the literature.[25,37] No such pattern was present in comparing the calculations of Meyerott[6,8,11] to the experimental results; in fact, there appeared to be a definite inconsistency. The calculations of Kivel and Bailey[7] were also not in agreement with the experimental results. Thus the theoretical calculations of Nardone et al[19] have been used as a basis for further analysis.

In Fig. 38 all of the experimental results obtained throught the use of the double layer Luster Black thin film gage are presented as a function of the simulated flight velocity, and are compared with the theoretical results of Nardone et al.[19] The region of disagreement is for conditions at which the continuum radiation from high temperature air dominates the shock layer emission. As indicated previously, present estimates of continuum radiation are highly approximate; thus the disagreement evident in Fig. 38 is not entirely unexpected. It should be noted that both contamination effects and effects due to non-equilibirum phenomena in the shock layer would have been expected to increase the radiative intensity; thus the present disagreement can not be attributed to those effects.

It would be presumptuous to try to extrapolate any detailed knowledge of the continuum radiation of high temperature air from the present measurements of the total radiative heat flux. However, it is clear that the existing estimates of Nardone et al[19] are, on the order of a factor of two, high at extreme temperatures. Biberman and Norman[37] have indicated that the existing calculations of the N^+ and O^+ de-ionization continuum radiation based on a hydrogen atom model should be expected to overestimate the emission. As a correction, they derive a modifying factor which is wavelength dependent and varies from 1.0 to 0.2. It would thus appear that as a first-order correction to existing calculations, a constant multiplying factor of 0.5 could be applied. The introduction of such a factor is, in essence, a correction to the cross section for the de-ionization process.

With the results of Nardone et al,[19] as a starting point, a revised estimate of the N^+ and O^+ de-ionization radiative emission from high temperature air has been carried out through the use of this correction factor of 0.5. These results, which are presented in Figs. 39 and 40, have been used to modify the radiance calculations of Nardone et al[19] at high temperatures where continuum radiation dominates. This revised theoretical estimate, together with the present experimental results, are shown in Figs. 41-43 where the radiance is presented as a function of temperature for the three shock layer densities at which measurements were performed. It may be seen that for all three shock layer densities, the experimental results appear to approach the present estimate of the radiance of high temperature air as temperature increases. In

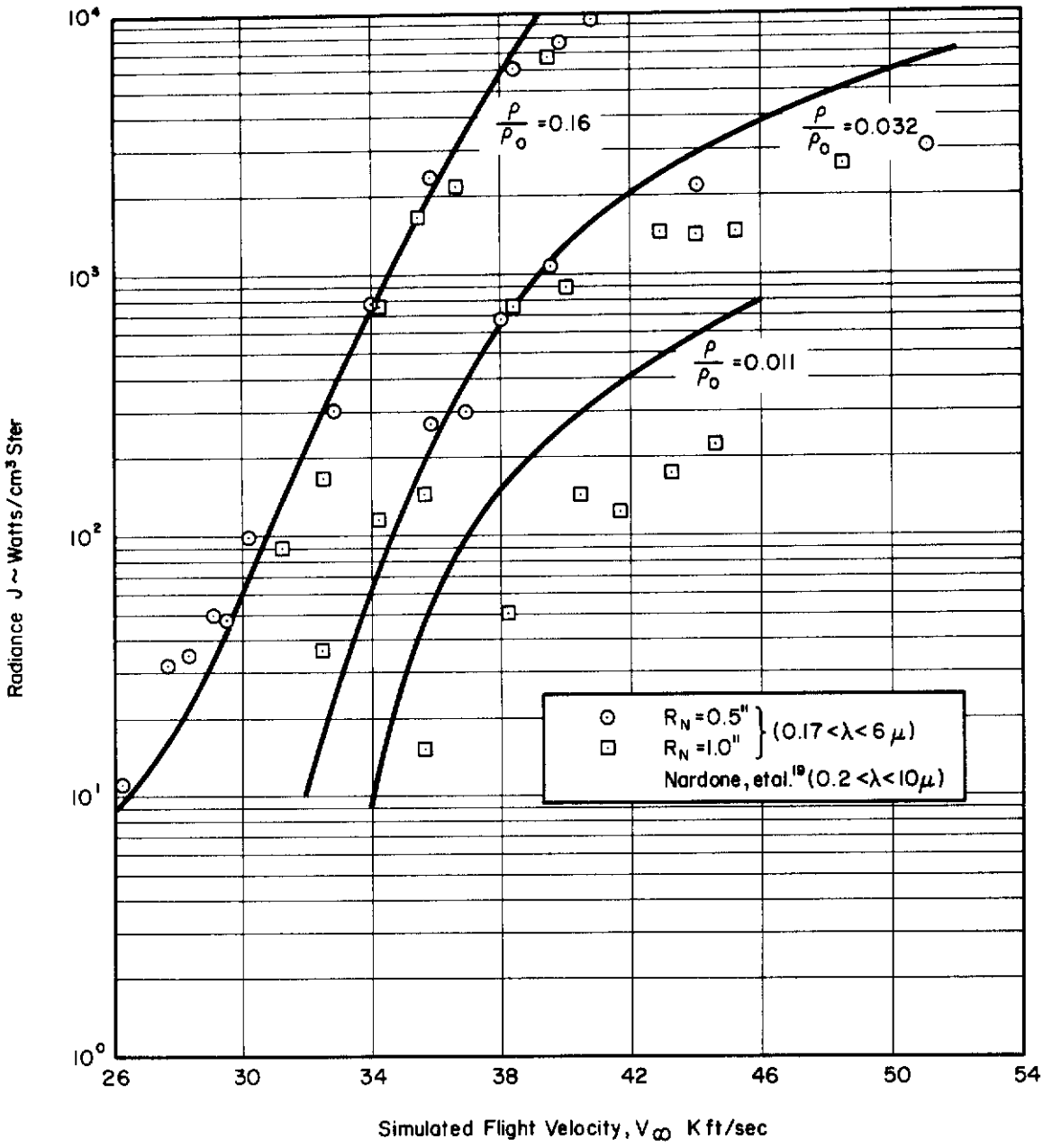

FIGURE 38. Comparison of Experimental Results and Theoretical Calculations of Nardone, et al[19]

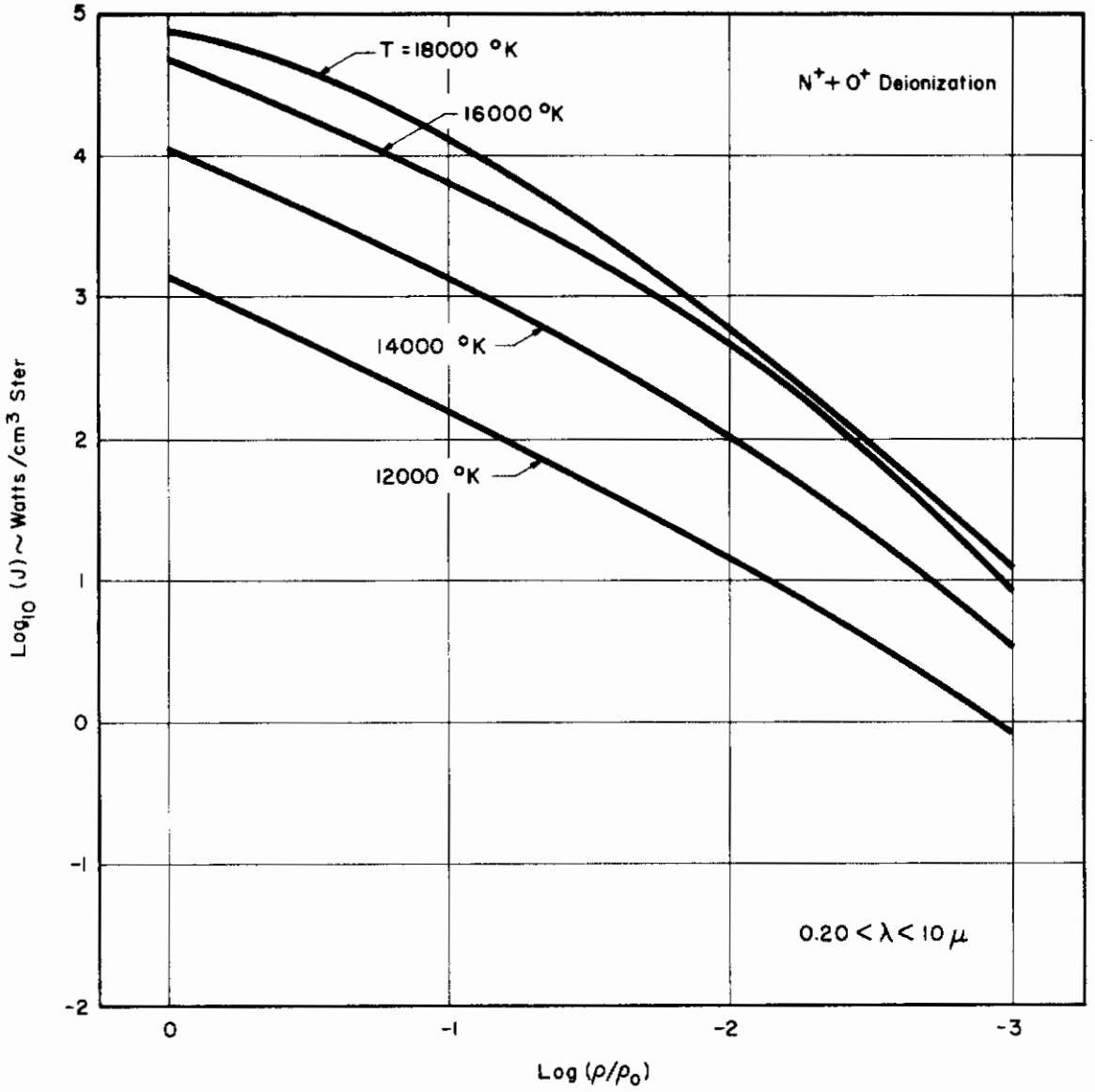

FIGURE 39. Estimate of Radiative Emission in High Temperature Air Due to N^+ and O^+ Deionization ($0.2 < \lambda < 10\mu$)

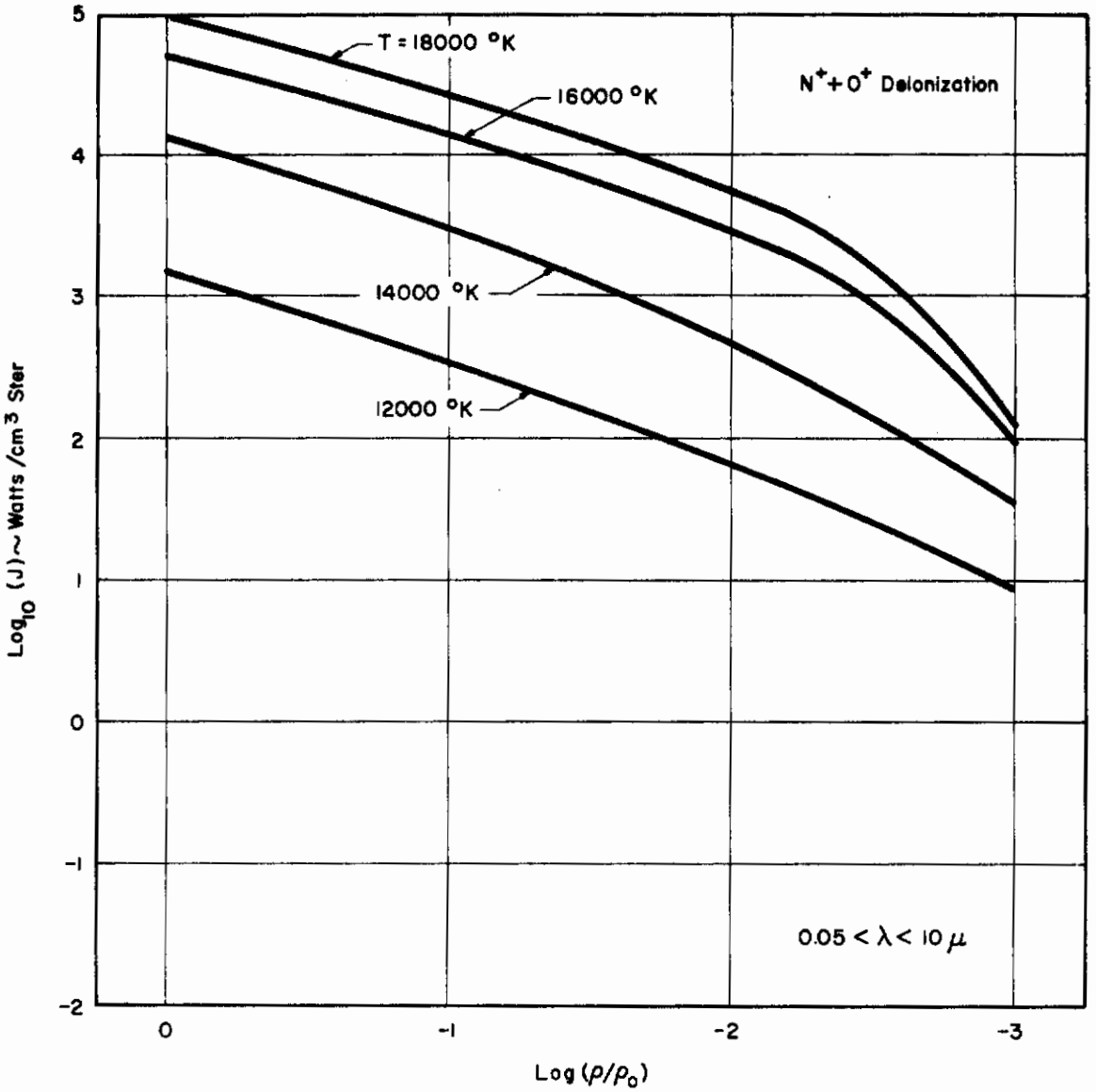

FIGURE 40. Estimate of Radiative Emission in High Temperature Air Due to N^+ and O^+ Deionization ($0.05 < \lambda < 10\mu$)

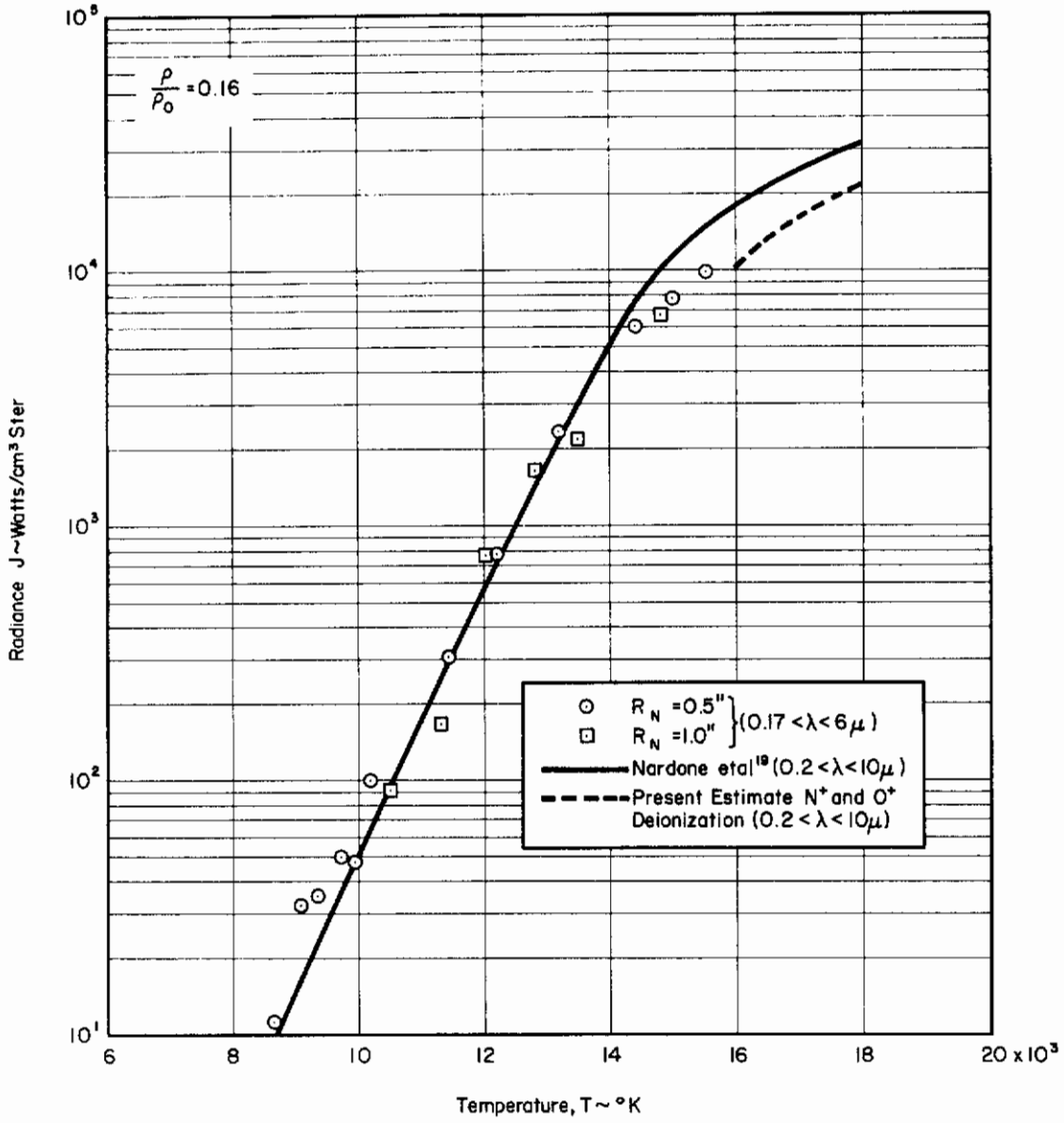

FIGURE 41. Comparison of Experimental Results and Theoretical Calculations of Radiance of High Temperature Air, P_i = 1 mm Hg

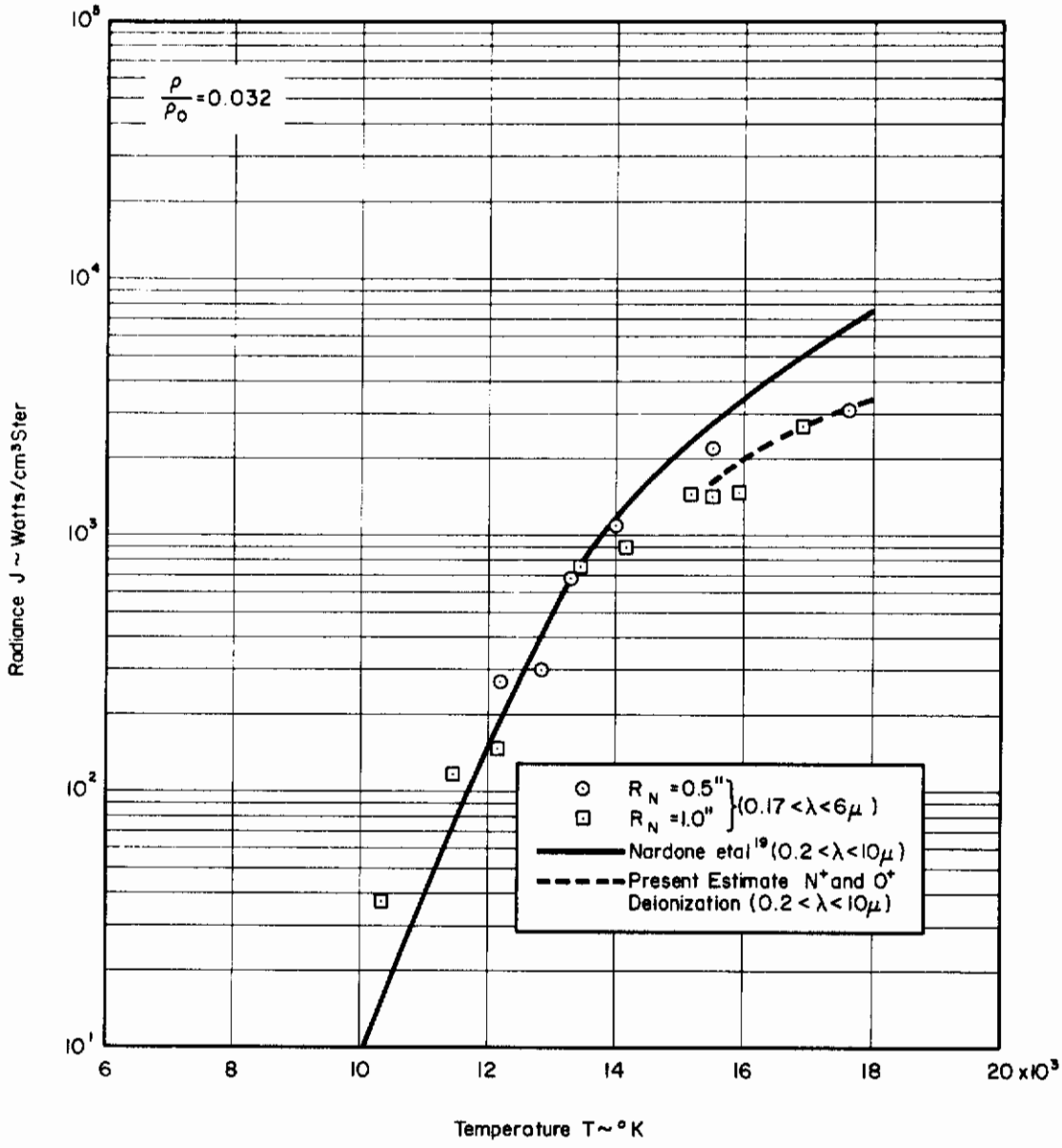

FIGURE 42. Comparison of Experimental Results and Theoretical Calculations of Radiance of High Temperature Air, P_1 = 0.2 mm Hg

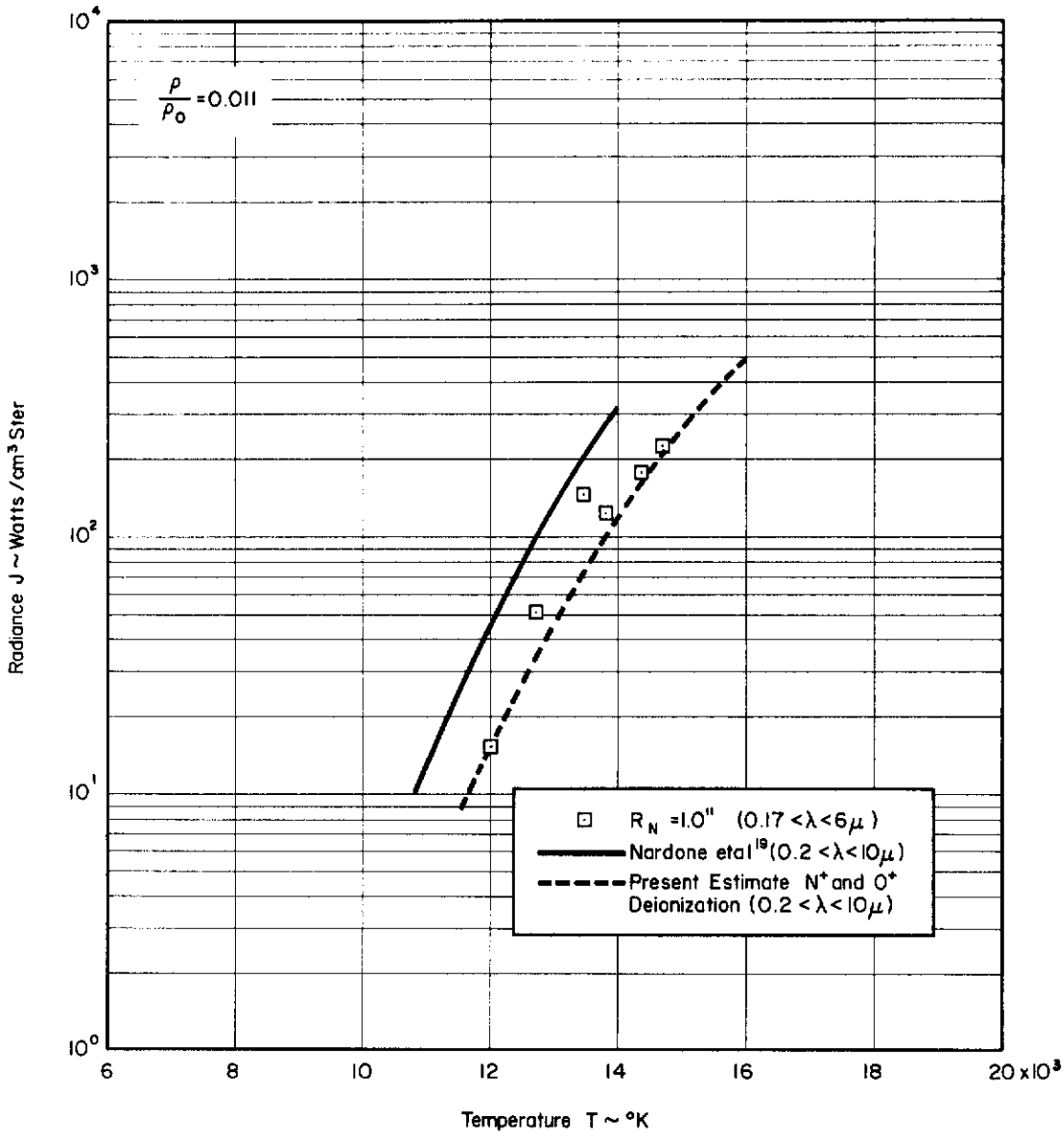

FIGURE 43. Comparison of Experimental Results and Theoretical Calculations of Radiance of High Temperature Air, P_1 = 0.06 mm Hg

fact, for a shock layer density of $\rho/\rho_o = 0.011$, the experimental results are in good agreement with the present estimate.

However, there is a range of temperatures within which the experimental data are in better agreement with the results of Nardone et al[19] than with the present estimate, even though continuum radiation is known to dominate the emission there (see Figs. 10-12). This can be explained if the presence of emission due to the photo attachment of an electron to N, as suggested by Boldt[36] and Allen and Textoris,[25] is important. Figure 44 shows the region of the density-temperature map where the calculations of Allen and Textoris,[25] at a wavelength of 5000 Å, indicate the N^- photo attachment emission to be important and also where the N^+ de-ionization emission is to be important. It can be seen that in the region of importance for the continuum due to N^+ de-ionization, the present emperimental results are in good agreement with the revised estimate based on the application of a correction factor of 0.5 to the emission rate. However, the region of importance for N^- photo attachment radiation corresponds to the region of Figs. 41 and 42 where the experimental results lie above the present revised estimate and are actually in better agreement with the results of Nardone et al.[19]

It thus appears that in certain ranges of temperatures and densities, the calculations of Nardone et al,[19] though overestimating the de-ionization radiation and not including the N^- photo attachment radiation, still are in good agreement with the experimental results since the two effects appear to cancel. In this range the results of Nardone, Breene et al[19] may be used for engineering calculations. However, at higher temperatures the N^- photo attachment emission becomes negligible and estimates of the de-ionization radiation must be corrected, as done here, in order for calculations of the total radiance of high temperature air to be correct.

It should be noted that the estimate of the radiative emission due to the N^+ de-ionization process (Figs. 39 and 40) are slightly higher than that of Biberman and Norman,[37] as calculated by Allen.[25] This can be seen in Fig. 45 where the present estimate is compared with that of Nardone et al,[19] and that of Biberman and Norman.[37] Thus the present estimate may be conservative. However, as was indicated earlier, it would be presumptuous to propose detailed modifications to the calculations of Nardone et al,[19] based on the present measurements of the integrated radiative heat flux. The present estimate is proposed only as a first-order correction which may be used as a modification to be applied in engineering design calculations.

With the present experimental results as a basis, the calculations by Nardone et al[19] of the radiance of high temperature air have been modified at high temperatures through the use of the correction factor previously discussed. The range of temperatures and densities, in which the correction factor was applied, was determined from the experimental results. The resulting estimates for the radiance of high temperature air are shown in Figs. 46 and 47. Also shown in Fig. 47 are the original results of Nardone et al.[19] It can be seen that at low densities the correction is sizable.

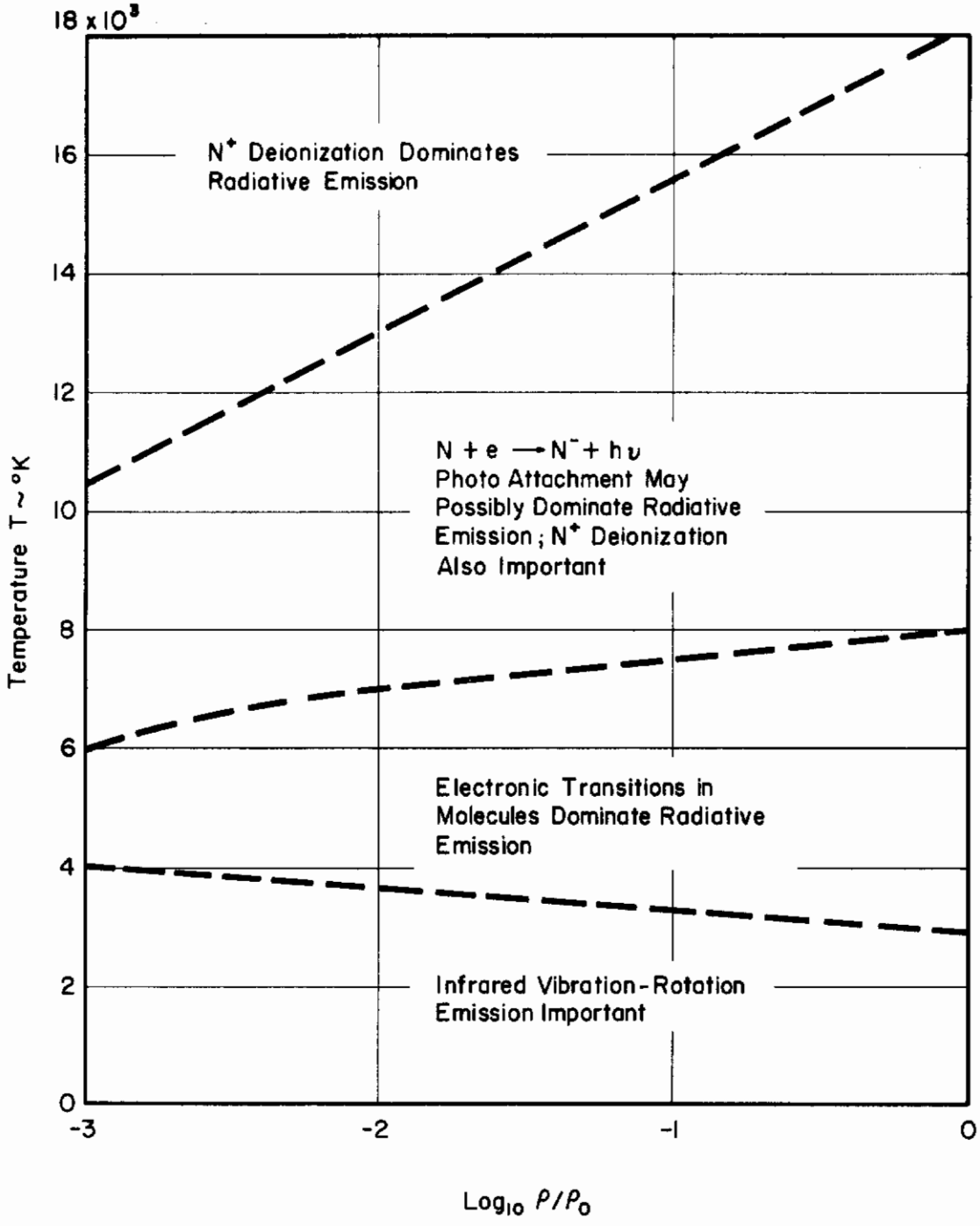

FIGURE 44. Regions Where Various Emission Processes Are Important

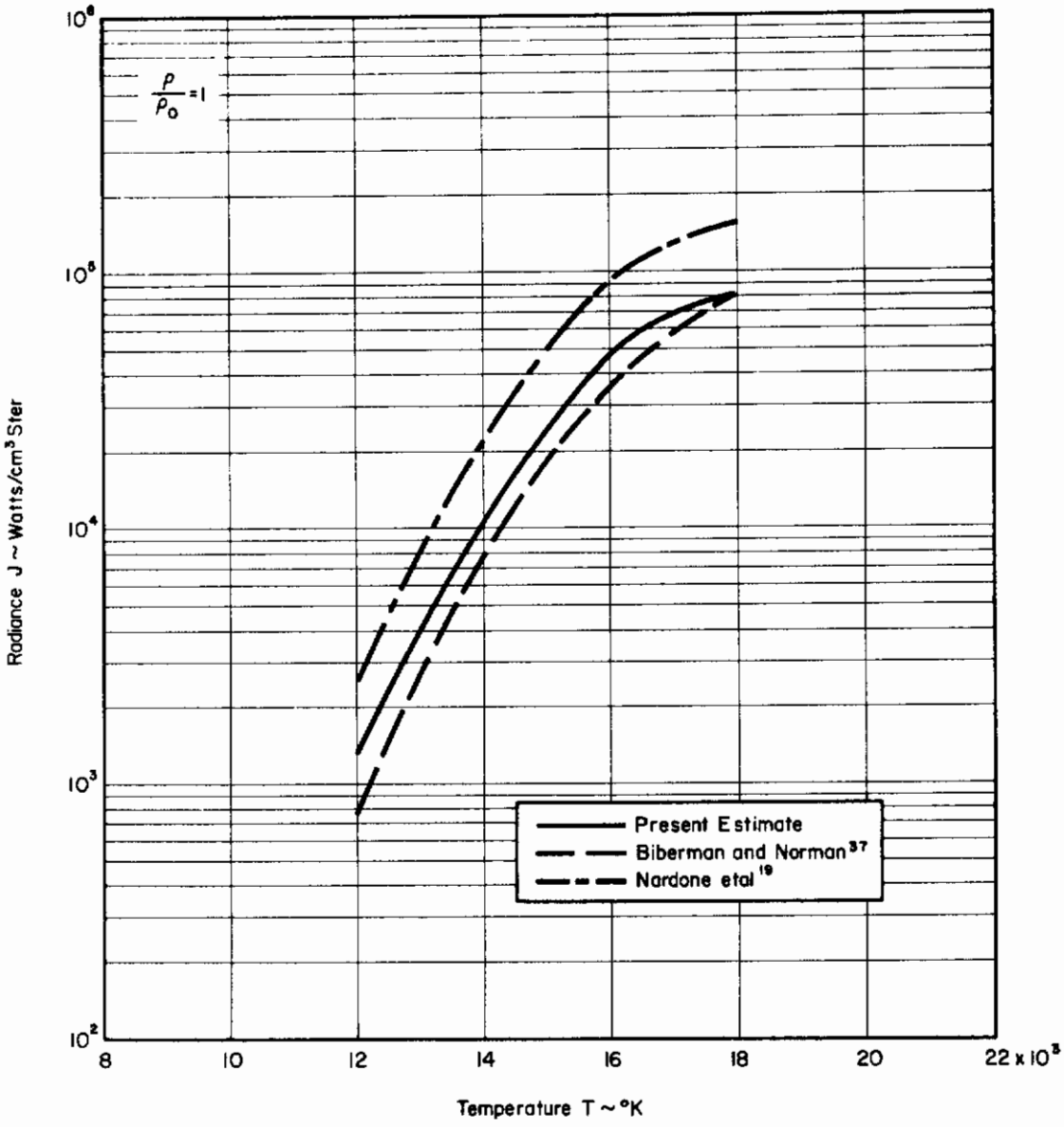

FIGURE 45. Comparison of Various Estimates of N^+ Deionization and N Free-Free Radiative Emission

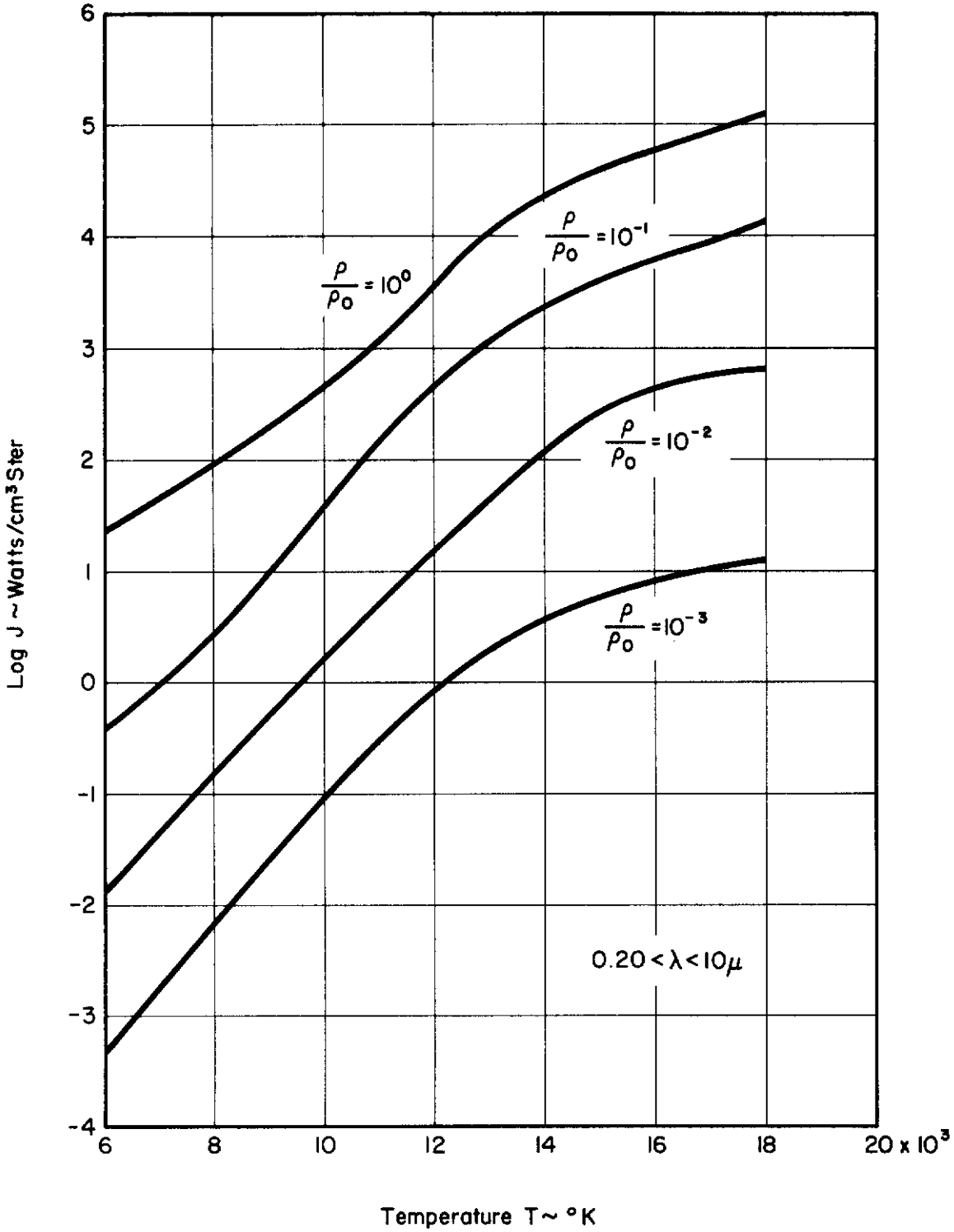

FIGURE 46. Estimate of Radiance of High Temperature Air ($0.20 < \lambda < 10\mu$)

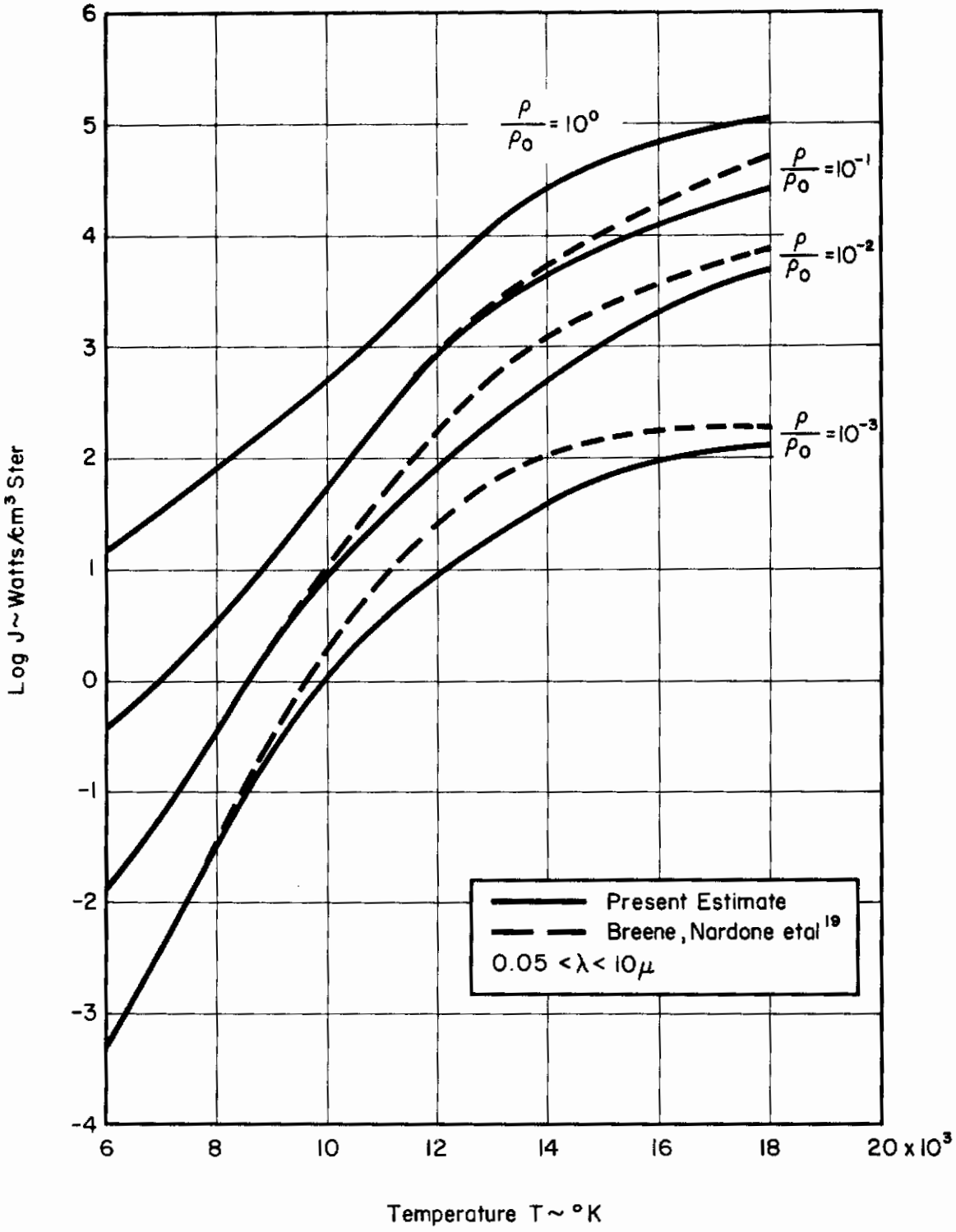

FIGURE 47. Estimate of Radiance of High Temperature Air ($0.05 < \lambda < 10\mu$)

It should be noted that there have been other investigations of the radiance of high temperature air. At the NASA Ames Research Center, experimental measurements have been carried out through the use of a series of photomultipliers to determine the spectral distribution of the shock layer emission for a blunt body.[15,17] Flight velocities up to 44,000 feet per second have been simulated with gun-launched models in a counterflow facility.[15,58] These measurements have shown general agreement with the theoretical results of Kivel and Bailey,[7] and thus are in considerable disagreement with the present results. However, in order to achieve flight velocities in excess of 30,000 feet per second, plastic models were used. These models ablate at such extreme conditions, and although corrections for the ablation product radiation were attempted,[17] it would seem rather impossible to separate the air radiation and the contamination radiation in certain portions of the spectrum. Thus this author feels that these results must be considered as highly questionable.

H. Hoshizaki[20] has also carried out stagnation point radiative heat transfer measurements using a combustion driven shock tube generated flow.[20] These measurements, which have been performed only at an initial driven tube pressure of 1 mm Hg and over a very limited range of temperatures, are shown in Fig. 48 with the present experimental results. It can be seen that there is good agreement.

The present experimental results are also in agreement with recent interpretations of the radiative emission from high temperature equilibrium air.[25] The lower emission rate associated with de-ionization continuum radiatiom as proposed by Biberman and Norman,[37] and the suggestion of significant radiation being contributed by the N^- photo attachment process[25] have both appeared plausible based on analysis of the data. Thus a revised estimate of equilibrium radiative emission has been carried out. The application of this to re-entry heating calculations will be discussed in the next section.

VIII. STAGNATION POINT RADIATIVE HEAT TRANSFER DURING RE-ENTRY AT HYPERVELOCITIES

The revised estimate of thermal radiation from high temperature equilibrium air, which is presented in Section VII, has an obvious importance for the problem of re-entering the Earth's atmosphere at super-orbital velocities. As an example, consider a manned Mars mission where Earth entry velocities ranging from 45,000 to 75,000 feet per second are anticipated.[59] The stagnation point heat load for such a re-entry will be dominated by the shock layer radiative emission, with the maximum stagnation point radiative heat transfer rate being a factor of ten or more greater than the maximum convective rate. Here the present results, which indicate that the radiative heating at flight velocities in excess of 40,000 feet per second will be on the order of a factor of two less than the existing estimates of Nardone et al,[19] have a definite bearing on the design of the re-entry vehicle thermal protection system.

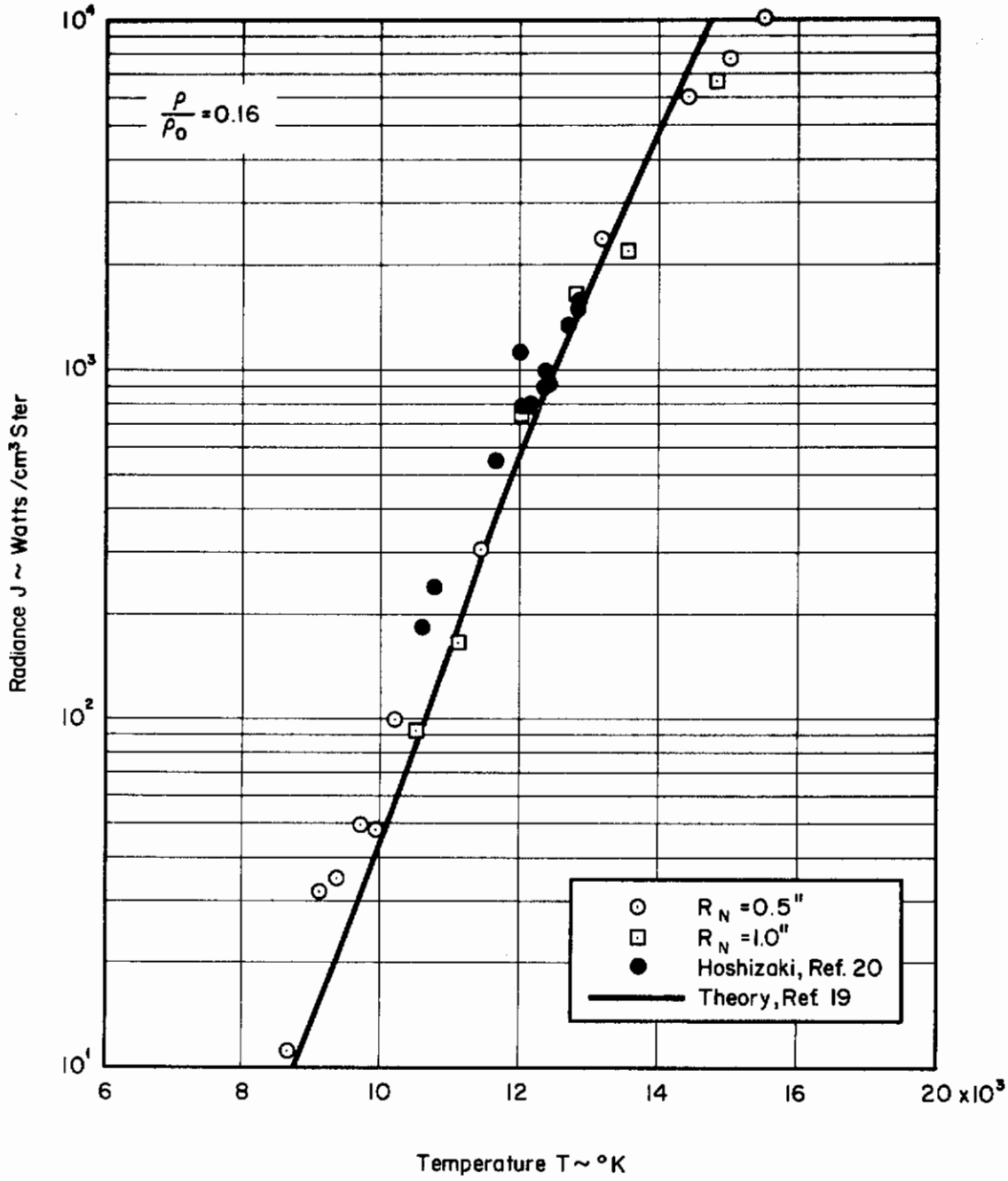

FIGURE 48. Comparison of Existing Shock Tube Results on Radiative Emission from Equilibrium Air

In order to present the results of this investigation in a form usable for design calculations, the total equilibrium radiative emission per unit volume into 4π steradians, denoted as $E_t = 4\pi J$, is shown in Fig. 49 as a function of flight velocity and altitude and for stagnation point equilibrium conditions.[24] For an optically thin shock layer, the stagnation point equilibrium radiative heat transfer rate to a surface with an absorptivity of 100 per cent may be expressed in terms of E_t as

$$\dot{q}_{rad} = \left(\frac{E_t}{2}\right) F_1 \delta \quad , \qquad (27)$$

where F_1 is a shock layer shape factor (see Section II) and δ is the shock detachment distance. Wick[32] has evaluated this shape factor for flight conditions in terms of the normal shock density ratio and his results are presented in Fig. 50. A value of 0.84 is recommended by Wick for the range of present interest in re-entry calculations. δ may be evaluated from any of several hypersonic flow theories or from experimental data.[33,40]

The results presented in Fig. 49 have been approximated by a correlation of the form

$$E_t = C\left(\frac{\rho_\infty}{\rho_o}\right)^m \left(\frac{V_\infty}{10^4}\right)^n \quad , \qquad (28)$$

where it has been necessary to use different values for the exponents m and n, and the constant C, in various flight velocity ranges. The results of this correlation are shown in Table 7. The R.M.S. deviation, σ, of the results in Fig. 49 from this correlation (Eq. (28) together with Table 7) is less than 36 per cent. The correlation for the range of flight velocities less than 28,000 feet per second has application to ICBM and satellite re-entries. For such re-entries, radiative heating is unimportant. The correlation for the range of 28,000 to 38,000 feet per second has application to vehicles re-entering at velocities on the order of the escape velocity and would include return from lunar missions. For these re-entries, radiative heating is important, but not necessarily dominant. The correlation for flight velocities in excess of 38,000 feet per second is applicable to the Earth re-entry of Venus and Mars missions in which the radiative heating dominates the heat load.

In the flight velocity range of 20,000 to 60,000 feet per second at altitudes from 100,000 feet to 240,000 feet, F_1 is approximately constant at the value of 0.84, and δ/R_N is approximately 0.045 for a hemispherical nose body.[32] Thus combining Eqs. (27) and (28), the stagnation point radiative heat transfer

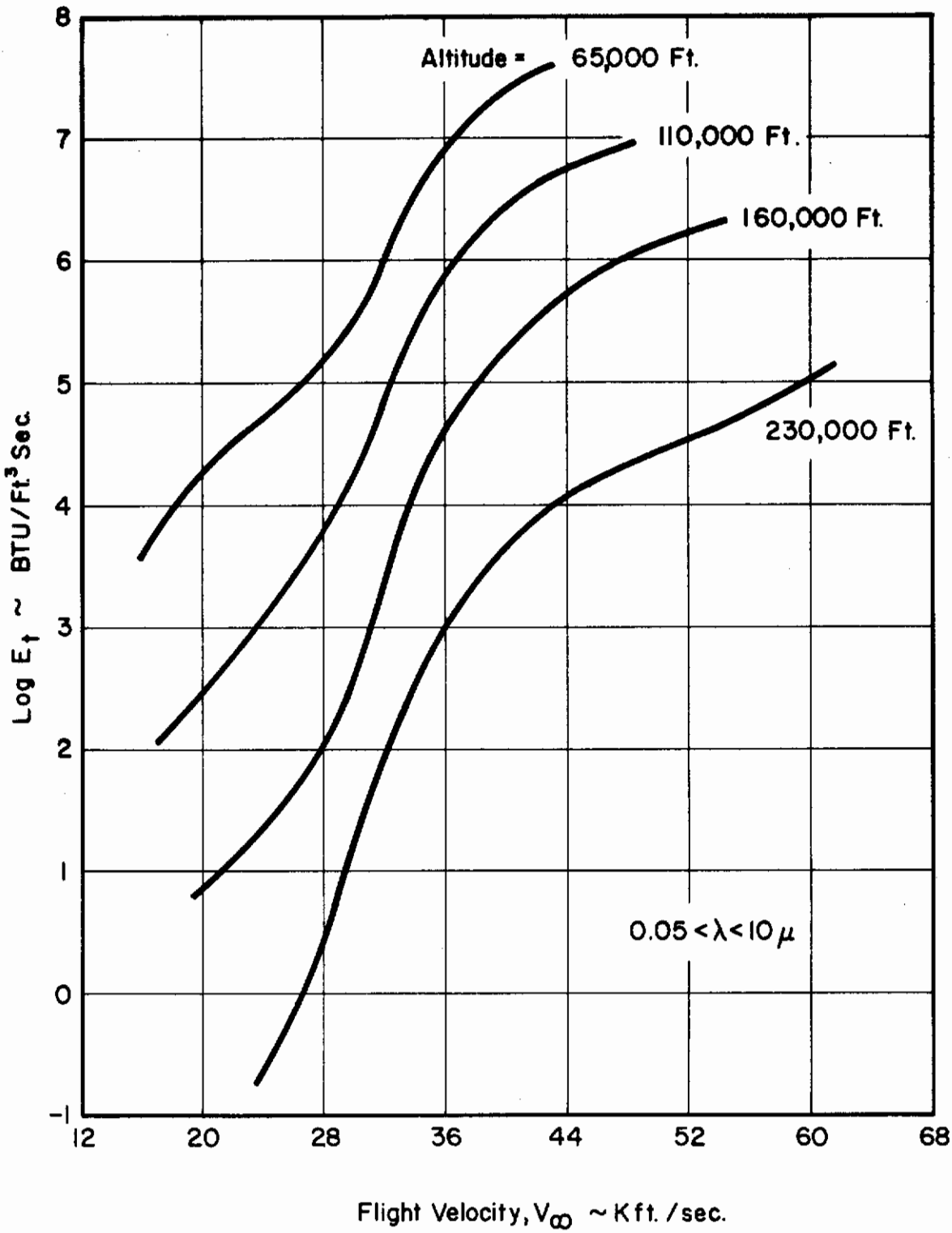

FIGURE 49. Stagnation Point Equilibrium Radiative Emission

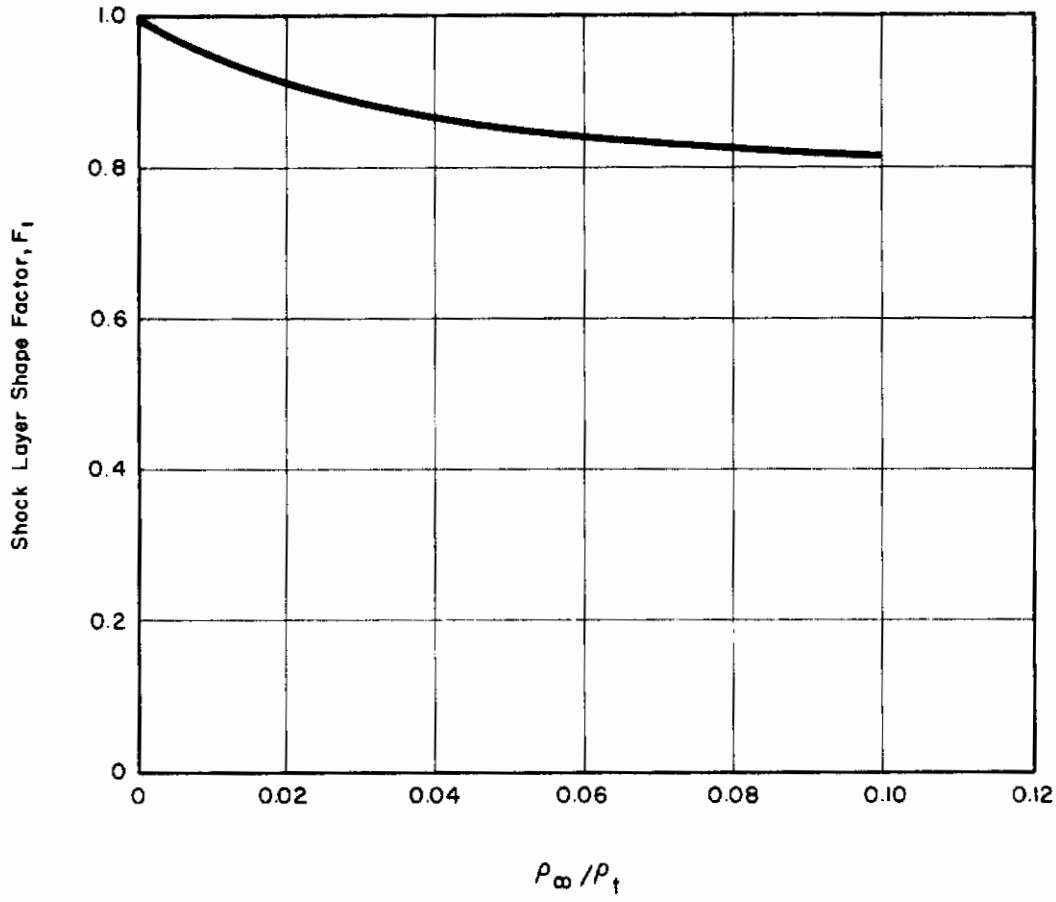

FIGURE 50. Shock Layer Shape Factor, F_1 (Reference 32)

TABLE 7

CONSTANTS IN RADIATIVE EMISSION CORRELATION

Flight Velocity Range Fps	C BTU/Ft^3 sec	m	n	σ
$V_\infty < 28{,}000$	6.83×10^{3}	1.68	7.4	0.3579
$28{,}000 < V_\infty < 38{,}000$	4.30×10^{-3}	1.41	20.0	0.3581
$38{,}000 < V_\infty$	2.10×10^{4}	1.30	8.00	0.3295

rate for an optically thin shock layer becomes, in units of BTU/Ft^{2}sec,

$$\dot{q}_{rad} = 1.3 \times 10^{3} R_N \left(\frac{\rho_\infty}{\rho_o}\right)^{1.68} \left(\frac{V_\infty}{10^4}\right)^{7.4}, \qquad V_\infty < 28000 \text{ Fps}$$

$$= 8.16 \times 10^{-5} R_N \left(\frac{\rho_\infty}{\rho_o}\right)^{1.41} \left(\frac{V_\infty}{10^4}\right)^{20.0}, \qquad 28000 < V_\infty < 38000 \text{ Fps} \qquad (29)$$

$$= 3.99 \times 10^{3} R_N \left(\frac{\rho_\infty}{\rho_o}\right)^{1.30} \left(\frac{V_\infty}{10^4}\right)^{8.00}, \qquad 38000 \text{ Fps} < V_\infty \; .$$

Equation (29), though somewhat approximate, is convenient for rapid engineering calculations. For higher accuracy in design calculations, Eq. (27) should be used together with Fig. 49 and an accurate shock detachment distance.

For extreme shock layer conditions, the radiative energy emission may be significant with the result that the stagnation region flow is non-adiabatic. This radiative energy loss is important if the ratio of the energy radiated by an element of fluid to the initial total energy of the element, Γ, is appreciable. For stagnation region flow and for the optically thin case, Γ may be expressed as

$$\Gamma = \frac{E_t \, \delta}{\frac{1}{2} \rho_\infty V_\infty^3} \; . \qquad (30)$$

Γ/δ is presented as a function of flight velocity and altitude for stagnation region conditions in Fig. 51. Wilson and Hoshizaki[60] have considered the decrease in the stagnation point radiative heat transfer rate due to the existence of non-adiabatic shock layer conditions. Results are presented in Fig. 52 where the ratio of the radiative flux for a non-adiabatic shock layer to that for an adiabatic shock layer is shown as a function of Γ. It can be seen that for a value of $\Gamma = 0.2$, the decrease in the radiative heat transfer rate would be on the order of 70 per cent. This value of Γ would correspond to a flight velocity in excess of 60,000 feet per second, an altitude of 200,000 feet, and a stagnation point nose radius of 5 feet.

The stagnation point radiative heat transfer rate can thus be predicted with Eq. (27), together with either Fig. 49 or Eq. (28), for an optically thin shock layer; while for a non-adiabatic shock layer, Fig. 52 must be used in order to correct for radiant energy losses. Away from the stagnation point, the radiative heating rate falls off rapidly. Wilson and Hoshizaki[60] have considered the distribution in equilibrium radiative heating over a blunt nose body with a radius of 5 feet, and the present author has noted that these results may be quite satisfactorily expressed as

$$\frac{\dot{q}(\theta')}{\dot{q}(o)} = (\cos\theta')^{4.65} \quad , \qquad (31)$$

where θ' is the angle between the tangent to the stagnation point and the tangent to some local point. This correlation formula is also in reasonable agreement with the earlier results of Strack,[16] and may be used in re-entry heating calculations.

IX. CONCLUDING DISCUSSION

The objective of this investigation has been to assess the accuracy of existing theoretical calculations of the radiance of high temperature air, and if necessary, modify these analyses so as to provide more accurate information on radiative heating during re-entry for use in engineering design calculations. It has been found that the existing calculations by Nardone et al[19] are more consistently in agreement with the present data than other available theoretical results.[6-8,11] However, at high temperatures where continuum radiation is dominant, this theory overestimates the radiative emission by a factor of two. This has been explained through the use of the recent spectroscopic results by Allen and Textoris,[25] and the theoretical analysis by Bibermann and Norman.[37]

The present results disagree with those obtained at the NASA Ames Research Center.[17] Although this author questions the NASA results due to effects of ablation product radiation, which he believes are not accounted for, it is clear that additional information is required before these differences can be resolved.

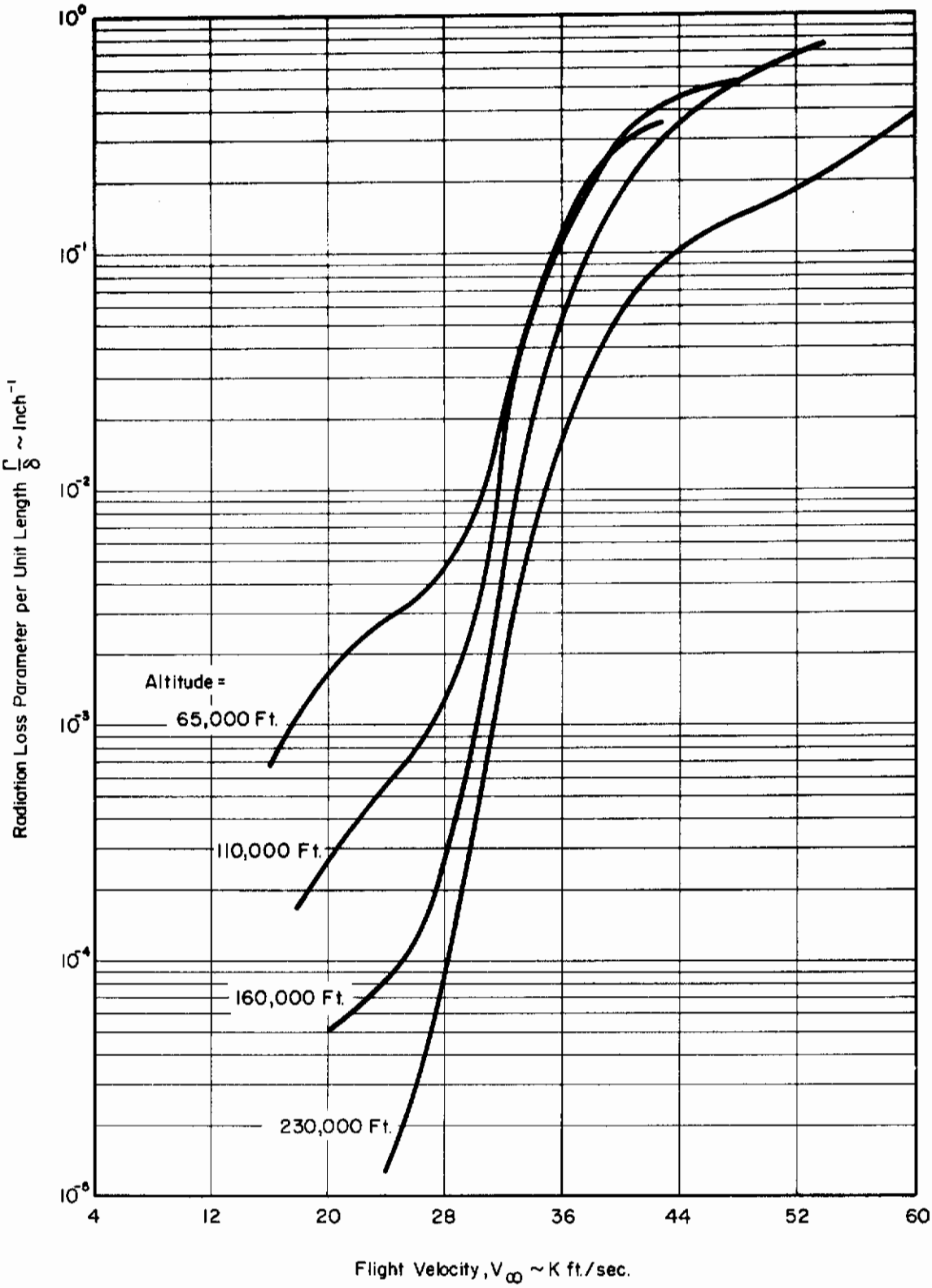

FIGURE 51. Energy Loss Parameter for Free-Flight Stagnation Conditions

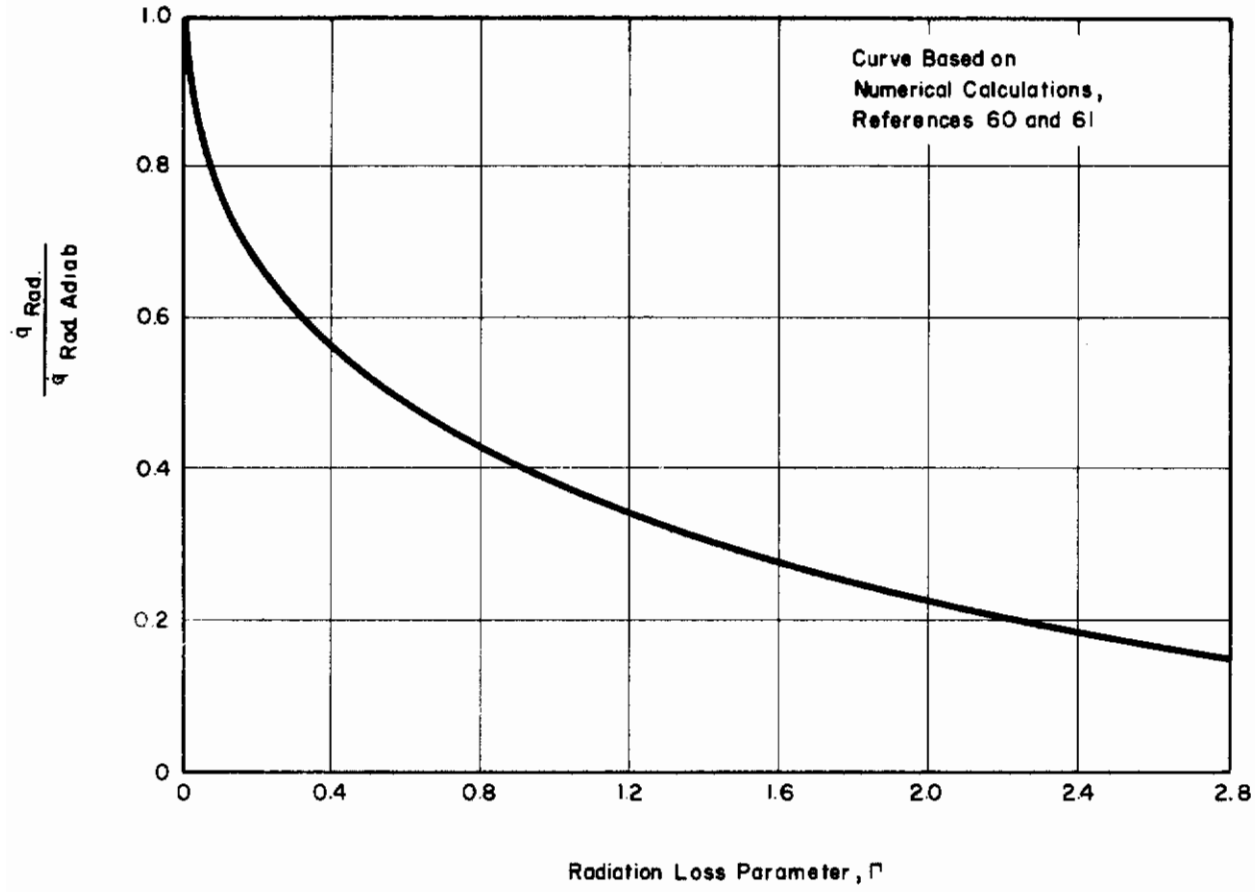

FIGURE 52. Stagnation Point Radiative Heat Flux Reduction from Adiabatic Value (Reference 60)

Of particular interest would be results from spectroscopic studies designed to determine which species and processes in high temperature equilibrium air are the dominant ones in terms of radiative energy emission.

An associated problem that should receive attention in the future is the measurement of radiative heat transfer at wavelengths below 0.15 micron, where Nardone, Breene et al[19] have indicated the presence of an important contribution. The difficulty with the performance of such a measurement is that no materials will transmit light at wavelengths much below 0.15 micron. Lithium fluoride, which this author believes to transmit furthest into the far ultraviolet, cuts off at 0.11 micron. Thus techniques other than those described here may need to be developed to measure radiation intensities at wavelengths less than 0.15 micron.

Based on the experimental results of this investigation, a revised estimate of the radiance of high temperature air has been presented. These results have been discussed with regard to determining the stagnation point equilibrium radiative heat transfer rate for blunt nose or blunt leading edge re-entry vehicles. Because of the strong dependence of radiative heating on flight velocity, free stream density, and the bluntness of the vehicle, future vehicles designed for re-entry in the 50-100,000 feet per second velocity range may well be of the slender, lifting body type of configuration. From an engineering standpoint, it is thus important that the effect of various vehicle configuration factors on re-entry radiative heating be investigated in the near future.

REFERENCES

1. Dorrance, W. H., Viscous Hypersonic Flow, McGraw-Hill New York, 1962.

2. Fay, J. A., and Riddell, F. R., "Theory of Stagnation Point Heat Transfer in Dissociated Air," J. Aero/Space Sci., Vol. 25, No. 2, February, 1958.

3. Lees, L., "Laminar Heat Transfer over Blunt Bodies at Hypersonic Flight Speeds," Jet Propulsion, Vol. 26, No. 4, April, 1956, pp. 259-269.

4. Rose, P. H.; Probstein, R. F.; and Adams, M. C., "Turbulent Heat Transfer through a Highly Cooled, Partially Dissociated Boundary Layer," J. Aero/Space Sci., Vol. 25, No. 12, December, 1958, pp. 751-760.

5. Nerem, R. M., and Stickford, G. H., "Stagnation Point Heat Transfer in High Enthalpy Gas Flows. Part I: Convective Heat Transfer in Partially Ionized Air," The Ohio State University Aerodynamic Laboratory, Final Report prepared under Contract AF 33(657)-10110, Research and Technology Division, Air Force Systems Command, United States Air Force, Wright-Patterson Air Force Base, Ohio. (FDL-TDR-64-41 Part I).

6. Meyerott, R. E., "Absorption Coefficients of Air from 6000°K to 18,000°K," USAF Project Rand RM-1554, The Rand Corporation, Santa Monica, California, September, 1955.

7. Kivel, F., and Bailey, K., "Tables of Radiation from High Temperature Air," Res. Rep. 21, AVCO Research Lab., 1957.

8. Meyerott, R. E., "Radiation Heat Transfer to Hypersonic Vehicles," Presented at the Third AGARD Colloquium on Combustion and Propulsion, Palerno, Sicily, March 17-21, 1958.

9. Keck, J.; Camm, J.; Kivel, B.; and Wentink, T., "Radiation from Hot Air, Part II," Annals of Physics, Vol. 7, May, 1959.

10. Camm, J. C.; Kivel, B.; Taylor, R. L.; and Teare, J. D., "Absolute Intensity of Non-Equilibrium Radiation in Air and Stagnation Heating at High Altitudes," Avco-Everett Research Laboratory RR93, December, 1959.

11. Meyerott, R. E.; Sokoloff, J.; and Nicholls, R. W., "Absorption Coefficients of Air," GRD-TR-60-277, Geophysics Research Directorate, AF Research Division, ARDC, Bedford, Massachusetts, July, 1960.

12. Kivel, B., "Radiation from Hot Air and its Effect on Stagnation Point Heating," J. Aero Sci., 28, 96 (1961).

13. Kennet, H., and Strack, S. L., "Stagnation Point Radiative Transfer," ARS Journal, 31, 370 (1961).

14. Teare, J. D.; Georgiev, S.; and Allen, R. A., "Radiation from the Non-Equilibrium Shock Front," Avco-Everett Research Laboratory RR 112, October, 1961.

15. Page, William A.; Canning, Thomas N.; Craig, Roger A.; and Stephenson, Jack D., "Measurements of Thermal Radiation of Air from the Stagnation Region of Blunt Bodies Traveling at Velocities up to 31,000 Feet Per Second," NASA TM X-508, 1961.

16. Strack, S. L., "Radiant Heat Transfer Around Re-Entry Bodies," ARS Journal, Vol. 32, No. 9, May, 1962, pp. 744-748.

17. Page, W. A., "Shock-Layer Radiation of Blunt Bodies Traveling at Lunar Return Entry Velocities," Presented at the IAS 31st Annual Meeting, New York, New York, January 21-23, 1963.

18. Allen, R. A.; Rose, P. H.; and Camm, J. C., "Non-Equilibrium and Equilibrium Radiation at Super-Satellite Re-Entry Velocities," IAS Prepring No. 63-77, Presented at IAS 31st Annual Meeting, New York, New York, January 21-23, 1963.

19. Nardone, M. C.; Breene, R. G.; Zeldin, S. S.; and Riethof, T. R., "Radiance of Species in High Temperature Air," GE R63SD3, General Electric Space Sciences Lab., June, 1963. (AD 408564).

20. Hoshizaki, H., "Equilibrium Total Radiation Measurements in Air at Superorbital Entry Velocities," Lockheed Missiles and Space Co. Rept. No. 6-90-63-97, October, 1963.

21. Gilmore, F. R., "Equilibrium Composition and Thermodynamic Properties of Air to 24,000°K," Rand Corporation Rept. RM-1543, August 24, 1955.

22. Feldman, S., "Hypersonic Gas Dynamic Charts for Equilibrium Air," Avco Research Laboratory, Everett, Mass., 1957.

23. Ziemer, R. W., "Extended Hypervelocity Gas Dynamic Charts for Equilibrium Air," Space Technology Laboratories, Inc., Report STL/TR-60-0000-09093, April 14, 1960. (AD 242694).

24. Huber, P. W., "Hypersonic Shock-Heated Flow Parameters for Velocities to 46,000 Feet Per Second and Altitudes to 323,000 Feet," NASA TR-R-163, 1963.

25. Allen, R. A., and Textoris, A., "New Measurements and a New Interpretation for High Temperature Air Radiation," Presented at the AIAA Aerospace Sciences Meeting, New York, January 20-22, 1964, Preprint No. 64-72.

26. Lees, L., "Recovery Dynamics--Heat Transfer at Hypersonic Speed in a Planetary Atmosphere," Space Technology ed. by H. Siefert, John Wiley and Sons, Inc., New York, 1959.

27. Chandrassekhar, S., Radiative Transfer, Dover Publications, New York, 1960.

28. Kourganoff, V., Basic Methods in Transfer Problems, Dover Publications, New York, 1963.

29. Penner, S. S., Quantitative Molecular Spectroscopy and Gas Emissivities, Addison-Wesley, Reading, Mass., 1959.

30. Herzberg, G., Molecular Spectra and Molecular Structure. I. Spectra of Diatomic Molecules, Van Nostrand, New York, 1950.

31. Zhigulev, V. N.; Romishevskii, Ye. A.; and Vertushkin, V. K., "Role of Radiation in Modern Gas Dynamics," AIAA Journal, Vol. 1, No. 6, Russian Supplement, June, 1963, pp. 1473-1475.

32. Wick, B. H., "Radiative Heating of Vehicles Entering the Earth's Atmosphere," Presented to the AGARD Fluid Mechanics Panel, Brussels, Belgium, April 3-6, 1963. (NASA Document No. N62-12453).

33. Hayes, W. D., and Probstein, R. F., Hypersonic Flow Theory, Academic Press, New York, 1959.

34. Truitt, R. W., Hypersonic Aerodynamics, Ronald Press, New York, 1959.

35. Branscomb, L. M.; Burch, D. S.; Smith, S. J.; and Geltman, S., "Photodetachment Cross Section and the Electron Affinity of Atomic Oxygen," Phys. Review, Vol. III, 1958, p. 504.

36. Boldt, G., "The Recombination and Minus Continua of Nitrogen Atoms," Z Physik, Vol. 154, 1959, pp. 330-338.

37. Biberman, L. M., and Norman, G. E., "On the Calculation of Photoionization Absorption," Opt. i Spektroskopiya, Vol. 8, 1960, pp. 433-438.

38. Bennett, R. G., and Dalby, F. W., "Experimental Determination of the Oscillator Strength of the First Negative Bands of N_2^+," J. Chem. Physics, 31, 435, (1959).

39. Lee, John D., and Nerem, Robert M., "Theory and Performance of a Shock Tube Having an Arc Heated Driver," The Ohio State University Aerodynamic Laboratory Report No. 1021-18, June 15, 1962. (AD 277192).

40. Caldecott, R.; Lee, J. D.; and Nerem, R. M., "The Development and Application of an Arc Driven Hypervelocity Shock Tube," Presented at the 8th Midwestern Mechanics Conference, Case Institute of Technology, Cleveland, Ohio, April 1-3, 1963.

41. Nerem, R. M.; Lee, J. D.; and Caldecott, R., "The Development of an Arc Discharge Driven Shock Including Some Initial Results on Aerodynamic Plasmas," The Ohio State University Aerodynamic Laboratory Report No. 1573-1, December 1, 1962. (AD 408273).

42. James, C. S., "Experimental Study of Radiative Transport From Hot Gases Simulating in Composition the Atmosphere of Mars and Venus," Presented at the AIAA Conference on Physics of Entry, Cambridge, Mass., August 26-28, 1963; Preprint No. 63-455.

43. Graber, B., and Nerem, R. M., "Test Duration Measurements in an Arc Driven Hypervelocity Shock Tube," The Ohio State University Aerodynamic Laboratory Report No. 1573-2, October 15, 1963. (AD 423711).

44. Graber, B. C., "An Experimental Study of Real Gas Effects on Shock Detachment Distances and Shock Shapes for a Group of Spherically Blunted Bodies," M. Sc. Thesis, The Ohio State University, November, 1963, (to be published as an RTD TDR, 1964).

45. Rose, P. H., and Stankevics, J. O., "Stagnation Point Heat Transfer Measurements in Partially Ionized Air," Presented at the IAS 31st Annual Meeting, New York, January 21-23, 1963, IAS Paper No. 63-61.

46. Eckert, E. R. G., and Drake, R. M., Heat and Mass Transfer, McGraw-Hill, New York, 1959.

47. Vidal, R. J., "Transient Surface Temperature Measurements," Presented at the ASME Hydraulic Division Conference, May 21-23, 1962.

48. Hall, J. G., and Hertzberg, A., "Recent Advances in Transient Surface Temperature Thermometry," Jet Propulsion, Vol. 28, No. 11, November, 1958.

49. Hanovia Liquid Gold Division, Engelhard Industries, "Ultraviolet, Visible, and Infrared Transmission and Reflection of Hanovia Metallic and Luster Films," Bulletin No. 22, 1962.

50. Vidal, R. J., "Model Instrumentation Techniques for Heat Transfer and Force Measurements in a Hypersonic Shock Tunnel," Cornell Aeronautical Laboratory Report No. AD-917-A-1, February, 1956. (WADC TN 56-315).

51. Private Communication with Leonard Bogdan, Cornell Aeronautical Laboratory, February, 1964.

52. Skinner, G. T., "Calibration of Thin-Film Gage Backing Materials," ARS Journal, Vol. 31, No. 5, May, 1961.

53. Hartunian, R. A., and Varwig, R. L., "A Correction to Thin-Film Heat Transfer Measurements," Aerospace Corp. Report No. TDR-594 (1217-01) TN-2, May, 1961.

54. Malitson, I. H.; Murphy, F. V.; and Rodney, W. S., "Refractive Index of Synthetic Sapphire," Journal of the Optical Society of America, Vol. 48, No. 9, September, 1958, pp. 629-631.

55. Bauple, R.; Gilles, A.; Romand, J.; and Vodar, B., "Absorption Spectra of Samples of Quartz and Corundum in the Ultra-Violet, Electric, and Thermic Treatment of Quartz," Journal of the Optical Society, Vol. 40, 1958, p. 788.

56. Linde Industrial Crystals Bulletin No. F-917B, "Synthetic Sapphire, An Optical Material," October 2, 1961.

57. Jeppesen, M. A., "Some Optical, Thermo-Optical, and Piezo-Optical Properties of Synthetic Sapphire," Journal of the Optical Society of America, Vol. 48, No. 9, September, 1958, pp. 629-631.

58. Sieff, A., "A Free-Flight Wind Tunnel for Aerodynamic Testing at Hyper-Sonic Speeds," NACA Report 1222, 1955.

59. Pritchard, E. B., "Survey of Velocity Requirements and Re-Entry Flight Mechanics for Manned Mars Missions," Presented at the AIAA Aerospace Sciences Meeting, New York, January 20-22, 1964, Preprint No. 64-13.

60. Wilson, K. H., and Hoshizaki, H., "Inviscid, Non-adiabatic Flow about a Blunt Body," Presented at the AIAA Aerospace Sciences Meeting, New York, January 20-22, 1964, Preprint No. 64-70.

61. Howe, J. T., and Viegas, J. R., "Solutions of the Ionized Radiating Shock Layer, Including Reabsorption and Foreign Species Effects, and Stagnation Region Heat Transfer," NASA TR-159, 1963.